Development and evaluation of freeform surface descriptions

Dissertation zur Erlangung des akademischen Grades

doctor rerum naturalium (Dr. rer. nat.)

vorgelegt dem Rat der Physikalisch-Astronomischen Fakultät

der Friedrich–Schiller-Universität Jena

von Dipl. Phys. Anika Brömel

geboren am 19. September 1984 in Waren(Müritz)

Gutachter:

1. Prof. Dr. Herbert Gross, Friedrich-Schiller-Universität Jena
2. Prof. Dr. Alois Herkommer, Universität Stuttgart
3. apl. Prof. Dr. Norbert Lindlein, Friedrich-Alexander-Universität Erlangen-Nürnberg

Tag der Disputation: 13. September 2018

Abstract

In recent years, great efforts can be observed in the community of optical design to use the additional degrees of freedom afforded by freeform surfaces in optical systems. If commercial software tools are considered, only very limited support of freeform surface systems is currently found. In particular one important question at the beginning of the concept and design of a freeform system is the decision how to mathematically describe the surface itself. If the development of an optical system with freeform surfaces is considered, not only the optical design, but also the mechanical design, the manufacturing and the assembly of the component inside the whole system are important. The focus in this PhD is on the design phase. Therefore only functions are considered which are globally defined on the computational area inside the boundary. The main approaches of describing freeform surfaces are discussed from a more mathematical point of view, either known from literature or new definitions according to the aforementioned opportunities. More two new polynomial sets the A-polynomials 1st and 2nd kind are introduced.

Based on these possibilities, the next question of an optical designer would be how to select the surface type optimal for an efficient optimization process with a comfortable result.

The choice of description is often limited by the available options in the commercial software. Therefore a systematic study of the different options can still not be found. To overcome this problem we evaluated the selected descriptions in a comprehensive assessment. The results are collected in the form of a benchmark which compares different freeform surface descriptions for optical systems with one freeform for various applications with different types of symmetry, including refractive, reflective and catadioptric systems. The representations under the viewpoint of different initial systems, symmetry of the system, sensitivity in optimization and quality of the final result are compared and discussed. In particular the influence of the basic shape selection, the basic geometry to be Cartesian or polar and the importance of the orthogonality are investigated. Finally, in a conclusion the major results are summarized and a recommendation for practical work is formulated.

Contents

Chapter 0 Motivation

Classically optical systems are using rotationally symmetric surfaces, described by spheres or conic sections. More than 100 years ago in 1905 Schwarzschild introduced aspheric surfaces to the optical design world [1]. This new form of surface description is still rotational symmetric, but with much higher degrees of freedom. Therefore, he could show in his telescope-design, that it is possible to correct for 2 Seidel conditions with only two aspheric mirrors [1]. Nevertheless, it took another 80 years until the new shape was used in a mass-produced commercial device [2]. Hereby Kodak achieved a similar performance with one aspheric lens in a four-element camera, as with a classical approach with five spherical lenses at only two-thirds of the cost.

With the development of design methods and example [1-7], as well as new strategies for cost-effective manufacturing [8-9] and metrology [10] in the last twenty years, aspherical surfaces became more and more standard in the optical design. Moreover, the huge success in industrial products like mobile phone cameras laid the foundation for increasing the degrees of freedom even further into optical systems with non-rotationally symmetric freeform surfaces. Giving up the rotational symmetry in an optical system is generally only beneficial for specialised applications like mirror systems without central obscuration or systems with special application needs for compactness like a spectrometer or head-mounted displays. The very first approaches of using a freeform in an optical system came from Kitajima in 1925 with a patent of "a combination lens made of two or more superimposed cylindrical lenses, which are movable longitudinally with respect to one another have a regularly increasing refrangibility from one end to another. "[11]. Also, Birchall in 1935 [12] and Alvarez in 1967 [12] acquired patents, which were using non-rotational symmetric surfaces. One of the first commercial applications for freeform imaging optics was the in 1972 launched Polaroid SX-70, designed by J.G. Baker and later described by W.T. Plummer [14]. The design was achieved with the use of two freeform lenses, described by a simple power series in x and y up to the eighth order. The manufacturing was quite cost-intensive, and the yield was not very high. So, for the next 25 years, freeform surfaces were either used in low-performing systems like eyeglasses and illumination. A few designers were thinking about non-rotational systems for

more advanced systems, like Tatian [15], who investigated “unusual optical surfaces” for unobscured reflective systems in the mid-80s.
With the beginning of the new century, non-rotational symmetric systems came back into the focus. The need for more compact systems with better image quality and higher field of view (FOV) encouraged the community to think of optical systems beyond the rotational symmetry.

Unfortunately, with the break of rotational symmetry we, as a designer, must rethink most of what we know about optical design, specifically in imaging. In recent years many novel approaches for designs [16-21], initial systems [22-27] and performance evaluation [28-37] were presented. Moreover, the tolerancing [38-39], fabrication [40-43], alignment [44-45] and metrology [40-41, 46-48] of freeform systems were investigated.
A very special question in the design process is the choice of description. For classical spherical or conical surfaces this is quite simple, but for freeform surfaces, there is a wide range of very different concepts: either locally defined [49-51] or globally defined polynomial descriptions, well-known from optical design [52-53] and mathematics [54-55]. Furthermore, there is a range of newly developed representations specifically for describing freeform surfaces [56-60]. Generally, it is desired for the description to achieve a superior result, with only a few significant parameters and fast convergence in the optimisation. The choice is hereby also influenced by the feasibility of tolerancing or fit of data. However, in the practical results of optical freeform design work, found in the literature [16-21], typically, the representation of the freeform surface used by the authors is governed by the available options in the commercial design programs. Previous investigations on the impact of the description choice on the performance of the system are limited by a small variety of representations and systems [56, 60—64]. Therefore, a more systematic comparison and critical review of different options are missing until today.
The main objective of this PhD work is to investigate the existing surface description for optical freeform system, concentrating on the globally defined polynomial representations. With the A-polynomials 1st and 2nd kind, two new descriptions were specifically developed for freeform surface. Hereby the aspect of a fast, robust and efficient calculation, known from a well-established polynomial set [65] was combined with a newer approach of better feasibility for the tolerancing and mechanical design [59]. In a second step, the two new descriptions and a selection of well-known freeform descriptions are evaluated in a so-called

benchmark with for various aspects regarding their performance to gain a better understanding of the behaviour of the different descriptions in the optimization of four typical freeform systems. The properties of the representations, which are of main impact on the performance, are emphasised. With this knowledge, a sufficient description can be selected.

For this, in chapter 1 a brief overview of classical design for circular symmetric systems is given. Moreover, the general definition and some typical freeform systems are introduced and the main difference in the design process, the performance evaluation and the realisation of freeform surfaces is emphasized. The chapter concludes with the consequences of the design requirements on the choice of the surface description.

In chapter 2 a detailed insight in the general approach of polynomial description and the structure of polynomial sets are given. Additionally, a selection of well-known and new descriptions is presented with their main mathematics and properties.

In chapter 3 the extension made for the basic shape is shown and the development and properties of the new A-polynomials 1st and 2nd kind are introduced. The new polynomial sets and their properties are summarized with the descriptions, presented in chapter 2, in an overview at the end of the section.

Chapter 4 opens with an introduction to the benchmark method and systems before it starts with the investigations for the impact of the basic shape, convergence and final performance of the polynomial descriptions, the impact of the orthogonality on the convergence speed and the convergence behaviour for different algorithms. At the end of this section, a summary and conclusion regarding the choice of the description are given.

Chapter 5 gives conclusions and an outlook on the development and evaluation of freeform surface descriptions for imaging applications.

Finally, in the appendix the conversion between the different sorting schemes of the description can be found.

Chapter 1 Introduction

In the following chapter, a brief overview of the design of circular systems is given. Moreover the benefits and design aspects of a freeform imaging system - specifically concerning the description of such surfaces – are introduced and finally the consequences for the choice of freeform descriptions are shown.

1.1 Circular symmetric systems

In geometrical optics, the ideal imaging of a system can be described by the perfect transfer of a single point in the object space to a single point in the image space. Hereby the ray bundle emitted by the point source forms a spherical surface with a constant phase, called wavefront. With propagation through the system, the wavefront keeps spherical and results into a perfect image point. In reality, the image quality of an imaging system is often degraded by diffraction and by geometrical aberrations [66].

Diffraction is caused by the interaction of the light with the aperture of the system. This results in spreading of the spot in the image plane, which is often also called blur. The image of a point source from infinity without geometrical aberrations is named Airy disk. Systems without spreading are called diffraction limited. The diameter of the Airy disk is thereby primarily influenced by the aperture of the system and the wavelength of the light [67]. Wave aberrations, on the other hand, are the deviation of the real wavefront from an ideal spherical one, caused by the optical components in the system. The aberrations can be expressed as a function of field of view and the aperture, simplified by the symmetrical properties of the system [66].

There are mainly two ways of representing the wave aberrations: as a Taylor-Expansion with Seidel-coefficients and as Zernike-polynomials. In both ways, the emerging wavefront data is than fitted to the different representations. The primary aberrations can be calculated by paraxial ray trace, for higher order aberrations a finite ray tracing is necessary. Using a Taylor-expansion, the wave aberration up to 4th order can be written as [66]:

$$\begin{aligned} W(\eta,\rho,\phi) = {} & W_{020}\rho^2 + W_{111}\eta\rho^2\cos(\phi) + W_{040}\rho^4 + W_{131}\eta\rho^3\cos(\phi) \\ & + W_{222}\eta^2\rho^2\cos^2(\phi) + W_{220}\eta^2\rho^2 + W_{311}\eta^3\rho^1\cos(\phi) \end{aligned} \tag{1.01}$$

η is hereby the normalised height of the object. Furthermore ρ and ϕ are the (normalised) ray

coordinates in the pupil. The coefficients W of the primary aberrations can be replaced by the Seidel sums S in the following way[67]:

$$W(\eta,\rho,\phi)=\frac{1}{8}S_I\rho^4+\frac{1}{2}S_{II}\eta\rho^3\cos(\phi)+\frac{1}{8}S_{III}\eta^2\rho^2\cos^2(\phi)+\frac{1}{4}(S_{III}+S_{IV})\eta^2\rho^2+\frac{1}{2}S_V\eta^3\rho\cos(\phi) \quad (1.02)$$

The coefficients S are hereby the Seidel sums of the aberrations over all surfaces for the primary aberrations (table 1.1).

Table 1.1 Primary aberrations and corresponding Seidel coefficients

Aberration	Seidel coefficient [length]
spherical aberration	S_I
Coma	S_{II}
astigmatism (half astigmatic difference)	S_{III}
sagittal field	$S_{III}+S_{IV}$
tangential field	$3S_{III}+S_{IV}$
Petzval curvature	S_{IV}
Distortion	S_V

With Zernike-polynomials the wave aberrations of a chosen field can be written as [68]:

$$W(\rho,\phi)=\sum_n\sum_{m=-n}^{n}a_{mn}Z_n^m(\rho,\phi) \quad (1.03)$$

The Zernike polynomials are orthogonal function systems over the unit circle, which directly relates to the primary aberration types, shown in table 1.2 and figure 1.1.

Table 1.2 Zernike terms and corresponding interpretation

Zernike polynomial	interpretation	
$\mathbf{Z_1=1}$	piston	lower order properties
$\mathbf{Z_2=\rho\cos(\phi)}$	tilt in x	
$\mathbf{Z_3=\rho\sin(\phi)}$	tilt in y	
$\mathbf{Z_4=2\rho^2-1}$	defocus /field curvature	
$\mathbf{Z_5=\rho^2\cos(2\phi)}$	astigmatism in 0°	primary aberrations
$\mathbf{Z_6=\rho^2\sin(2\phi)}$	astigmatism in 45 °	
$\mathbf{Z_7=(3\rho^3-2\rho)\cos(\phi)}$	coma in x	
$\mathbf{Z_8=(3\rho^3-2\rho)r\sin(\phi)}$	coma in y	
$\mathbf{Z_9=6\rho^4-6\rho^2+1}$	primary spherical aberration + defocus + piston	

The main goal in designing an optical system is to minimise the aberrations as good as possible to achieve a good performance within the desired specifications. For this, the specifications, including all optical parameters, packaging constraints, performance goals and environmental requirements are the starting point of every design.

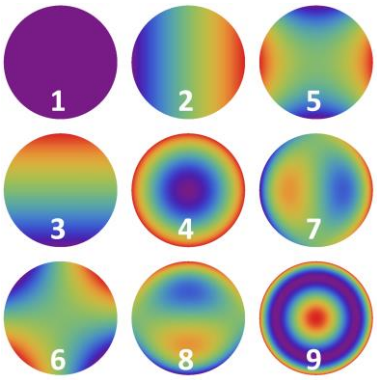

Figure 1.1 Primary aberrations represented by Zernike polynomials.

With the knowledge about the desired final performance, it is necessary to select a sufficient starting system. This can be either an already existing system with slightly different parameters, like an existing patent or a completely new setup with simpler starting configuration (e.g. reduced number and simpler shape of surfaces). In a next step, the variables and constraints of the systems have to be set. At the very beginning of the system development, depending on the experience, the design starts with only a few variables. The number is usually increased within the design process to gain more degrees of freedom for the system. Nevertheless, a high number of variables can be problematic in complex systems. Therefore the choice of variables needs to be done with care. After the system and constraints are set a performance error function, also called merit function, has to be established. The merit function is defined as the sum of the weighted (w_i) squared difference of the target values ($f_{tar,i}$) and the objective function components $f_i(\vec{x})$ [67]:

$$M(\vec{x}) = \sum_{i=1}^{m} w_i [f_{tar,i} - f_i(\vec{x})]^2 \tag{1.04}$$

The target for the merit function $M(\vec{x})$ is usually zero.

In practice, most often local optimisation algorithms like damped least square-based methods (DLS) are used in commercial software, due to a good and robust convergence. The damping term γ is hereby involved to avoid divergence of the change vector $\vec{f}$ and to control the size of the improvement steps.

The DLS can then be described by the change of the parameter vector as:

$$\Delta\vec{x} = -(J^T \cdot J + \gamma \cdot I)^{-1} \cdot J^T \cdot \vec{f}\ , \tag{1.05}$$

where J is the Jacobian-matrix of the derivatives of each operand vs each variable and I is

the identity matrix. In case of CODE V [69] and OSLO [70] the user has access to the damping factor and increment, in Zemax/OpticStudio [71] this is set automatically.
Additionally, other local algorithms like orthogonal descent (Zemax) or rough optimisation (CODE V) and different versions of global optimisers can be found in the different tools.
The target values have to be established according to the performance goal and quality criteria of the system. Typically, the root-mean-square (RMS) of the spot or wavefront are used as image quality criteria. Moreover, the modulation transfer function (MTF), as the ratio of the modulation in the image to the modulation in the object as a function of the spatial frequency, the encircled energy and in case of afocal systems the angular radius of the spot can be selected [66].
After the optimisation the performance needs to be evaluated according to the chosen criteria and the variables and constraints adjusted. Usually several of these iterations are necessary to achieve a good result. If the system configuration does not offer sufficient degrees of freedom, it is sometimes necessary to change or modify elements and materials, may even change the complete starting system and repeat the optimisation.
Is the final performance within the specification, the system is ready for the manufacturing and adjustment preparations. Hereby the design is analysed for its sensitivity regarding manufacturing errors and miss-adjustments. The so-called tolerancing is the final, but nevertheless an important step in designing a system. Hereby the system performance is evaluated for the miss-alignment of components and manufacturing errors of the surfaces in a realistic range. It shows the feasibility of the system within the required specifications.

1.2 Freeform systems: definition and benefit

When we speak of freeform systems, strictly, we talk about systems with surfaces without symmetry at all. Nevertheless, with the break of rotational symmetry, many of what we know about optical design is not valid anymore, or only in a very limited way. Therefore, a freeform is often defined as a surface without rotational symmetry, which can be for example a plane-symmetric or double-plane-symmetric surface, but also an off-axis used sub-aperture of an asphere.
The additional degrees of freedom of a freeform surface compared to a spherical or conical/ aspherical enables the potential for improving the image quality like F/number (F/#) and increasing the field of view. Moreover, the higher complexity of the surface can reduce the

volume and so help in the packaging, illustrated in figure 1.2. This can be beneficial in case of obscuration free mirror systems, which are non-symmetric, due to application needs (e.g head-mounted displays, head-up displays, spectrometers …)

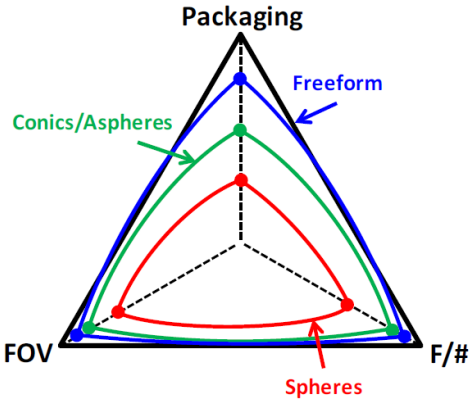

Figure 1.2 Illustration of the improving capabilities by a freeform for the image quality (F/#), field of view (FOV) and the volume of the system (packaging) [72]

1.3 Typical freeform systems

A typical application in design for freeforms are reflective surfaces for astronomical systems, like the plane-symmetric three mirror anastigmat (TMA) [73-74]. The idea is to avoid central obscuration by using the mirrors under finite incident and achieve a high resolution, with a relatively small system size. Other reflective applications are head-up-displays [75] and grating spectrometers [76]. One of the few completely symmetry-free systems is the so-called Yolo-reflector, a special kind of Schiefspiegler with two mirrors, each tilted in x and y independently, designed by A.S. Leonard [77].

A well-known application for refractive systems using freeforms are eyeglasses for varifocals. Another application are anamorphic systems [78], which generate a different magnification in x and y and therefore need independent correction. Alvarez plates and similar compensator concepts use freeforms for the correction of specific aberrations [79]. For inspection, the so-called Scheimpflug systems are used. Due to the tilted object plane, the systems have variant magnification in imaging and suffers from non-rotationally symmetric aberrations [80].

In recent years virtual reality and augmented reality applications came into the focus of development. Often used here are catadioptric head-mounted display (HMD), which combine refractive and reflective freeform surfaces to obtain large FOVs and high performance, in numerous design forms [81-82].

1.4 Design process

The design process of an optical system generally starts with the choice of a sufficient initial system. In case of a freeform system the complexity of possible system geometries is much larger than for rotational symmetric systems. Additionally the number of existing designs for starting systems is quite small. Nevertheless a good starting system is essential for a successful optimization and final result. Optimal is to find a starting system with enough degrees of freedom to achieve a superior result, but not more than necessary to avoid unwanted complexity of the surfaces and system, which impedes the optimization.

The classical thin lens and paraxial approaches works for symmetry-free systems only limited. Therefore, other approaches are necessary, like the conical-confocal method [22] for wide-field off-axis refractive imaging systems, evaluation of third-order aberration for reflective systems by Korsch [23] or general systems by Araki [37] and a pre-optimization method based on the thin-component-theory by Li and Cen for zoom-systems [24]. These methods generate rotational symmetric starting surfaces, which gives no indication of where to put the freeform and how many are needed for correction, specifically since the approaches are often limited to a certain number of surfaces.

A very direct method is the simultaneous multiple surface method (SMS) [25]. Here rays for specific fields are mapped with specific image points using a freeform, defined by a point cloud, where each point corresponds to one pair of object and image point. The number of surfaces and coupled field and image point is limited to a very small number by the approach. The resulting point cloud needs to be fitted to a freeform in the aftermath to achieve the starting system. Nie and Duerr [83] extended this approach to the “direct design method” for more fields.

A very different approach is the Gaussian bracket-method combined with the Nodal aberration theory [26]. Here the aberrations of the rotational symmetric system are derived analytically by the paraxial fast ray trace and extended to the paraxial environment based on nodal-aberration theory (NAT). This method is limited by the complexity of the calculation (non-linear equations) for a higher number of field points and surfaces, on the other hand, the starting values and boundary conditions for the system of equations are essential for finding a good minimum. Nevertheless, the huge advantage is that it can be used for refractive [27] and reflective systems.

Table 1.3 Overview initial systems concepts (+: incorporated)

concept	Initial system rot. sym.	initial system freeform	position of freeform	number of freeforms	Systems
conic-confocal		+			off-axis reflective imaging systems
Korsch 3rd order aberration	+				reflective systems
thin-component-theory	+				zoom lens systems
3D-SMS		+	+	+	arbitrary
direct design method		+	+	+	arbitrary
Gaussian bracket-method	+		+	+	arbitrary

The decision for a sufficient mathematical description of the freeform surface is influenced by several criteria. The remaining symmetry of the system is one very essential one, for example in case of plane- or double-plane symmetric systems another aspect is the outer boundary of the light footprint. For more circular shaped footprints, polar descriptions seem to be more feasible, on the other hand for more rectangular footprints, Cartesian descriptions with an adapted normalisation for the circumscribed rectangle make more sense.

Many different descriptions for freeform surfaces are proposed in the literature. These descriptions can be divided into local and global descriptions.

Locally defined surface representations like splines, specifically non-uniform rational basis-spline (NURBS) [49], wavelets [50] or radial basis functions (RBF) [51], are well known from describing real surfaces or illumination profiles but are also used for imaging applications. It is possible to describe local deviations with high accuracy since the parameters have local support, but generally, a very high number of parameters depending on the sampling is needed. This is a huge drawback for calculation and optimisation. Therefore, these kinds of descriptions are only of limited availability in commercial software and usually used for data import.

More preferred in design are polynomial expressions [52-60], normally as an addition to a basic shape, which can be a sphere or a circular symmetric conic section, a double-plane-symmetric toric or a biconic surface. The few parameters here describe the major part of the surface sag, but need an additional description for higher order correction, which is performed by the polynomial expression. In chapter 2 a comprehensive overview of the general approach and properties is given. Moreover, a selection of descriptions is introduced. Unfortunately, although many descriptions are proposed only limited experience in the usage

is given so far.

The optimisation for freeform systems is due to the lack of symmetry much more challenging than for rotationally symmetric systems. First of all, many of the existing definitions in optical design like pupil, focal length, optical axis, paraxility, principal planes and others are basing on circular symmetric conditions. Therefore, these definitions need to be generalised, which is not always easy. Moreover, the merit function becomes much more complex due to the dramatically larger number of degrees of freedom for the surfaces as well as the larger number of sampling points, e.g. for the fields and pupil, due to the loss of the symmetry. This can lead to multiple minima of the merit function, from which not all solutions are practically useful. Therefore, the systems need potentially more restrictions and limitations.

For optimisation mostly the well-known DLS algorithms are used. Other local algorithms like orthogonal descent (Zemax) or rough optimisation (CODE V) and different versions of global optimiser seem not sufficient for freeform systems, due to long calculation time and complexity. In 2013 CODE V released the so-called STEP optimisation as an optional extension of their DLS algorithm [69]. An early investigation indicates that the new algorithm is faster and better in result than the conventional DLS [64]. Nevertheless, regarding optimisation algorithms and freeform systems, the community is still learning since there was no further work done on this topic so far.

1.5 Performance evaluation

In case of a freeform system, the classical Seidel approach [84] is no longer valid since it is based on rotational symmetry. Nevertheless, evaluating the performance of an optical system is crucial for understanding the system structure and determine necessary structural changes. Compared to rotational symmetric systems, the interaction between different components is much more complicated, specifically in mirror systems with large incident angles and the aberrations are now depending on the full 2D field of view.

To incorporate this new complexity it is helpful to develop a surface resolved representation and distinguish between intrinsic –caused by the actual surface- and induced – caused by previous surfaces- contributions [85] to the total wavefront error in the aberration theory (figure 1.3). After evaluation, additional information about the correction, specifically the shape of the surfaces and the sensitivity can be gained.

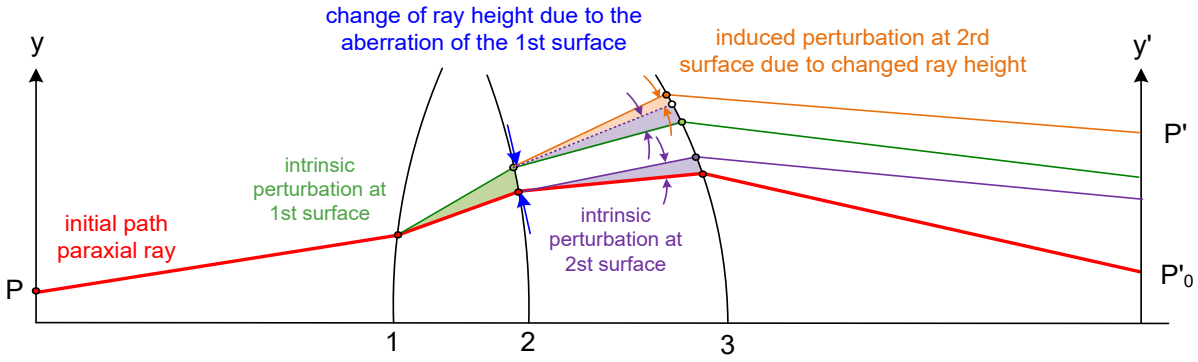

Figure 1.3 schematic scheme intrinsic –caused by the actual surface- and induced – caused by previous surfaces- contributions of aberrations [86]

There are several approaches for describing aberrations, but only a few of them incorporates this concept.

In 1980 Shack and Thompson[28] introduced the nodal-aberration theory, which was later further developed by Thompson [29] and most recently by Fuerschbach [30] to include 6th order aberrations and non-rotational symmetric surfaces. Sasian published 2010 another approach, were he combines the initial concept of Shack, Seidel and Hoffmann. His theory involves similar to the NAT 6th order contributions but distinguishes between intrinsic and induced parts for each surface. Another analytical concept is the generalised Aldis theorem by Brewer [31], which involves all orders of wave aberrations, but only locally for one single ray and spherical surface and the extended generalised Aldis theorem by Liu [87] for freeforms and 3D. Furthermore, it is not incorporating field dependence in comparison to the previous ones. There are also numerical approaches like Welford's [32] extension of the idea by Hopkins [33]. Here the aberrations for all orders can be determined with the help if the optical path difference (OPD), but only for one ray. A very recently published concept by Oleszko [34] combines this OPD-idea with the intrinsic and induced contributions for each surface of Sasian [35]. A quite different approach is the calculation of surface contribution in phase space by Herkommer [36]. Another theoretical concept is the extension of the ray propagation matrix to 4x4 by Araki [37]. Table 1.4 shows an overview of the different approaches.

1.6 Realisation aspects

A very important often underestimated aspect of the optical design is the tolerancing. Specifically in case of freeform surfaces, this is not trivial. Since there isn't much experience, neither in design nor manufacturing, it is quite difficult to estimate realistic values for the tolerancing.

With the power spectral density (PSD) – a Fourier transform of the surface topography for a range of spatial frequencies, which contains just the power, but not the phase information- of a freeform surface (shown in figure 1.4) can be divided roughly into 3 parts: low frequency, represents the typical figure errors, which result in a loss of resolution. The mid-frequency range is a result of the diamond turning process, often by regular structures, which can lead to ghost images. Moreover, the high-frequency part, which are mostly statistical errors.

Table 1.4 Approaches for describing aberrations (+: incorporated)

approaches	order (wave aberration)	analytical/ numerical	non-centred	freeforms	field dependence	single ray	decomposition in intrinsic and induced
4th order (Seidel)	4	analytical			+		
4th order (Araki)	4		+	+ (4th order)	+	+	
6th order (Sasian)	6		+	+ (6th order)	+		+
Nodal-Aberration Theory (Shack/Thompson)	6		+		+		
Nodal-Aberration Theory (Thompson/Fuerschbach)	6		+	+	+		
generalised Aldis theorem(Brewer)	all					+	
extended generalised Aldis theorem (Liu)	all		+	+		+	
Wavefront (Hopkins/Welford)	all	numerical	+	+		+	
Wavefront, Zernike decomposition with multiple rays (Oleszko)	all		+	+			+
Phase-space approach (Herkommer)	all		+	+		+	

Tolerancing figure errors is a procedure often with using additional Zernike Fringe terms and simulate certain patterns. Alternatively, in recent past, Forbes suggested using the coefficients of his Q-polynomials [59] for tolerancing. The benefit compared to Zernike is, that the Qs are gradient-orthogonal and therefore represent only a very narrow frequency band. The coefficients are hereby directly related to the slopes of the surface and small changes of the coefficients are directly related to a change of the PSD. Tolerancing mid-frequency errors is not as simple. There are approaches using the Q-polynomials also for this range [88], but with up to several hundred thousand terms needed to describe mid-frequency errors, the number of parameters is too high. Another approach of describing such errors is to use a combination of Radial basis functions for local errors and a special radial and azimuthal depending representation for the ring (or spiral) shaped deviations [89]. With this description it is

possible to describe the mid-frequency errors with only a few hundred parameters and to also tolerance with certain patterns of sinusoidal perturbations with specific intervals and amplitudes, to see the impact on the system performance.

However, the way to describe the different errors are one point, but the criteria another one. Due to the lack of experience, there isn't a standardised procedure. Possible options are RMS or peak-to-valley (PV) values, slope values in specific surfaces subapertures or limitations or accepted thresholds of the PSD, to name only some.

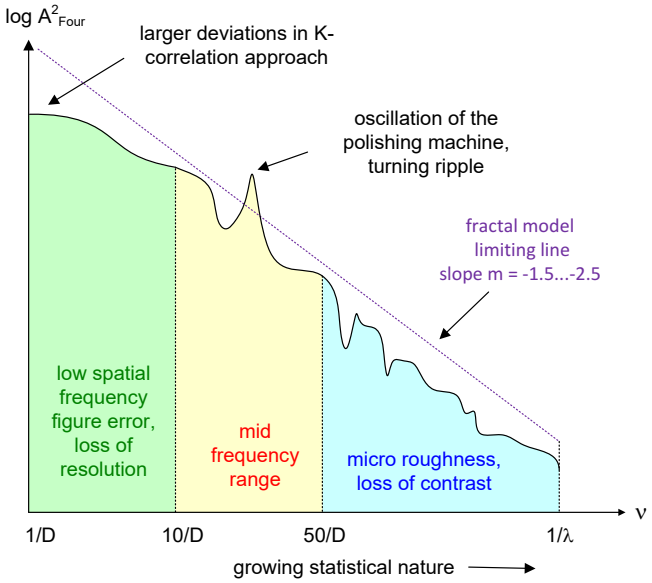

Figure 1.4 Power spectral density curve of a typical freeform surface [90]

With the tolerancing, the main work on the design is normally finished on the designer's part and data is transferred to the mechanical design and manufacturing. In a later step the designer is also involved in the adjustment and simulation of the system. In case of freeform, this workflow is not simple since the system geometry is quite complex. Specifically, the surface description is a problem [91], since most computer-aided design software (CAD) for mechanical design work with splines, which are rarely used for design, as discussed before. The mechanical design prepares the mounting and potential reference marks of the surfaces, which means the surface diameter needs to be enlarged, so the mechanical parts are not obstructing with the ray path and the reference marks are positioned near to the region of interest with sufficient accuracy (no high slopes). Additionally, the coordinate system is transformed, if necessary, to reduce the non-rotational symmetric part of the surface. Depending on the machine, material and process the maximum deviation from the rotational symmetry, azimuthal gradients and azimuthal accelerations are limited [40], which needs to

be incorporated in the optical and mechanical design.

After manufacturing, it is necessary to evaluate the surface compared to the original design with a re-import of the real surface into the system. Hereby it is necessary to describe the measured surface mathematically. Normally the designed surface is subtracted from the measured one and the deviation is given as a point cloud or Zernike fit. As shown in figure 1.4 and introduced before a sufficient description for the mid-frequency part and a fit with lower order polynomial descriptions is possible to describe this real surface quite accurate for a re-import into the design [89] to analyse the impact of the deviations on the system performance. Alternatively a polynomial set with very high orders can be used [88]. The resulting accuracy is a bit lower and the number of terms is up to several hundred thousand, which can be problematic for data processing in the re-import.

1.7 Consequences for the choice of a good surface description

As presented the surface description plays an important role throughout the design process of a freeform system.

The choice is mainly influenced by the following aspects of the design:

- an efficient and robust calculation of the entire process chain,
- a fast calculation of intersection points and local slopes in the ray trace
- a significant description of usual surfaces with only a few characteristic parameters,
- easy access to aberrations,
- a fast convergence in optimisation with superior results.

Moreover, for the entire process:

- a simple and robust import and export, as well as a conversion of data,
- direct relation to tolerancing,
- a simple fit of measured data,
- a simple extension of the region of interest to a larger area for fixing the mounting (no high gradient at the edges) is desirable

With polynomial descriptions, it is possible to achieve these goals. In the following chapter, a deeper introduction to polynomial representations for freeform surfaces is given. Furthermore, two new polynomial sets are introduced, who were specifically developed to incorporate these requirements (chapter 3) and an evaluation of these new sets compared with the most important classical representations is presented (chapter 4).

Chapter 2 Freeform surface representations

As emphasised in the previous section globally defined polynomial descriptions can fulfil the requirements on a freeform surface representation in a much better way than locally defined ones. Specifically, when it comes to an easy and robust calculation and fast convergence with a low number of terms, polynomial descriptions are the preferred choice. The most common description is the Monomial series [52], a simple Taylor-expansion, which is often used for data transfer. Furthermore, the classical Zernike polynomials [53], well-known for describing wavefront errors and aberrations are widely implemented in the existing commercial software.

In recent years many suggestions for polynomial freeform descriptions were made, e.g. the two-dimensional product of either Chebyshev polynomials 1st kind by Liu [54] - and later implemented into Zemax [92] - or Legendre polynomials by Nicolic [55] or Ye [93]. Also, different polynomial sets, using Zernikes as a basis where presented. One approach by Ochse is based on Zernike differences [56]. Others have proposed orthogonal polynomial sets for various aperture shapes like for a square aperture by Muslimov [57] or as "Legendre 2D" by Bray [58], for elliptical apertures by Díaz [94] or hexagonal apertures by Mahajan [95]

Specifically, for freeform surfaces developed are the Q-polynomials by Forbes [59], an approach based on the widely used Q_{bfs}, or also called "mild asphere" –aspheric description [4]. Here the focus was to develop a description, which is beneficial for design and manufacturing with introducing a "best-fit"-basic shape and a projection-factor, with the gradient-orthogonal polynomial set. This approach also influenced other developments like the Q-Legendre [60], a gradient-orthogonal set basing on a two-dimensional product of Legendre polynomials.

Table 2.1 gives an overview of the main properties of the most important approaches.

For this work in total six existing descriptions were selected to be investigated more in detail. These descriptions were chosen because they are already available in commercial software and therefore broadly in use like Monomials, classical Zernikes and 2D Chebyshev 1st kind. Moreover, to investigate the impact of different weightings over the aperture, the 2D Chebyshev 2nd kind and Legendre were added to the selection. As the last description, the Q-polynomials are part of the investigation. The chosen representations differ in various

aspects: the domain of definition, orthogonality or weighting function. For a better understanding, the general approach of these descriptions is explained (section 2.1) and insight into the structure of a polynomial set, in general, is given (section 2.2). In the final 2.3 of this chapter a detailed overview of the selected descriptions is presented.

Table 2.1 Overview of possible polynomial freeform surface descriptions

description	Orthogonality	Basic symmetry	Boundary
off-axis asphere	-	polar	circle
Monomials [52]	-	Cartesian	arbitrary
Chebyshev 2D 1st [54] **Chebyshev 2D 2nd** **Legendre [55]**	spatial	Cartesian	unit square
Zernike [53]	spatial	polar	unit circle
elliptical Zernike [91]	spatial	polar	unit ellipse
square Zernike [57]	spatial	polar	unit square
"Legendre 2D" [58]	spatial	polar	unit square
Q-Legendre [60]	gradient	polar	unit square
Zernike differences [56]	gradient	polar	unit circle
Q-Polynomials [59]	gradient	polar	unit circle

2.1 General approach of polynomial based descriptions

A simple way to describe a freeform surface is a modular decomposition into two major parts: The so-called basic shape, e.g. sphere, conic or biconic incorporates mainly the quadratic contributions around the axis and are fixing the parabasal behaviour of the surface. This part is complemented by a higher order term, which describes additional deformations and is responsible for the aberration correction. The second term is typically much smaller in amplitude of the Δz-contribution than the basic shape and contains the freeform contributions, see figure 2.1 for illustration.

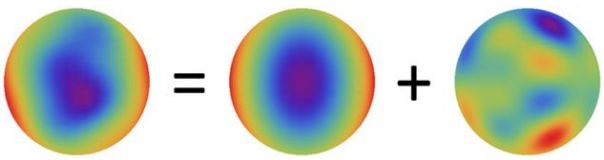

Figure 2.1 Decomposition of sag of a freeform surface (left) into the basic shape (middle) and higher order deformations (right)

The deformation terms can generally be described as a sum over a polynomial expansion set $F_i(\bar{x},\bar{y})$ and the corresponding set of coefficients a_i with a prefactor. The prefactor is defined as the boundary function $B(\bar{x},\bar{y})$ and an inverted projection factor $P(x,y)$. The function $B(\bar{x},\bar{y})$ controls the values of the deformation terms on the boundary line and centre of the surface. The prefactor allows in particular for steep surfaces to orient the additional sag correction along the local normal of the surface and not simply along the z-axis.
This decomposition is formally expressed with normalised coordinates for Cartesian–defined description as

$$z(x,y)=z_{basic}+\frac{B(\bar{x},\bar{y})}{P(x,y)}\sum_j^J a_j F_j(\bar{x},\bar{y}) \quad , \tag{2.1}$$

With normalized coordinates $\bar{x}=x/x_{max}$ and $\bar{y}=y/y_{max}$ for better comparability and numerical conditioning. Using the relations

$$\bar{x}=\bar{r}\cos(\varphi),\ \bar{y}=\bar{r}\sin(\varphi) \text{ and } \bar{r}=r/r_{max}, \tag{2.2}$$

it can also be written as

$$z(r,\varphi)=z_{basic}+\frac{B(\bar{r},\varphi)}{P(\bar{r},\varphi)}\sum_j^J a_j F_j(\bar{r},\varphi) \tag{2.3}$$

for polar defined descriptions.

Basic shape

The basic shape contains the major part of the 2nd order contribution of the freeform surface and is the dominating part in the neighbourhood of the z-axis. The simplest option is a sphere, with only one degree of freedom (radius of curvature R or curvature $c=1/R$):

$$z_{basic}^{(sphere)}(r)=\frac{cr^2}{1+[1-c^2r^2]^{1/2}}. \tag{2.4}$$

In case of the Q-polynomials of Forbes [4] the sphere is modified to a so-called "best-fit-sphere". Here the basic shape is defined as a sphere by the centre of the surface and the circular boundary of the aspheric surface

$$z_{basic}^{(bestfitsphere)}(r)=\frac{c_{bfs}r^2}{1+[1-c_{bfs}{}^2r^2]^{1/2}} \tag{2.5}$$

The freeform deviation has hereby no contribution to the centre but does not necessarily coincide with the boundary of the aspheric surface (figure 2.2). Later this concept was further developed for a "best-fit-conic" [96].

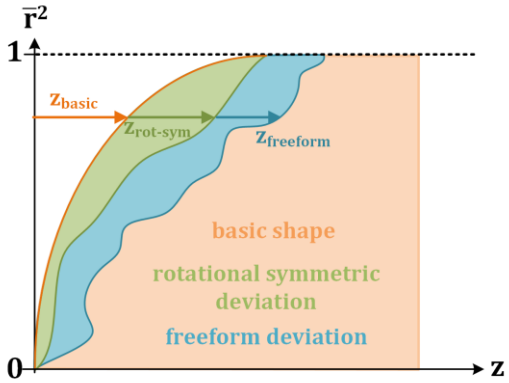

Figure 2.2 Concept of "best fit" basic shape, with no contribution of the rotational symmetric and freeform deviation in the centre ($\bar{r}^2 = 0$) and by the rotational symmetric deviation at the boundary ($\bar{r}^2 = 1$) of the freeform surface

Most descriptions are used with a circular symmetric conic section

$$z_{basic}^{(conic)}(r) = \frac{cr^2}{1+[1-(1+\kappa)c^2r^2]^{1/2}} \tag{2.6}$$

C describes the curvature of the conic section in the vertex point, κ is the conical constant of the surface. In particular in the case of mirror systems, one of the real problems is the occurrence of a large astigmatism for larger incidence angles of the axis ray. This can be considered in the second order approximation by a non-spherical basic shape function and corresponding large terms in the deviation expansion can be avoided. This is an advantage for the design and the convergence of the correction part of the freeform surface, from the viewpoint of manufacturing, where the non-circular contribution plays a major role. For a toric basic shape, in special cases, astigmatism and spherical aberration can be corrected. This is, in particular, an advantage if mirror systems are considered with large incidence angles of the axis ray

$$z_{basic}^{(biconic)}(x,y) = \frac{c_x x^2 + c_y y^2}{1+[1-(1+\kappa_x)c_x{}^2x^2-(1+\kappa_y)c_y{}^2y^2]^{1/2}} \,. \tag{2.7}$$

Boundary function

As already mentioned, the boundary function has the task to define or restrict the values of the additional deformation terms on the boundary of the surface. This is not a necessary condition, but in many practical cases, the behaviour at the edge is then quite better controlled. In reality, the footprint of light on the surface is mostly not perfectly matching the ideal geometrical boundary. An additional overflow is needed for the mechanical design, reference marks and the mountings. Furthermore, a clearly defined boundary value simplifies

the task to relate the surface to the necessary marks and fiducials to locate and orient the surface inside the system. Extrapolating the polynomial expansions beyond the optically-used diameter is an underestimated problem in practice. For simplicity, the boundary curve is selected by simple geometrical shapes. If there is a restriction of the deformation terms, it is usually either in the centre of the surface, at the outer boundary or both. Table 2.2 gives some examples of boundary functions for square ($B(\bar{x},\bar{y})$) and circular ($B(\bar{r})$) domains, as used later in section 2.3 and 3.2.

Table 2.2 Typical boundary functions $B(\bar{x},\bar{y})$ or $B(\bar{r})$ in freeform surface descriptions

Boundary function		
1	uniform, no special constraints (unit circle/ square)	
$(1-\bar{r}^2)\bar{r}^2$	centre and boundary forced to be zero (unit circle)	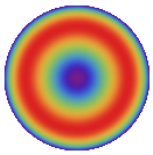
$(\bar{x}^2+\bar{y}^2)$	center forced to be zero (unit square)	

Projection factor

The projection factor $P(x,y)$ has the task to define the direction of the additional correction of the deviation term onto the basic shape. Therefore it couples both terms. Usually, the intention is to have a small correction contribution of higher orders. When the freeform surface is strongly bent and the slope of the surface against the z-axis is large, the projection of a small change in surface profile onto the axis direction generates a large difference. This is not comfortable and therefore a second opportunity measures the deviation along the local surface normal vector of the basic shape surface. This is also directly related to the necessary material removal and therefore grinding time. These two geometries are depicted in figure 2.3. The same consideration is already well known in case of aspheres [4]. If this additional prefactor is included in the representation of the surface, as it is seen in equation 2.1, the expression is no longer a polynomial. In particular, this has the consequence that an exact conversion between different representations is no longer possible and any conversion should consider the desired accuracy and the necessary number of terms.

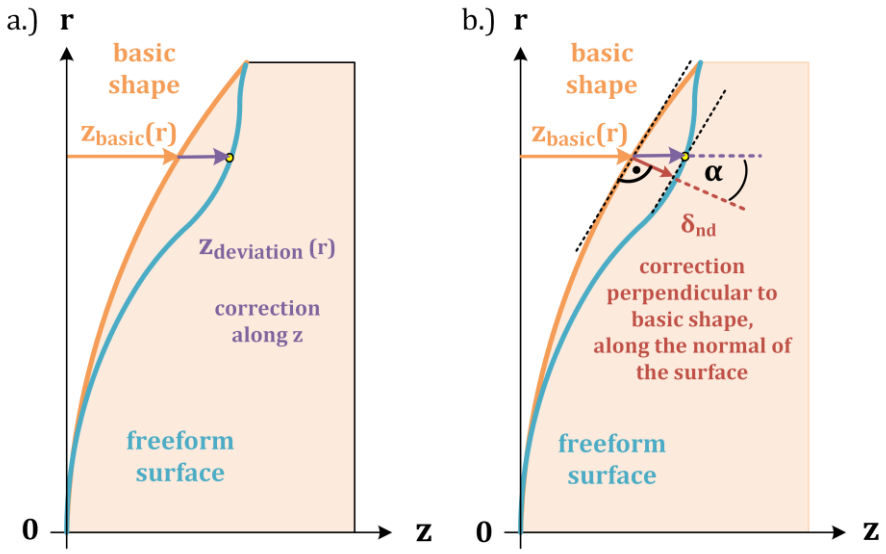

Figure 2.3 Direction of the correction term: a.) without projection: parallel to the z-axis, b.) with projection: perpendicular to the local basic shape orientation (δ_{nd}- normal departure)

For surface descriptions with a projection factor of one, the deformation is independent of the basic shape parameters.

If α is the angle between the local normal and the z-axis, the projection factor is given by cos (α). It is now a question of the selected basic shape to formulate the corresponding projection functions in Cartesian coordinates. The general expression is given by equation 2.8, and the formulas for a sphere and a circular symmetric conic are given in equation 2.9 and 2.10 respectively

$$P(x,y)=\cos(\alpha)^{-1} = \left[1+\left(\frac{d(z(x,y)_{basic})}{dx}\right)^2+\left(\frac{d(z(x,y)_{basic})}{dy}\right)^2\right]^{-1/2}, \tag{2.8}$$

$$P^{(sphere)}(x,y)=[1-c^2(x^2+y^2)]^{1/2}, \tag{2.9}$$

$$P^{(conic)}(x,y)=\left[\frac{1-c^2(x^2+y^2)(1+\kappa)}{1-c^2\,\kappa(x^2+y^2)}\right]^{1/2}. \tag{2.10}$$

2.2 Structure of polynomial set

Development

According to the discussion in the introduction, there are several aspects, possibilities and criteria to select and generate a system of functions for the deformation correction term. Mathematically, the geometry of the supported area, the weighting function, the selected orthogonality as well as the choice of the initial shapes as a starting point of the set are of importance. Since experience shows that an orthogonal set of function is quite an advantage [97], the algorithm for generating the series of functions is after the selection of the criteria above the most crucial step. The classical Gram-Schmidt method is usually applied to guarantee the orthogonality of functions with a different index. For the detailed algorithm, the reader is referred to corresponding textbooks [98]. A special question is the selection of the basis functions f^m and f^n, which define the functional shape of the polynomial set. A second point that should be noticed is the special case of slope orthogonality. In this case in the classical method, the calculation of the scalar product between two functions f^m and f^n must be replaced by

$$< f^m, f^n > = \iint_A w(\bar{x},\bar{y}) \cdot \nabla[B(\bar{x},\bar{y})\, f^m(\bar{x},\bar{y})] \cdot \nabla[B(\bar{x},\bar{y})\, f^n(\bar{x},\bar{y})]\, d\bar{x}\, d\bar{y}. \tag{2.11}$$

Here $w(\bar{x},\bar{y})$ is the weighting function, and the integration is performed over the domain. This leads to

$$\iint_D w(\bar{x},\bar{y}) \cdot \nabla[B(\bar{x},\bar{y})\, f^m(\bar{x},\bar{y})] \cdot \nabla[B(\bar{x},\bar{y})\, f^n(\bar{x},\bar{y})]\, d\bar{x}\, d\bar{y} = \begin{cases} C_m & \text{for m=n} \\ 0 & \text{otherwise} \end{cases}, \tag{2.12}$$

With C_m being a constant of a given m. In case of an orthonormal set $C_m = 1$ for all m.

Sorting

By definition, the functional systems have two ordering indices, describing their radial and azimuthal order or variation in x and y respectively. Very often a two-dimensional matrix scheme is cumbersome and therefore a one-dimensional vectorial scheme is preferred and easier from the viewpoint of the handling. If this mapping of the indices is done, a definition of the rule of conversion is necessary. From the optical point of view, it is most beneficial if with increasing index value the corresponding order or spatial frequency of the function is growing. In this case, the decision of fixing the maximum index make sense and fixes the needed largest order of correction. There are different approaches for such a scheme. One is

to sort the terms by radial orders and within one order by azimuthal orders, as it is used for Zernike polynomials in standard convention [65, 99].

Another often preferred possibility is to sort the Zernike by the aberration order of the terms. This is for example realised in the Zernike Fringe or often called "University of Arizona" approach [71, 100]. The aberrational order corresponds hereby to the sum of the polar and azimuthal order of the individual terms. The terms are starting with a piston (1st term) and 2nd order tilt in x and y (2nd and 3rd term) and are then sorted by aberrational order (with the cosine term first): defocus (4th term), primary astigmatism (5th and 6th term), coma (7th and 8th term) and spherical aberration (9th term) and so on. For the first eight terms of the Fringe sorting are hereby identical to the sorting by radial orders. If the series is truncated at square numbers for Zernikes in Fringe convention (e.g. 1, 4, 9, 16...) exactly a full higher order is included in the description. A similar sorting can be done for the Q-polynomials (here: at 2, 7, 14,). For Zernike and Q-polynomials with 9, respectively 7 terms, the primary aberrations of 4th order wave aberration are covered, with 16 (14) terms the 6th order is included and so on. Unfortunately, this rule is not easy to follow in case of Cartesian polynomial sets. As the aberrations are represented in the polar description with higher orders, it is not possible to represent them by a single term in the Cartesian description, except for astigmatism in 45°. Nevertheless with equation 2.2, it can be seen, that for example in case of the Monomials the series can be sorted similar for the first terms, starting with piston (1st term), 2nd order tilt in x and y (2nd and 3rd term), 4th order quadratic term in x (4th term), astigmatism (5th term), quadratic term in y (6th term) and so on. Hereby the quadratic terms (4th and 6th) can be combined for the other astigmatism term, or defocus. Moreover, the four 6th order terms can be interpreted individually as a combination of trefoil (0° or 30°) and coma (x or y) with different weightings. For higher orders, the polynomial terms can be either interpreted as a combination of several aberrations (6th, 10th, 14th, … order) or as a part of an individual aberration, which needs no be combined with certain terms to be interpreted as the complete aberration (4th, 8th, 12th… order). A similar ordering, here for Chebyshev 1st kind, was shown in the literature [101] for describing surface forms and figure irregularities.

Table 2.3 is showing the first 15 terms of Monomials sorted in this way, with the corresponding interpretation and order.

A similar pattern can be seen for other Cartesian description like Chebyshev 1st and 2nd kind, as well as Legendre polynomials. For these descriptions, a full order of aberrations is included

if the series is truncated at triangular numbers (e.g. 1, 3, 6, 10…). This means the number of terms corresponding to each order is smaller for Cartesian descriptions than for polar ones. As it was stated before, the (wave) aberration order is equivalent to the sum of radial and azimuthal order for polar descriptions, it can be seen that for Cartesian descriptions the (wave) aberration order can be described mathematically by two times the sum of order of x and y, due to the link via equation 2.2.

This sorting by aberration order gives the opportunity to compare polar and Cartesian descriptions although they are different. In the following chapters, this classification is generally named the polynomial order of each description. Moreover, the sorting, interpretation and polynomial order of the first terms for some existing description are given in the next section.

2.3 Descriptions of existing polynomial representations

In this section, the explicit mathematical terms, as well as the sorting and properties, are summarised for the most important sets of polynomials. The descriptions can be divided into Cartesian and polar defined descriptions. For all of the following descriptions, the coordinates of the polynomial set are normalised to the maximal dimensions.

Monomials

Monomials, as mentioned in the introduction, are a simple Taylor-expansion in x and y with no orthogonality at all [98]. The description can be expressed in Cartesian coordinates as follows:

$$z(x,y)=z_{basic}(x,y)+\sum_{m,n}^{M,N} a_{mn}\bar{x}^m\bar{y}^n \quad \text{with } m,n = 0, 1\ldots M,N. \tag{2.10}$$

Moreover, it can be expressed in polar coordinates with the relation (2.2) as:

$$z(x,y)=z_{basic}(x,y)+\sum_{m,n}^{M,N} a_{mn}\bar{r}^{m+n}\cos^m(\varphi)\sin^n(\varphi) \quad \text{with } m,n = 0, 1\ldots M,N. \tag{2.11}$$

With a simple transformation, the double-indices (m,n) can be transformed into a single-index j, which sorts the polynomials, similar to the Zernike Fringe, by aberrational order (see for more information appendix A). The first terms with the one single index sorting can be seen in figure 2.4 and table 2.3.

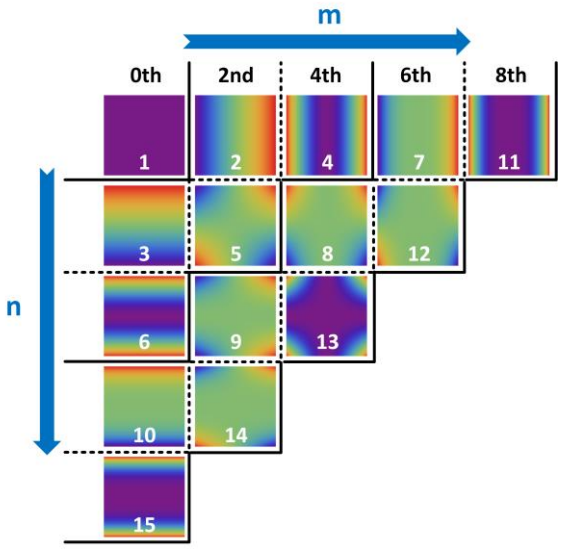

Figure 2.4 First terms in x and y for Monomials.

Table 2.3 First terms of Monomials with the corresponding interpretation and polynomial order

J	m	n	term	interpretation	polynomial order
1	0	0	1		0^{th}
2	1	0	x		2^{nd}
3	0	1	y		
4	2	0	x^2	with j=6: astigmatism 0° or defocus	4^{th}
5	1	1	xy	astigmatism 45°	
6	0	2	y^2	with j=4: astigmatism 0° or defocus	
7	3	0	x^3	each term corresponds to trefoil (either 0° or 30 °) and coma (x or y)	6^{th}
8	2	1	x^2y		
9	1	2	xy^2		
10	0	3	y^3		
11	4	0	x^4	combination of terms corresponds to spherical aberration, four sheet (0° and 22,5°) and secondary astigmatism	8^{th}
12	3	1	x^3y		
13	2	2	x^2y^2		
14	1	3	xy^3		
15	0	4	y^4		

Chebyshev 2D

The Chebyshev 2D polynomials are Cartesian products of the one-dimensional Chebyshev polynomials. The resulting set is spatial-orthogonal on a unit square [98]. There are various kinds, which are differing in weighting over the aperture. Here the 1st and 2nd kind are further discussed. The 1st kind Chebyshev 2D can be expressed as

$$z(x,y)=z_{basic}(x,y)+\sum_{m,n}^{M,N} a_{mn}\,T_m(\bar{x})\,T_n(\bar{y}) \quad \text{with } m,n = 0,\,1\ldots M,N \tag{2.14}$$

The one-dimensional terms $T_m(\bar{x})$, respectively $T_n(\bar{x})$ are orthogonal polynomials with respect to the weighting function $(1-x^2)^{-1/2}$:

$$\int_{-1}^{1} \frac{T_m(x)\,T_{m'}(x)}{\sqrt{(1-x^2)}}\,dx = \begin{cases} \frac{1}{2}\pi\,\delta_{mm'} & \text{for } m\neq 0,\, m'\neq 0 \\ \pi & \text{for } m=m'=0 \end{cases} \tag{2.15}$$

with the Kronecker delta $\delta_{mm'}$ and a strong weighting of the outer edge $x=\pm 1$.

The polynomial terms can be built by recurrence with the initial terms and the recurrence relation for the one-dimensional functions:

$$\begin{aligned} T_0(x) &= 1 \\ T_1(x) &= x \\ T_{m+1}(x) &= 2xT_m(x)-T_{m-1}(x) \end{aligned} \tag{2.16}$$

Alternatively, they can be calculated explicitly with:

$$T_m(x)=m\sum_{k=0}^{\lfloor m/2\rfloor}(-1)^k\frac{(m-k-1)!}{(m-2k)!k!}2^{m-2k}x^{m-2k} \tag{2.17}$$

The first terms of the Chebyshev 1st kind can be seen in figure 2.5. Moreover the mathematical expression with the corresponding ordering is shown in table 2.4.

The 2nd kind Chebyshev polynomials 2D are defined very similar to the 1st kind as

$$z(x,y)=z_{basic}(x,y)+\sum_{m,n}^{M,N} a_{mn}\,U_m(\bar{x})\,U_n(\bar{y}) \quad \text{with } m,n = 0,\,1\ldots M,N. \tag{2.18}$$

The one-dimensional terms $U_m(\bar{x})$, respectively $U_n(\bar{x})$ are orthogonal polynomials with respect to the weighting function $(1-x^2)^{1/2}$, with a strong weighting of the centre $x=0$:

$$\int_{-1}^{1} U_m(x)\,U_{m'}(x)\sqrt{(1-x^2)}\,dx = \begin{cases} 0 & \text{for } m\neq m' \\ \frac{\pi}{2} & \text{for } m=m' \end{cases} \tag{2.19}$$

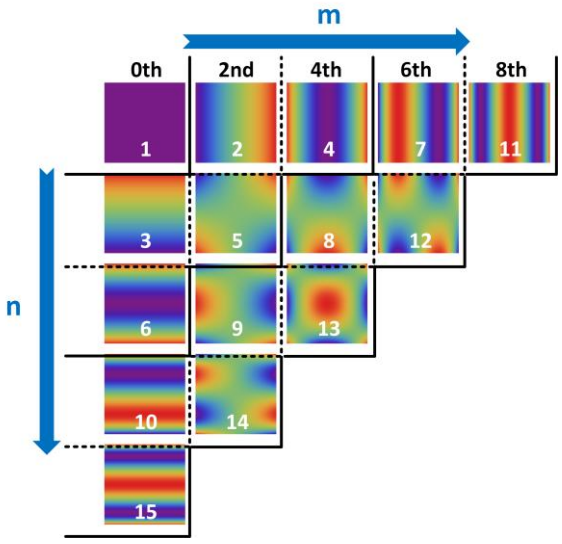

Figure 2.5 First terms of Chebyshev 1st kind with single-index sorting.

As the weighting is different, the initial terms and recurrence relation for the 2nd kind Chebyshev are changed:

$$\begin{aligned} U_0(x) &= 1 \\ U_1(x) &= 2x \\ U_{m+1}(x) &= 2xU_m(x) - U_{m-1}(x) \end{aligned} \quad (2.20)$$

They can also be calculated explicitly with

$$U_m(x) = m\sum_{k=0}^{\lfloor m/2 \rfloor} (-1)^k \frac{(m-k)!}{(m-2k)!k!} 2^{m-2k} x^{m-2k} \quad (2.21)$$

The first terms of the Chebyshev 2nd kind can be seen in figure 2.6. Moreover, the mathematical expression with the corresponding ordering is shown in table 2.4.

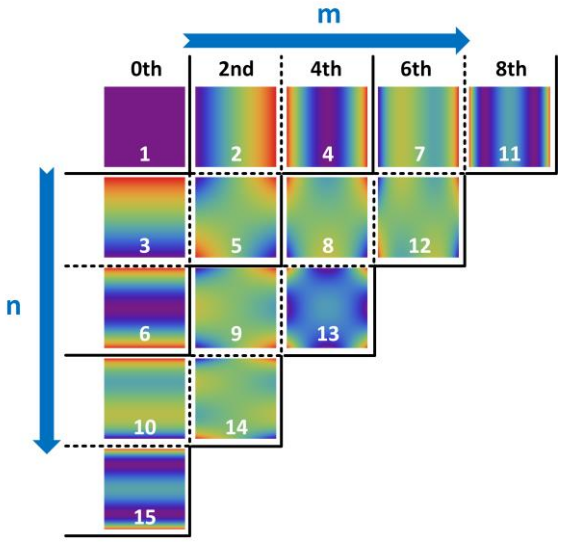

Figure 2.6 First terms in x and y for Chebyshev 2nd kind with single-index j

The double-index (m,n) for both Chebyshev sets can be converted into the single-index j with an algorithm introduced for the Monomials (see Appendix A).

Table 2.4 First terms of Chebyshev 1st and 2nd kind with double- and single-index

j	m	n	1st kind	2nd kind	interpretation	polynomial order
1	0	0	1	1	piston	0th
2	1	0	X	2x	tilt in x	2nd
3	0	1	y	2y	tilt in y	
4	2	0	$2x^2-1$	$4x^2-1$	with j=6: astigmatism 0° or defocus	4th
5	1	1	xy	4xy	astigmatism 45°	
6	0	2	$2y^2-1$	$4y^2-1$	with j=4: astigmatism 0° or defocus	
7	3	0	$4x^3-3$	$8x^3-4$	each term corresponds to trefoil (either 0° or 30 °) and coma (x or y)	6th
8	2	1	$(2x^2-1)y$	$(2x^2-1)y$		
9	1	2	$x(2y^2-1)$	$x(2y^2-1)$		
10	0	3	$4y^3-3x$	$8y^3-4x$		
11	4	0	$8x^4-8x^2+1$	$16x^4-12x^2+1$	combination of terms corresponds to spherical aberration, four sheet (0° and 22,5°) and secondary astigmatism	8th
12	3	1	$(4x^3-3x)y$	$(8x^3-4x)y$		
13	2	2	$(2x^2-1)(2y^2-1)$	$(4x^2-1)(4y^2-1)$		
14	1	3	$x(4y^3-3x)$	$x(8y^3-4x)$		
15	0	4	$8y^4-8y^2+1$	$16y^4-12y^2+1$		

Legendre 2D

The Legendre polynomials are defined similar to the Chebyshev polynomials as Cartesian products of one-dimensional functions [98].

$$z(x,y)=z_{basic}(x,y)+\sum_{m,n}^{M,N} a_{m,n}P_m(\bar{x})P_n(\bar{y}) \text{ with } m,n = 0, 1\ldots M,N. \tag{2.22}$$

The one-dimensional terms $P_m(\bar{x})$, respectively $P_n(\bar{x})$ are orthogonal polynomials with respect to a uniform weighting:

$$\int_{-1}^{1} P_m(x)\,P_{m'}(x)\,dx = \frac{2}{2m+1}\delta_{mm'} \tag{2.23}$$

The initial terms of the one-dimensional functions follow as

$$\begin{aligned} P_0(x) &= 1 \\ P_1(x) &= x \\ (m+1)P_{m+1}(x) &= (2m+1)xP_m(x) - mP_{m-1}(x) \end{aligned} \quad . \tag{2.24}$$

The explicit representation for the Legendre polynomials is

$$P_m(x) = \frac{1}{2^m}\sum_{k=0}^{\lfloor m/2 \rfloor}(-1)^k \frac{(2m-2k)!}{(m-2k)!(m-k)!k!}x^{m-2k} \tag{2.25}$$

In figure 2.7 the first terms for the Legendre 2D can be seen, as well as in table 2.5 with the corresponding interpretation and orders. The single-index sorting follows the same rule as for the Monomials and Chebyshev polynomials (see appendix A)

Table 2.5 First terms of Legendre with double- and single- index

j	p	q	Term	interpretation	polynomial order
1	0	0	1	piston	0th
2	1	0	X	tilt in x	2nd
3	0	1	y	tilt in y	
4	2	0	$\frac{3}{2}x^2 - \frac{1}{2}$	with j=6: astigmatism 0° or defocus	4th
5	1	1	xy	astigmatism 45°	
6	0	2	$\frac{3}{2}y^2 - \frac{1}{2}$	with j=4: astigmatism 0° or defocus	
7	3	0	$\frac{5}{2}x^3 - \frac{3}{2}x$	each term corresponds to trefoil (either 0° or 30 °) and coma (x or y)	6th
8	2	1	$\left(\frac{3}{2}x^2 - \frac{1}{2}\right)y$		
9	1	2	$\left(\frac{3}{2}y^2 - \frac{1}{2}\right)x$		
10	0	3	$\frac{5}{2}x^3 - \frac{3}{2}x$		
11	4	0	$\frac{35}{8}x^4 - \frac{30}{8}x^2 + \frac{3}{8}$	combination of terms corresponds to spherical aberration, four sheet (0° and 22,5°) and secondary astigmatism	8th
12	3	1	$\left(\frac{5}{2}x^3 - \frac{3}{2}x\right)y$		
13	2	2	$\left(\frac{3}{2}y^2 - \frac{1}{2}\right)\left(\frac{3}{2}x^2 - \frac{1}{2}\right)$		
14	1	3	$\left(\frac{5}{2}y^3 - \frac{3}{2}y\right)x$		
15	0	4	$\frac{35}{8}y^4 - \frac{30}{8}y^2 + \frac{3}{8}$		

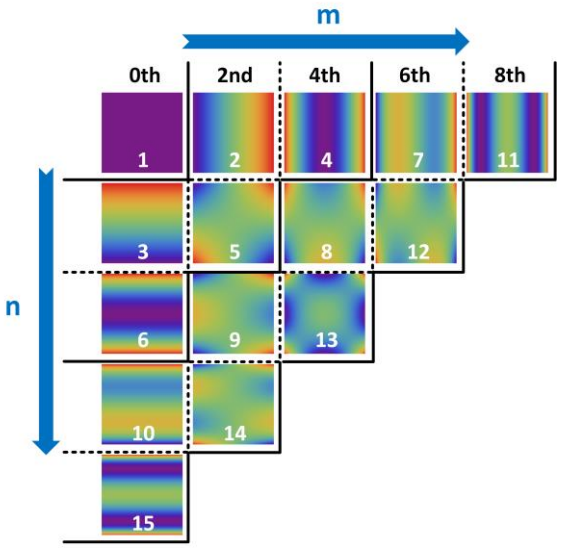

Figure 2.7 First terms in x and y for the Legendre polynomials 2D

Zernike

The Zernike polynomials are a spatial-orthogonal set, which is well known for describing wavefront errors and aberrations. There are different definition conventions for Zernike polynomials.

The most common ones are the standard definition [65, 99] and Fringe or "University of Arizona" convention [71, 100]. The latter one was specifically introduced for describing wavefront errors in optical metrology but is also often used in design.

The terms are defined in polar coordinates and have a constant weighting function [98].

$$z(\bar{r},\varphi)=\sum_{m,n} a_n^m Z_n^m(\bar{r},\varphi) \quad \text{with m,n=0,1...N} \tag{2.26}$$

Both sets defined as a product of a radial part $R_n^m(\bar{r})$ with an azimuthal part $\Phi^m(\varphi)$ and a normalisation factor $N(m,n)$. In the standard convention the Zernike polynomials are normalised to the RMS, whereas the Zernike in Fringe convention are normalised to peak-to-valley:

$$Z_n^m(\bar{r},\varphi)=N(m,n)\, R_n^m(\bar{r})\, \Phi^m(\varphi) \tag{2.27}$$

The normalisation factor for the standard Zernike ism

$$N(m,n)=\sqrt{\frac{2(n+1)}{1+\delta_{m0}}}, \tag{2.28}$$

whereas in Fringe convention it is

$$N(m,n)=1. \tag{2.29}$$

the radial part for both conventions is

$$\begin{aligned} R_n^m(\bar{r}) &= \sum_{k=0}^{\frac{n-|m|}{2}} (-1)^k \binom{n-m}{k} \binom{n-2k}{\frac{n-m}{2}-k} \bar{r}^{n-2k} \\ &= \sum_{k=0}^{\frac{n-|m|}{2}} (-1)^k \frac{(n-k)!}{k!\left(\frac{n-|m|}{2}-k\right)\left(\frac{n+|m|}{2}-k\right)} \bar{r}^{n-2k}, \end{aligned} \tag{2.30}$$

moreover, the azimuthal part

$$\Phi^m(\varphi) = \begin{cases} \sin(m\varphi), & m<0 \\ \cos(m\varphi), & m>0 \\ 1, & m=0 \end{cases}, \tag{2.31}$$

for the angle φ being measured against the x-axis.

The Zernike polynomials can be developed with the orthogonality over a unit circle [98]

$$\int_0^{2\pi}\int_0^1 Z_n^m(r,\varphi)\, Z_{n'}^{m'}(r,\varphi)\, r\, dr\, d\varphi = \frac{\pi(1+\delta_{m,0})}{2(n+1)} \delta_{m,m'}\delta_{n,n'}, \tag{2.32}$$

with $m-n$ and $m'-n'$ are even and $R_n^m(1)=1$.

As mentioned in the previous section, different single indexing schemes for Zernike polynomials exist. The definition of the terms and the sorting is not necessarily connected. Nevertheless, the standard definition is often used with the double-index or a single-index sorting by radial orders, whereas the Fringe definition is mainly used with the single-index sorting by aberration order, as introduced in section 2.2.

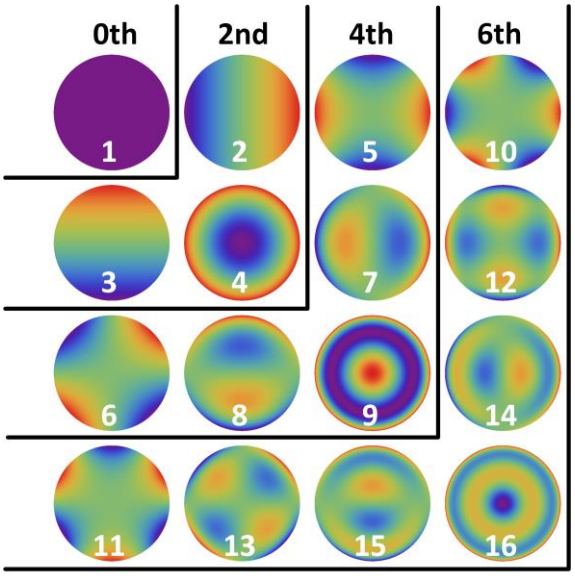

Figure 2.8 First terms of Zernike Fringe polynomials convention with single-index by aberration order

In figure 2.8 the terms are shown graphically. Additionally, in table 2.6 the first 16 terms of the Fringe convention with the interpretation and polynomial order of each are summarised.

Table 2.6 First terms of Zernike in Fringe indexing with interpretation and polynomial order

j	m	n	term	interpretation	polynomial order
1	0	0	1	piston	0^{th}
2	1	1	$r\cos(\varphi)$	tilt in x	2^{nd}
3	-1	1	$r\sin(\varphi)$	tilt in y	
4	0	2	$2r^2-1$	defocus	
5	2	2	$r^2\cos(2\varphi)$	astigmatism 0°	4^{th}
6	-2	2	$r^2\sin(2\varphi)$	astigmatism 45°	
7	1	3	$(3r^3-2r)\cos(\varphi)$	coma x	
8	-1	3	$(3r^3-2r)\sin(\varphi)$	coma y	
9	0	4	$6r^4-6r^2+1$	spherical aberration	
10	3	3	$r^3\cos(3\varphi)$	trefoil 0°	6^{th}
11	-3	3	$r^3\sin(3\varphi)$	trefoil 30°	
12	2	4	$(4r^4-3r^2)\cos(2\varphi)$	secondary astigmatism 0°	
13	-2	4	$(4r^4-3r^2)\sin(2\varphi)$	secondary astigmatism 45°	
14	1	5	$(10r^5-12r^3+3r)\cos(\varphi)$	secondary coma x	
15	-1	5	$(10r^5-12r^3+3r)\sin(\varphi)$	secondary coma y	
16	0	6	$20r^6-30r^4+12r^2-1$	secondary spherical aberration	

Q-polynomials

The Q-polynomials developed by Forbes are based on his “mild-asphere” approach [4, 59]. The gradient-orthogonal description, defined for circular boundaries, incorporates the concept of the “best-fit” basic shape, an individual boundary function for the aspheric terms and freeform terms, as well as the projection factor and a weighting function, which emphasise the centre and the boundary of the domain.

The mild-asphere set (m=0) is restricted at the centre and the outer area by the boundary function to achieve the “best-fit” basic shape where the surface sag is only defined by the basic shape in these two points. The further development of the freeform set (m>0), called Q-polynomials, is only restricted at the centre of the domain. Therefore, the surface sag at the centre of the freeform is still only defined by the basic shape, but the boundary incorporates freeform contributions. The goal of this specific boundary function, the projection factor and

the weighting is the limitation of the slopes, specifically on the boundary, to generate a manufacturing-friendly surface.

The complete surface description is hereby

$$\begin{aligned} z(r,\varphi) &= z_{\text{basic}}^{(\text{bestfitsphere})} + z_{\text{Mild-Asphere}}(\bar{r}) + z_{\text{Q-Polynomials}}(\bar{r},\varphi) \\ &= z_{\text{basic}}^{(\text{bestfitsphere})} + \frac{1}{\sqrt{1-c^2r^2}} \cdot \left[\bar{r}^2 \cdot \left(1-\bar{r}^2\right) \cdot \sum_{n=0} a_n^0 Q_n^0\left(\bar{r}^2\right) \right] \\ &+ \frac{1}{\sqrt{1-c^2r^2}} \cdot \left[\sum_{m=1} (\bar{r})^m \sum_{n=0} \left[a_n^m \cos(m\varphi) + b_n^m \sin(m\varphi) \right] \cdot Q_n^m\left(\bar{r}^2\right) \right] \\ &\text{with } m,\ n\ = 0,\ 1 \ldots M, N \end{aligned} \tag{2.37}$$

The trigonometric functions in (2.37) are automatically orthogonal for different azimuthal orders, shown in (2.33). The radial part with the boundary function follows the orthogonality condition:

$$\int_0^1 \nabla[z^n{}_{\text{Q-Polynomials}}(\bar{r})] \cdot \nabla[z^{n'}{}_{\text{Q-Polynomials}}(\bar{r})] \frac{d\bar{r}}{\sqrt{1-\bar{r}^2}} = \begin{cases} \pi & n = n' \\ 0 & \text{otherwise} \end{cases} \tag{2.38}$$

The Q-polynomials $Q_n^m(\bar{r}^2)$ were specifically designed to be orthogonal in gradient, the mean square gradient of the normal departure from the best-fit basic shape can then be expressed as the sum of the squares of the coefficients in the departure:

$$\left\langle \left| \nabla \delta_{\text{nd}}(\bar{r},\varphi) \right|^2 \right\rangle = \left\langle \left(\frac{\partial \delta_{\text{nd}}}{\partial \bar{r}} \right)^2 + \frac{1}{\bar{r}^2} \left(\frac{\partial \delta_{\text{nd}}}{\partial \varphi} \right)^2 \right\rangle = \sum_{m,n} \left[\left(a_n^m\right)^2 + \left(b_n^m\right)^2 \right] \text{ with } b_n^0 = 0 \tag{2.39}$$

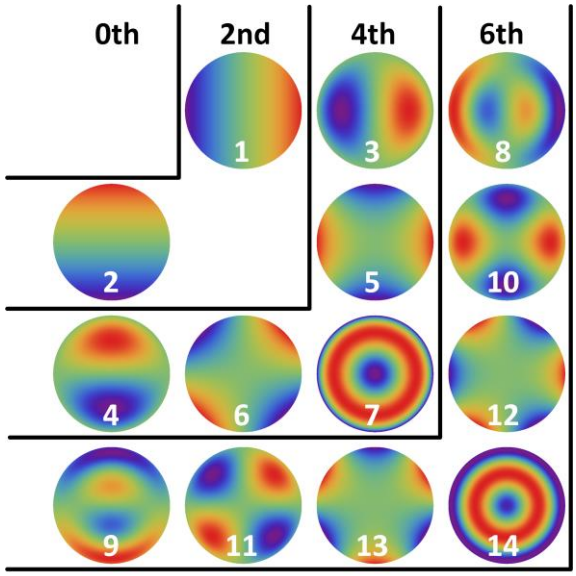

Figure 2.9 First terms of Q-polynomials with boundary function in single-index sorting

The normal departure δ_{nd} (shown Figure 2.2) is hereby given by the deformation terms without the projection factor

$$\delta_{nd}(\bar{r},\varphi) = \bar{r}^2 \cdot \left(1-\bar{r}^2\right) \cdot \sum_{n=0} a_n^0 Q_n^0\left(\bar{r}^2\right) + \bar{r}^2 \cdot \sum_{n,m=0} a_n^m Q_n^m\left(\bar{r}^2\right) \tag{2.40}$$

As discussed in the previous section the Q-polynomials can be sorted like the Zernike polynomials by order of aberration. Since the aspheric-part of the polynomial set (m=0) starts with the 4th order, due to the boundary function, the terms for piston and defocus are missing. Therefore, a full order is completed with quadratic number minus 2 (e.g. 2, 7, 14…).

In figure 2.9 the terms are shown graphically. Additionally, in table 2.7 the first 14 terms of the single index sorting with the interpretation and polynomial order of each are summarised

Table 2.7 First terms of Q-polynomials with boundary function with double- and single-index

j	m	n	coefficient	term	interpretation	polynomial order
1	1	0	a_0^1	$r\cos(\varphi)$	tilt in x	2nd
2	1	0	b_0^1	$r\sin(\varphi)$	tilt in y	
3	2	0	a_0^2	$\frac{1}{\sqrt{2}} r^2 \cos(2\varphi)$	astigmatism 0°	4th
4	2	0	b_0^2	$\frac{1}{\sqrt{2}} r^2 \sin(2\varphi)$	astigmatism 45°	
5	1	1	a_1^1	$\frac{(4r-4r^3)}{\sqrt{14}}\cos(\varphi)$	coma x	
6	1	1	b_1^1	$\frac{(4r-4r^3)}{\sqrt{14}}\sin(\varphi)$	coma y	
7	0	0	a_0^0	$r^2(1-r^2)$	spherical aberration	
8	3	0	a_0^3	$\frac{4}{3\sqrt{6}} r^3 \cos(3\varphi)$	trefoil 0°	6th
9	3	0	b_0^3	$\frac{4}{3\sqrt{6}} r^3 \sin(3\varphi)$	trefoil 30°	
10	2	1	a_1^2	$\frac{(9-8r^2)}{\sqrt{38}} r^2 \cos(2\varphi)$	secondary astigmatism 0°	
11	2	1	b_1^2	$\frac{(9-8r^2)}{\sqrt{38}} r^2 \sin(2\varphi)$	secondary astigmatism 45°	
12	1	2	a_2^1	$\frac{(50-176r^2+112r^4)}{\sqrt{1610}} r\sin(\varphi)$	secondary coma x	
13	1	2	b_2^1	$\frac{(50-176r^2+112r^4)}{\sqrt{1610}} r\cos(\varphi)$	secondary coma y	
14	0	1	a_1^0	$\frac{(13-16r^2)}{\sqrt{19}} r^2(1-r^2)$	secondary spherical aberration	

Chapter 3 Development of freeform descriptions

In the previous chapter, a selection of six of the most promising descriptions for freeform surfaces and the general approach behind were introduced.
It was shown, that with the extension of the basic shape to a biconic, it is possible to correct for primary astigmatism and spherical aberration in some cases. Moreover, it could be seen that the Zernike Fringe and Q-polynomial offer the easy access to the aberrations, whereas the latter ones, also incorporate manufacturing and tolerancing friendly restrictions, as desired for a freeform surfaces description (see section 1.7).
With the development of two polynomial sets – called A-polynomials, these aspects are combined in each of the descriptions in the following way:

- biconic basic shape for better astigmatism correction
- projection-factor for an easier access to tolerancing
- a gradient-orthogonal polynomial set for a faster convergence
- Zernike-polynomials as the basis function for an easier access to the aberrations
- developed on a square domain for better accordance with non-circular shaped domains

The two new sets differ only in their weighting over the aperture and boundary function.
In the first section, the necessary adaption of the projection factor for an extended basic shape is shown. Moreover, in section 3.2 the development of the A-polynomials 1st and 2nd kind is shown and the representations are introduced. The chapter closes with an overview over the most important properties of the previously in chapter 2 presented six descriptions together with the two new descriptions, sorted by Cartesian and polar descriptions and short guideline of conversion between the different description.

3.1 Extension of the basic shape

In section 2.1 the general way of describing a biconic was introduced as (equation 2.7)

$$z_{\text{basic}}^{(\text{biconic})}(x,y)=\frac{c_x x^2+c_y y^2}{1+[1-(1+\kappa_x)c_x{}^2x^2-(1+\kappa_y)c_y{}^2y^2]^{1/2}}\ . \tag{3.1}$$

With the projection factor defined as (equation 2.8):

$$\begin{aligned} P(x,y) &= \cos(\alpha)^{-1} \\ &= \left[1+\left(\frac{d(z(x,y)_{basic})}{dx}\right)^2+\left(\frac{d(z(x,y)_{basic})}{dy}\right)^2\right]^{-1/2}, \end{aligned} \tag{3.2}$$

It follows for the projection factor of a surface with a biconical basic shape:

$$P(x,y)=\frac{1}{\sqrt{\left(1+\frac{c_x x^2\left(\frac{c_x(1+\kappa_x)c_x(1+\kappa_x)(c_x x^2+c_y y^2)}{\sqrt{1-c_x^2(1+\kappa_x)x^2-c_y^2(1+\kappa_y)y^2}}+2\left(\sqrt{1-c_x^2(1+\kappa_x)x^2-c_y^2(1+\kappa_y)y^2}+1\right)\right)^2}{\left(\sqrt{1-c_x^2(1+\kappa_x)x^2-c_y^2(1+\kappa_y)y^2}+1\right)}+\frac{c_y y^2\left(\frac{c_y(1+\kappa_y)c_y(1+\kappa_y)(c_x x^2+c_y y^2)}{\sqrt{1-c_x^2(1+\kappa_x)x^2-c_y^2(1+\kappa_y)y^2}}+2\left(\sqrt{1-c_x^2(1+\kappa_x)x^2-c_y^2(1+\kappa_y)y^2}+1\right)\right)^2}{\left(\sqrt{1-c_x^2(1+\kappa_x)x^2-c_y^2(1+\kappa_y)y^2}+1\right)}\right)}} \tag{3.3}$$

In the following all descriptions using the projection factor and biconic basic shape, like Q- and A-polynomials 1st and 2nd kind are calculated by this scheme.

3.2 A-polynomials

The A-polynomials are a new set, specifically developed for rectangular domains [102]. The surface description is based on the approach by Forbes [4], combining a projection factor and a gradient-orthogonal set for better access to manufacturing and tolerancing. Additionally, the basic shape was extended to a biconic, to include lower order astigmatism. Due to the adjustment to a rectangular domain and a biconic basic shape, a “best-fit-shape” is no longer meaningful.

In general, the A-polynomials are described by:

$$z(x,y)=z_{basic}^{(biconic)}+\frac{B(\bar{x},\bar{y})}{P_{Biconic}(x,y)}\sum_j a_j A_j(\bar{x},\bar{y}) \text{ with } j=0,\ 1\ldots J, \tag{3.4}$$

Previous polynomial sets for rectangular domains, like Monomials or Chebyshev polynomials or the Q-Legendre [60] base on Cartesian products of one-dimensional functions depending on x and y. As discussed earlier, these descriptions have some drawbacks for design. Therefore, the approach of Bray [58] with the Zernike Fringe set was used. The polar description, defined on a unit circle, was hereby converted to a Cartesian grid and the original domain is circumscribed by the definition area of the new set, a unit square. The Zernikes will

be extrapolated to the corners of the unit square.

The two sets of A-polynomials were developed with the following parameter:

For the 1st kind, with no restrictions for the boundary

$$B_{A-1st}(\bar{x},\bar{y}) = 1 \tag{3.5}$$

and a uniform weighting

$$w_{A-1st}(\bar{x},\bar{y}) = 1, \tag{3.6}$$

as well as for the 2nd kind, with restricting the centre with the boundary function

$$B_{A-2nd}(\bar{x},\bar{y}) = (\bar{x}^2 + \bar{y}^2), \tag{3.7}$$

And emphasising the boundary with the weighting function:

$$w_{A-2nd}(\bar{x},\bar{y}) = \frac{1}{\sqrt{[1-\bar{x}^2][1-\bar{y}^2]}}. \tag{3.8}$$

Both polynomial sets were developed with the Gram-Schmidt process and the modified relation to ensure slope orthogonality (see section 2.2 for more details):

$$< f^m, f^n > = \frac{\int_{-1}^{1}\int_{-1}^{1} w(\bar{x},\bar{y}) \cdot \nabla[B(\bar{x},\bar{y})\, f^m(\bar{x},\bar{y})] \cdot \nabla[B(\bar{x},\bar{y})\, f^n(\bar{x},\bar{y})] d\bar{x}\, d\bar{y}}{\int_{-1}^{1}\int_{-1}^{1} w(\bar{x},\bar{y}) d\bar{x}\, d\bar{y}} \tag{3.9}$$

with $\bar{x} = \bar{r}\cos(\varphi)$ and $\bar{y} = \bar{r}\sin(\varphi)$.

The functions f_m and f_n are hereby the basis functions of the Zernike Fringe set in Cartesian coordinates.

For the A-polynomials of the 1st kind equation 3.2 turns into:

$$< f^m_{A-1st}, f^n_{A-1st} > = \int_{-1}^{1}\int_{-1}^{1} \nabla[f^m_{A-1st}(\bar{x},\bar{y})] \cdot \nabla[f^n_{A-1st}(\bar{x},\bar{y})] d\bar{x}\, d\bar{y} \tag{3.10}$$

In contrast, the 2nd kind A-polynomials are developed with:

$$\begin{aligned} &< f^m_{A-2nd}, f^n_{A-2nd} > \\ &= \frac{\int_{-1}^{1}\int_{-1}^{1} \frac{1}{\sqrt{1-\bar{x}^2}\sqrt{1-\bar{y}^2}} \cdot \nabla[(\bar{x}^2+\bar{y}^2)\, f^m_{A-2nd}(\bar{x},\bar{y})] \cdot \nabla[(\bar{x}^2+\bar{y}^2)\, f^n_{A-2nd}(\bar{x},\bar{y})] d\bar{x}\, d\bar{y}}{\int_{-1}^{1}\int_{-1}^{1} \frac{1}{\sqrt{1-\bar{x}^2}\sqrt{1-\bar{y}^2}}) d\bar{x}\, d\bar{y}} \end{aligned} \tag{3.11}$$

.

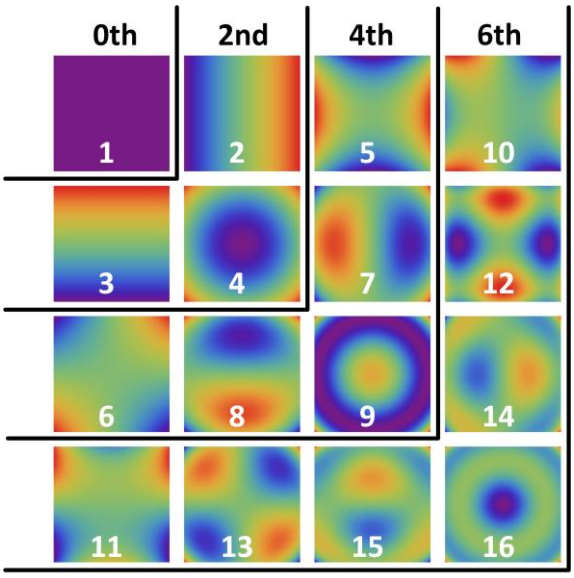

Figure 3.1 First terms of A-polynomials 1st kind

The resulting A-polynomials kept the main structure of the Zernike-Fringe set, as well as the polar character. Moreover, the order and sorting of the A-polynomials 1st kind is equivalent to the Zernike Fringe set, as seen in figure 3.1. The similarities can also be seen in table 3.1, with the first 16 terms of the A-polynomials 1st kind in polar expression. For the first nine terms, the terms are corresponding to the individual aberrations, whereas for the 6th order terms a smaller contribution by a 4th order aberration is added, due to the orthogonalisation process. The single-index of the A-polynomials 1st kind corresponds to the single-index of the Zernike Fringe sorting

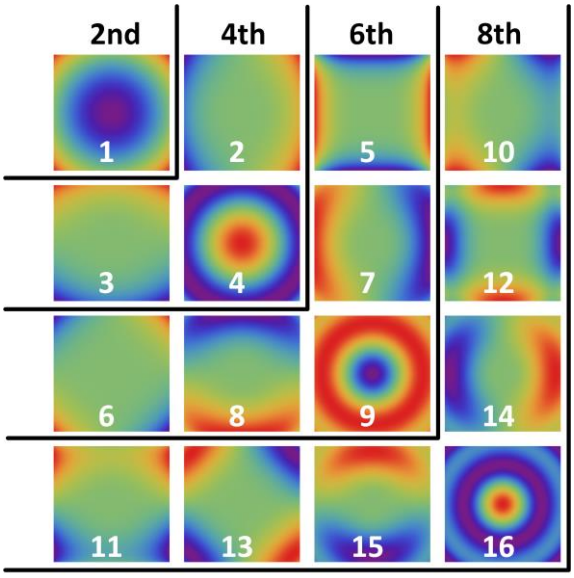

Figure 3.2 First terms of A-polynomials 2nd kind with boundary function

For the A-polynomials 2nd kind the sorting and order of the polynomial set itself is following the structure of the 1st kind, but with the boundary function (equation 3.7), each term is multiplied by $(\bar{x}^2 + \bar{y}^2) = \bar{r}^2$, which results first into a one-order higher contribution (starting with 2nd instead of 0th order) and a different interpretation of terms compared to the A-polynomials 1st kind. Moreover the function system involving the boundary function is not complete anymore. In table 3.2 the first 16 terms for the first eight orders, starting with the 2nd order defocus term, are shown. It can be directly seen, that the two primary astigmatism terms are missing. It is also not present as a lower order contribution for higher order terms. Therefore, an extension of the basic shape was necessary, so the whole primary astigmatism correction can be done by the biconic.

The advantages of initially using Zernikes, like the direct link to the aberrations are still given, specifically for the 1st kind A-polynomials, but now defined on a unit square with the possibility of direct tolerancing. The similarities between the 1st kind A-polynomials and Zernike Fringe can be specifically seen in the centre region of the surface. For the outer boundary, the A 1st kind appear as Zernike stretched into the corner.

Due to the use of a projection factor, the direct conversion of A-polynomials into a polynomial is no longer possible. Nevertheless, in-between the As and Qs a direct conversion can be done. For the other descriptions, an approximation via fitting is necessary.

Table 3.1 First terms of the A-polynomials 1st kind with the corresponding interpretation and polynomial order in polar coordinates

j	Term	interpretation	polynomial order
1	1	piston	0th
2	$\frac{1}{2}\,r\cos(\varphi)$	tilt in x	2nd
3	$\frac{1}{2}\,r\sin(\varphi)$	tilt in y	
4	$\sqrt{\frac{3}{128}}(2r^2-1)$	defocus	
5	$\sqrt{\frac{3}{128}}r^2\cos(2\varphi)$	astigmatism 0°	4th
6	$\sqrt{\frac{3}{32}}r^2\sin(2\varphi)$	astigmatism 45°	
7	$\sqrt{\frac{1}{48}}(3r^2-4)r\cos(\varphi)$	coma x	
8	$\sqrt{\frac{1}{48}}(3r^2-4)r\sin(\varphi)$	coma y	
9	$\frac{\sqrt{651}}{992}(15r^4-28\,r^2+9)$	spherical aberration	
10	$\frac{\sqrt{2}}{32}(5r^3\cos(3\varphi)+(3r^3-4r)\cos(\varphi))$	trefoil 0° + coma x	6th
11	$\frac{\sqrt{2}}{32}(5r^3\sin(3\varphi)-(3r^3-4\,r)\sin(\varphi))$	trefoil 30° + coma y	
12	$\frac{\sqrt{14}}{32}(5r^4\cos(2\varphi)-6r^2\cos(2\varphi))$	secondary astigmatism 0°	
13	$\frac{\sqrt{399}}{304}(5r^4\sin(2\varphi)-8r^2\sin(2\varphi))$	secondary astigmatism 45°	
14	$\frac{\sqrt{1077}}{17232}((315r^5-690r^3+332\,r)\cos(\varphi)+30r^3\cos(3\varphi))$	secondary coma x + trefoil 0°	
15	$\frac{\sqrt{1077}}{17232}((315r^5-690r^3+332r)\sin(\varphi)-30r^3\cos(3\varphi))$	secondary coma y + trefoil 30°	
16	$\frac{\sqrt{2046}}{372992}(4340r^6-12600r^4+10128\,r^2+1949)$	secondary spherical aberration	

Table 3.2 First terms of the A-polynomials 2nd kind including boundary function with the corresponding interpretation and polynomial order in polar coordinates

j	Term	interpretation	polynomial order
1	$\frac{1}{2\sqrt{\pi}} r^2$	defocus	2nd
2	$\frac{2}{5\sqrt{\pi}} r^3 \cos(\varphi)$	coma x	4th
3	$\frac{2}{5\sqrt{\pi}} r^3 \sin(\varphi)$	coma y	
4	$\frac{1}{2\sqrt{3\pi}} r^2(2r^2-5)$	spherical aberration	
5	$\frac{1}{\sqrt{10\pi}} r^4 \cos(2\varphi)$	secondary astigmatism 0°	6th
6	$\frac{1}{5\sqrt{\pi}} r^4 \sin(2\varphi)$	secondary astigmatism 45°	
7	$\frac{8}{5\sqrt{4749\pi}}(25r^5-56r^3)\cos(\varphi)$	secondary coma x	
8	$\frac{8}{5\sqrt{4749\pi}}(25r^5-56r^3)\sin(\varphi)$	secondary coma y	
9	$\frac{\sqrt{105}}{210\sqrt{\pi}}(16r^6-58r^4+61r^2)$	secondary spherical aberration	
10	$\frac{4(1583r^5\cos(3\varphi)+(3415r^5-5750r^3)\cos(\varphi))}{\sqrt{885167693\pi}}$	secondary coma x + secondary trefoil 0°	8th
11	$\frac{4(1583r^5\sin(3\varphi)-(3415r^5-5750r^3)\sin(\varphi))}{\sqrt{885167693\pi}}$	secondary coma y + secondary trefoil 30°	
12	$\frac{\sqrt{790}}{2370\sqrt{\pi}}(80r^6-127r^4)\cos(2\varphi)$	higher order astigmatism 0°	
13	$\frac{(400r^6-929r^4)\sin(2\varphi)}{15\sqrt{4951\pi}}$	higher order astigmatism 45°	
14	$\frac{(26840208r^7-95655952r^5+89595533r^3)\cos(\varphi)}{\sqrt{3277113215902131\pi}} + \frac{55056r^5\cos(3\varphi)}{\sqrt{3277113215902131\pi}}$	higher order coma x + secondary trefoil 0°	
15	$\frac{(26840208r^7-95655952r^5+89595533r^3)\sin(\varphi)}{\sqrt{3277113215902131\pi}} - \frac{55056r^5\sin(3\varphi)}{\sqrt{3277113215902131\pi}}$	higher order coma y + secondary trefoil 30°	
16	$\frac{(560r^8-2544r^6+3822r^4-2139r^4)}{2\sqrt{55195\pi}}$	higher order spherical aberration	

3.3 Overview of surface descriptions

In table 3.3 and 3.4 the most important properties like domain, orthogonality, boundary and weighting function, as well as the first times are compared for each description sorted by the defining grid.

Table 3.3 Cartesian defined freeform surface representations

surface representation	Domain	orthogonality	boundary function	weight function
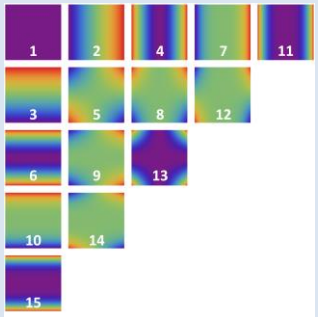	**Monomials**			
	arbitrary	none	none	none
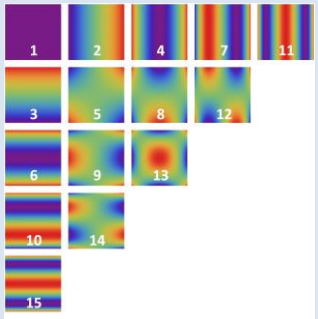	**Chebyshev 1st kind (2D)**			
	unit square	spatial	1	$\frac{1}{\sqrt{[1-\bar{x}^2][1-\bar{y}^2]}}$
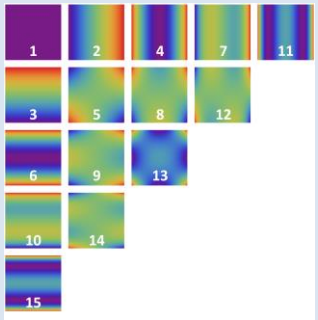	**Chebyshev 2nd kind (2D)**			
	unit square	spatial	1	$\sqrt{[1-\bar{x}^2][1-\bar{y}^2]}$
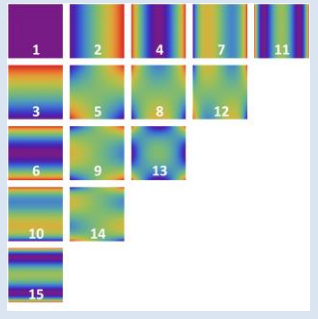	**Legendre 2D**			
	unit square	spatial	1	1

Table 3.4 Polar defined freeform surface representations

surface representation	domain	orthogonality	boundary function	weight function
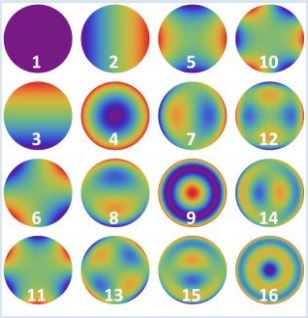	**Zernike Fringe**			
	unit circle	spatial	1	1
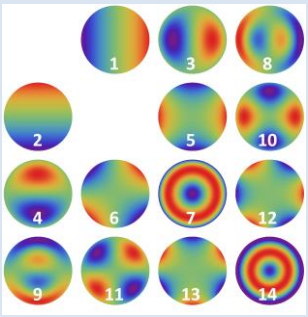	**Q-polynomials**			
	unit circle	gradient	$(1-\bar{r}^2)\,\bar{r}^2$ rot. sym. terms $\bar{r}^2$ freeform terms	$\frac{1}{\bar{r}\sqrt{1-\bar{r}^2}}$
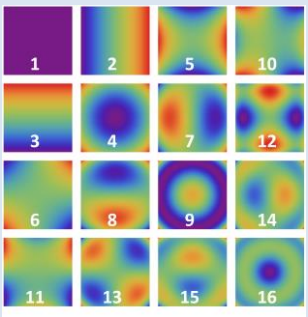	**A-polynomials 1st kind**			
	unit square	gradient	1	1
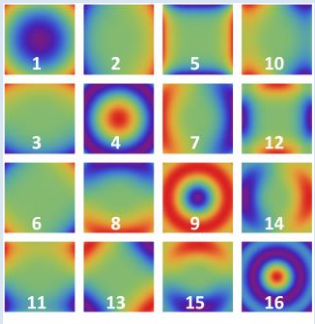	**A-polynomials 2nd kind**			
	unit square	gradient	$(\bar{x}^2+\bar{y}^2)$	$\frac{1}{\sqrt{[1-\bar{x}^2][1-\bar{y}^2]}}$

Conversion between different descriptions

The description introduced in the previous section are except for the Q- and A-polynomials simple polynomial expressions, which allow for direct conversion into each other, as it can be seen in table 3.5. Hereby each term of the representation A will be converted into a sum of terms of description B. For the Q-and A-polynomials the projection factor prevents a direct conversion, only in case of a plane basic shape, which results in a projection factor of 1, the deformation terms of the Q- and A-polynomials are directly convertible with the other descriptions, otherwise an approximation via a fitting procedure is necessary.

Table 3.5 Conversion options for the different descriptions

<table>
<tr><th></th><th>Monomials</th><th>Chebyshev 1st</th><th>Chebyshev 2nd</th><th>Legendre</th><th>Zernike</th><th>Q</th><th>A 1st</th><th>A 2nd</th></tr>
<tr><td>Monomials</td><td colspan="5" rowspan="5">direct conversion</td><td colspan="3" rowspan="5">approximation necessary</td></tr>
<tr><td>Chebyshev 1st</td></tr>
<tr><td>Chebyshev 2nd</td></tr>
<tr><td>Legendre</td></tr>
<tr><td>Zernike</td></tr>
<tr><td>Q</td><td colspan="5" rowspan="3">approximation necessary</td><td colspan="3" rowspan="3">direct conversion</td></tr>
<tr><td>A 1st</td></tr>
<tr><td>A 2nd</td></tr>
</table>

A conversion of a polynomial set with single-index from description A to description B follows hereby the algorithm:

1. Conversion of the single-index convention to the double-index convention for the polynomial terms
2. Multiplication with conversion matrix to Monomials
3. Multiplication with conversion Matrix from Monomials to description B
4. Conversion to the single-index convention of description B

Chapter 4 Evaluation of freeform descriptions

In chapter 2 and 3 some opportunities how freeform surfaces can be described from the mathematical point of view were introduced. Based on these possibilities, the next question of an optical designer would be, how to select the surface type optimal for an efficient optimisation process with a comfortable result. In this chapter, the results of an assessment of the previously introduced description from the design application viewpoint are presented. The issues of the surface representation in the design phase are restricted without considering questions of sensitivity, tolerancing and manufacturing. Therefore, the results are collected in the form of a benchmark, which compares different freeform surface descriptions for optical systems for various applications with different properties. To limit the complexity and make the results easier for interpretation, here only a small number of four sample systems is selected. Due to the complexity of the problem, all examples are restricted to the use of only one freeform surface. The setups are selected to be practical relevant with diverse types of symmetry, including refractive, reflective and catadioptric systems. The benchmark method and systems are presented in section 4.1.

From the viewpoint of practical work and efficiency, there are several criteria for the selection of special surface representation. The surface representation should allow for a fast ray trace, the parametrisation should be flexible with a small number of parameters, and the optimisation of the parameters should be robust and converge quickly with a good result in the design process. Therefore, the evaluation of the benchmark is mainly focusing on the following aspects:

- Impact of the basic shape (section 4.2)
- Convergence over the orders and final performance for the different polynomial types (section 4.3)
- Impact of orthogonality on convergence (section 4.4.)
- Convergence behaviour of other algorithms (section 4.5)

Finally, conclusions for the choice of freeform descriptions are given (section 4.6).

4.1 Benchmark method and systems

The goal of this investigation is to evaluate the criteria for choosing an appropriate representation for a given task with a freeform system. Therefore, each of the chosen representations is used to optimise the benchmark systems over several polynomial orders and the performance is evaluated [103].

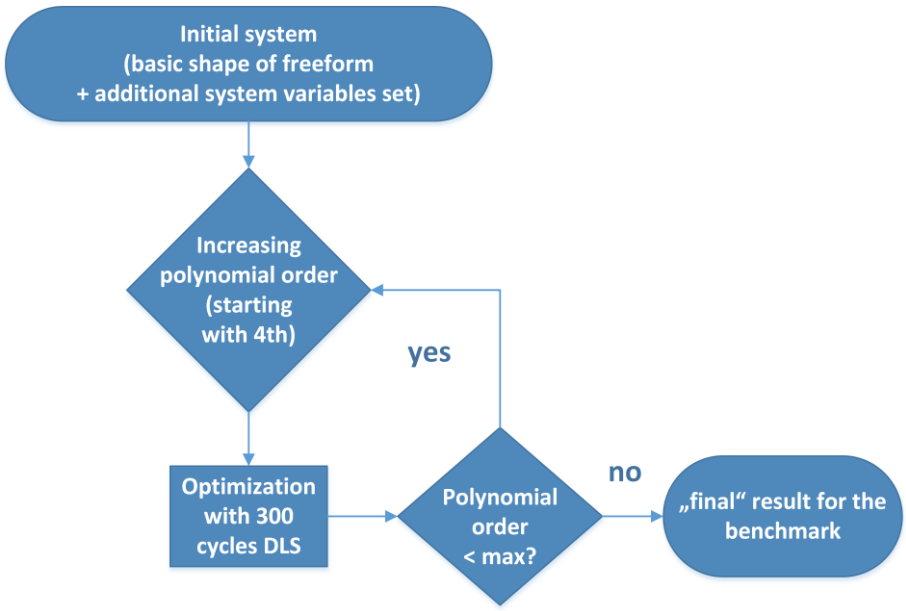

Figure 4.1 Benchmark process

Benchmark method

To investigate the convergence of the polynomial order and specific contribution by each order, the optimisation proceeds stepwise. Starting with the initial system (figure 4.1), setting the basic shape and additional system variables (see table 4.3), the parameter of the deformation terms of the freeform surface were increased order by order (beginning with the 4^{th}) and re-optimized each time with 300 cycles of DLS up to the 14^{th} polynomial order. The used surface parameters are limited to those who contribute to the symmetry of the system. Moreover, the lower order terms, like tilts and offset, as well as defocus, are not used for the correction.

The optimisation algorithm used for the investigation of the impact of the basic shape and convergence in section 4.2 to 4.4 is a local damped least square-provided by Zemax/OpticStudio™. Additionally, in section 4.5 for the comparison of the optimisation algorithms, the equivalent local algorithms of DLS (with/without Step) by CODE V™ and DLS by OSLO™ are used. An overview of the used settings and definitions can be found in table 4.1.

The main criteria for all systems were the default root-mean-square of the spots radius/size for all field points. In CODE V™ this is called transverse ray aberration. The sampling grid was polar with 15 rings and 8 arms. In case of OSLO, the number criteria for the merit function is limited. Therefore, the rings had to be reduced to 14, due to the larger number of defined field points (12). The later evaluated RMS values were calculated with respect to the centroid of the spots.

Table 4.1 Overview over the used settings and the different definition for the optical design software.

	Zemax /OpticStudio	**CODE V**	**OSLO**
local optimisation algorithms	DLS	DLS optional with Step	DLS
merit function criteria	RMS spot radius	transverse ray aberration	RMS spot size
sampling grid	polar 15 rings, 8 arms	polar 15 rings, 8 arms	polar 14 rings, 8 arms

For the benchmark, the descriptions discussed in chapter 2 were chosen, as well as the newly developed A-polynomials 1st and 2nd kind from chapter 3. Table 4.2 shows the investigated descriptions: Cartesian (blue) and Polar (red) with their corresponding orthogonality and definition domain. The descriptions were chosen to evaluate the performance, namely the merit function, as well as the corresponding RMS spot sizes and surface sag contributions by the basic shape, deformation terms and the total surface. They were selected to represent the different properties like orthogonality, domain or defining grid. Moreover, to investigate the influence of a different weighting over the domain, the Chebyshev 1st kind, 2nd kind and Legendre (each in 2D) were chosen for the spatial-orthogonal description defined on a unit square. With the Monomials, they represent the descriptions of Cartesian definition. The Zernike and Q-polynomials, as well as A-polynomials 1st and 2nd kind, are polar defined descriptions, varying in the defining domain and orthogonality.

In literature, mostly only spherical or conical basic shapes are used. For the investigations of the basic shape additionally, biconical basic shapes were evaluated for their benefit in the design. For all further investigations only biconic was used. In case of Q-polynomials, the projection factor for biconic basic shape must be adapted (see section 3.1) to enhance its functionality.

Since our investigations have shown no significant impact of the projection factor on the performance of these systems, this was not addressed here. In case of systems with a stronger

inclination of the rays at the boundary, this aspect might be of importance.

All descriptions used in the benchmark were implemented as a User-defined-surface Dynamic Link Library (DLL).

Table 4.2 Investigated representations

domain / orthogonality	(unit) circle	(unit) square
none	Monomials	
spatial	Zernike Fringe	Chebyshev 2D 1st kind Chebyshev 2D 2nd kind Legendre 2D
gradient	Q-polynomials	A-polynomials 1st kind A-polynomials 2nd kind

Benchmark Systems

For the benchmark, four systems with different symmetry representing typical refractive, reflective and catadioptric applications of freeform surfaces are investigated (figure 4.2):

A symmetry-free Yolo-type two mirror telescope, a plane-symmetric folded three-mirror-anastigmat (TMA), a plane-symmetric head-mounted display (HMD) in a recently suggested folded setup and a double-plane-symmetric anamorphic system with a straight optical axis.

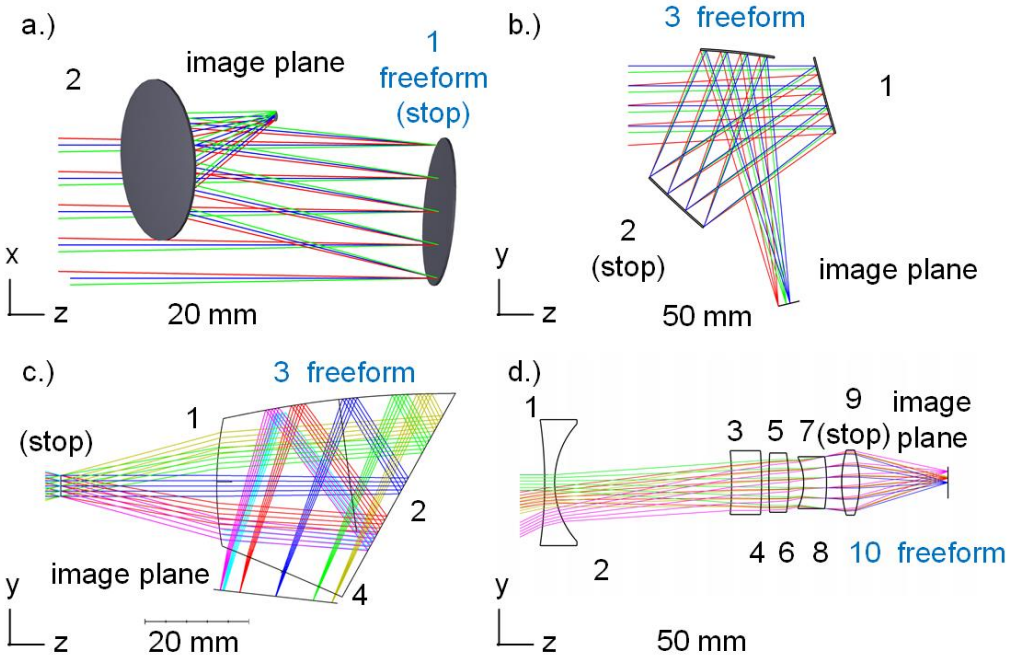

Figure 4.2 Layouts of investigated systems: a.) Yolo-telescope, b.) TMA, c.) HMD, d.) anamorphic system

All systems are imaging setups and should be corrected for an improved resolution by one freeform. Due to simplification and comparability with the original design, the correction of distortion was not considered. For all examples, the effective focal length (EFFL) is kept constant during re-optimisation. For simplification, only one wavelength is considered. The norm radius respectively norm width was adapted to the semi-diameter plus a small offset of 2 mm after each cycle to make sure the domain of the surface description and the optical region of interest are equivalent. The basic data for the initial systems, shown in figure 4.2, are collected in table 4.3.

The Yolo-telescope (figure 4.2a) is based on two tilted mirrors (the first one bending in y and the second one in x, both by 30°), which leads to a symmetry-free system with a small field of view (1.5° x 1.5°) and F-number of 1.9 (table 4.3). The first mirror is hereby the freeform and the second a conic. The footprint on the freeform surface is almost entirely circular with all nine fields. The main criterion for the performance is the averaged resolution over each field (RMS spot). In addition to the surface parameters of the freeform, the radius and conic of the second surface, as well as the final distance and the tilt of the image plane, are used as optimisation variables. The system suffers on axis and in the field mainly from astigmatism in 0° (-6.492, respectively -3.077 to -10.114 λ), larger coma in x (-10.668 λ, respectively -8.852 to -12.389 λ) and smaller coma in y (-4.139, respectively -2.472 to -5.820 λ). Moreover, for the outer field points, there are additional contributions by astigmatism 45° (1.808 to -4.542 λ), as seen in the summary of the wavefront data for the on-axis and outer field points in table 4.3.

The folded TMA is a reflective plane-symmetric system (figure 4.2b). The first and second mirror is spherical and the third one a freeform. With a small F-number of 2.14 and field of view (table 4.3) the separation of the field bundles is very poor, seen on the nearly circular footprint of the freeform for the three fields. The criteria for optimisation are the resolution (RMS spot) with a small contribution by effective focal length, as well as restrictions for the obscuration. The radii of the first two mirrors plus the final distance are additional variables for the optimisation. The system needs to be correct simultaneously for large astigmatism 0° (-209.254, respectively -119.255 λ) and coma y (44.101, respectively 36.202 λ) on axis and in the outer field (see table 4.3). The non-existing contributions by astigmatism 45° and coma in x results from the 0° field in x-direction.

The folded head-mounted-device (figure 4.2c) based on the recently published design by Chen [104] is slightly simplified for the benchmark. The plane-symmetric catadioptric system was modified to have a spherical refractive entrance (1st) and exit (4th) surface and a plane mirror as a second surface. The third surface is freeform, which is used in reflection. The system has a large field of view (50° x 30°), with the field points only defined for the positive x-direction, due to symmetry and a large F-number of 10.89 (table 4.3). The good separation of the field bundles can be seen in the rectangularly shaped footprint of the twelve fields1 on the freeform surface. The optimisation criteria are like the TMA, namely the resolution (RMS spot) with obscuration restrictions. For the optimisation, only the radii of the front and rear surface are additional variables. Moreover, the final distance was not used as a parameter to avoid unphysical solutions during the optimisation. Nevertheless, initial tests have shown, that the fixing of the final distance is of no significant impact on the performance of the different descriptions. For comparability with the original design, distortion was not considered in the merit function. This simplification may distort the final results slightly. The system suffers on-axis only from a small contribution of astigmatism 0° (-1.539 λ), which is for the outer field points of higher value (2.493 to 6.718 λ). Moreover, in the field the wavefront contains large astigmatism in 45 ° (-9.741 to 27.094 λ) and for the positive y field also smaller coma in x and y (2.490 and 2.240 λ).

The anamorphic system (figure 4.2d) is a double-plane-symmetric refractive freeform system based on a patent by Wartmann [105], which is simplified for the benchmark. The first nine surfaces are spherical, except the second and the fourth, which are cylinders. The last surface in front of the image plane is the freeform. The system has a medium field of view and F-number (0° x 3°), only in y-direction. The imperfect separation of the field bundles is again seen on the footprint of the last surface. The optimisation criteria are like the Yolo-telescope, namely the resolution (RMS spot). The radii of the 9 non-freeform-surfaces, as well as the final distance, are additional variables for the optimization. The system mainly needs to be corrected for astigmatism 45° (9.175 λ) and smaller part of spherical aberration (2.975 λ) on axis. For the field, the wavefront contains mainly large astigmatism 0° (-13.713 λ) and small contributions by astigmatism in 45°, coma in x and y (2.248 to -4.529 λ).

Table 4.3 System data of initial benchmark-systems with a spherical basic shape for the freeform surface: Yolo-telescope, three-mirror-anastigmat, head-mounted-display and an anamorphic System [EPD: entrance pupil diameter]

	Yolo-telescope	**Three-mirror-anastigmat**	**Head-mounted display**	**Anamorphic system**
symmetry	-	plane	plane	double-plane
specification: **EPD** **FOV** **field points** **F-number** **wavelength** **stop position**	 21 mm 1.5° x 1.5° 9 1.9 0.55 µm surface 1	 28 mm 0° x 3° 3 2.14 0.66µm surface 2	 4 mm 50° x 30° 12 10.89 0.5775 µm In front of system	 7.49 mm 12° x 25° 5 4.0 0.587 mm surface 9
optimization criteria	RMS spot+ EFFL	RMS spot + EFFL+ restrictions for obscuration		RMS spot + EFFL
surfaces	1: freeform 2: conic	1 & 2: sphere 3: freeform	1 & 4: sphere 2: plane 3: freeform	1, 3, 5 -9: sphere 2 & 4: cylinder 10: freeform
footprint freeform surface	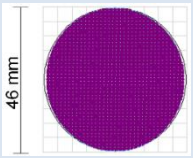	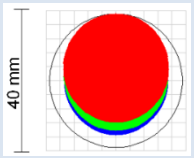	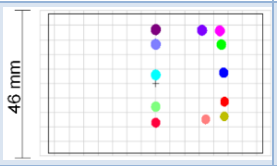	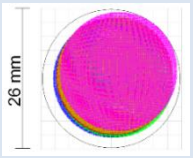
additional variables	radius and conic surface 2, tilt x & y image plane final distance	radii of surface 1 & 2, final distance	radii of surface 1 & 4	radii of surface 1 to 9, final distance
wavefront data of the initial system (spherical basic shape) in [λ]:				
on axis				
Z_5/Z_6	-6.492/0.672	-209.254/0.000	-1.539/0.000	9.175/0.000
Z_7/Z_8	-10.668/-4.139	0.000/44.101	0.000/0.715	0.000/0.000
Z_9	-0.032	1.269	0.001	2.975
field 1				
Z_5/Z_6	-9.009/2.568	-119.255/0.000	2.493/27.094	-13.713/-3.751
Z_7/Z_8	-12.836/-5.760	0.000/36.202	2.490/2.240	-4.529/2.248
Z_9	0.055	0.980	0.163	-1.705
field 2				
Z_5/Z_6	-3.077/1.808	-	6.718/-9.741	-
Z_7/Z_8	-12.389/-2.528	-	1.052/-0.377	-
Z_9	0.075	-	0.037	-
field 3				
Z_5/Z_6	-10.114/-2.509	-	-	-
Z_7/Z_8	-8.852/-5.820	-	-	-
Z_9	-0.108	-	-	-
field 4				
Z_5/Z_6	-4.191/-4.542	-	-	-
Z_7/Z_8	-8.848/-2.472	-	-	-
Z_9	-0.087	-	-	-

4.2 Impact of the basic shape

To evaluate the impact of the chosen basic shape to the performance of the description, for each system and description a spherical, conical and biconical basic shape was used and the performance over the orders was compared. Exemplarily shown here are the final results for each order for Chebyshev 1st kind, as a Cartesian description, Zernike polynomials, as a polar description and the newly developed A-polynomials 1st kind.

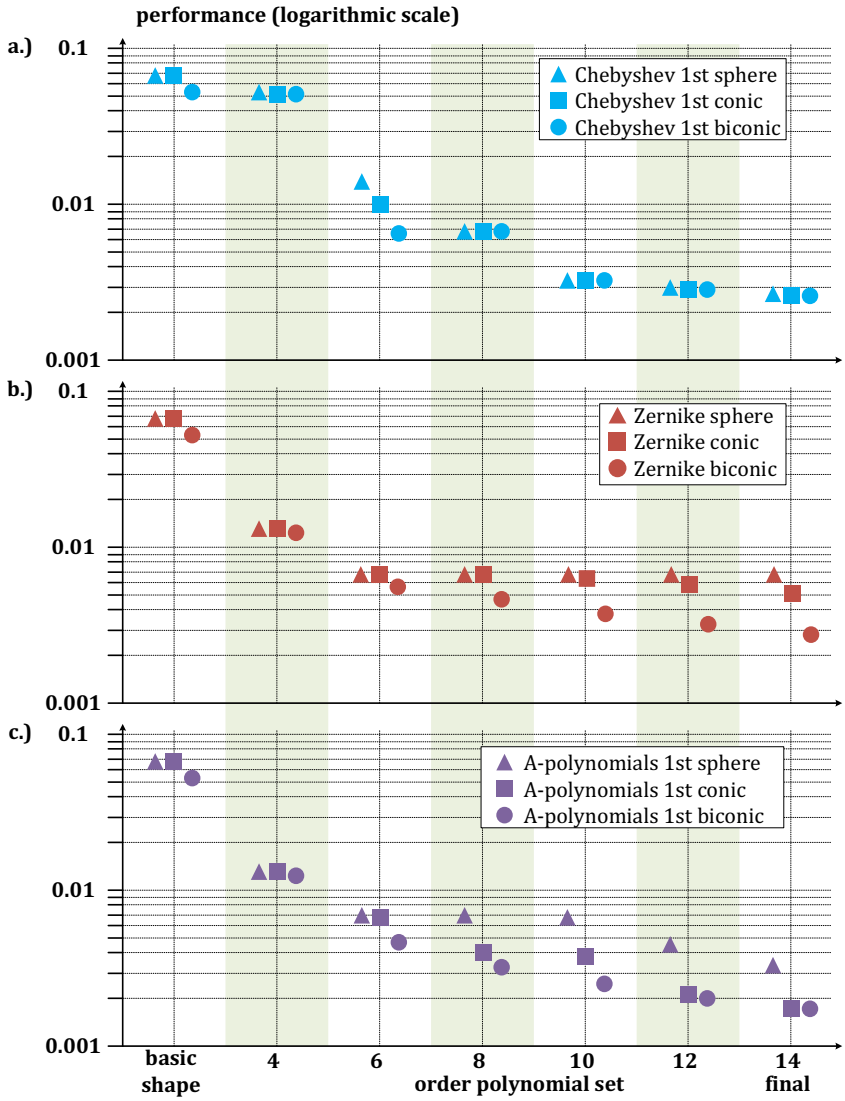

Figure 4.3 Performance for different basic shapes for Yolo-telescope: a.) Chebyshev 1st kind, b.) Zernike polynomials, c.) A-polynomials 1st kind

Yolo-telescope

It can be seen, that the descriptions have different ability to show the effect of the biconic. In case of the Chebyshev 1st kind (figure 4.3a) a variation of the performance can only be identified for the 6th order. For higher orders, the basic shape has no influence on the performance, which means the polynomial terms can completely cover the correction by the biconic in case of a basic shape of less complexity like sphere or conic.

For the Zernike polynomials (figure 4.3b) the impact is different. The conic and spherical basic shape has almost the same performance for all orders, which indicates that the polynomial terms can compensate to a certain extend (except for very high orders) the effect of the conic with respect to a sphere. Nevertheless, the effect of the biconic basic shape compared to the other two cannot be covered by the deformation terms. Therefore, this performance is almost better by a factor of two.

For A-polynomials 1st kind (figure 4.3c) the conical and biconical basic shape have equivalent performance, so the difference in basic shape can be fully compensated by the polynomials. Nevertheless, for spherical basic shape, the polynomial set is not able to cover the effect of the basic shape, which results in two times worse final.

It can be seen, that the final result in case of a sphere and a conic for Zernike, respectively sphere for A-polynomial 1st kind, can be reached already by the biconic shape with up to only 6th, respectively 8th order polynomial terms.

Three-mirror-anastigmat

In contrary to the Yolo –telescope, the Chebyshev 1st kind (figure 4.4a) can only compensate the conic complexity, but not the biconic. The final result here is more than a factor of 2 better than for the other basic shapes. Alternatively, the final result of the spherical and conical basic shape is similar to the performance of a biconic shape after the 6th polynomial order. In case of Zernike (figure 4.4b) and A-polynomials (figure 4.4c), the effect is almost the same. Both descriptions have huge differences for lower orders for a sphere, a conic and a biconic, but with increasing number of degrees of freedom, the results for conic and biconic become comparable. The final results comparing the spherical basic shape are a factor of 5 for Zernike and 2 for A- polynomials better. For either description, the polynomial terms cover the effect of conic and biconic, which result in a final result for spherical basic shape, which is worse than the performance of a simple biconic, and in case of Zernikes even simple conic.

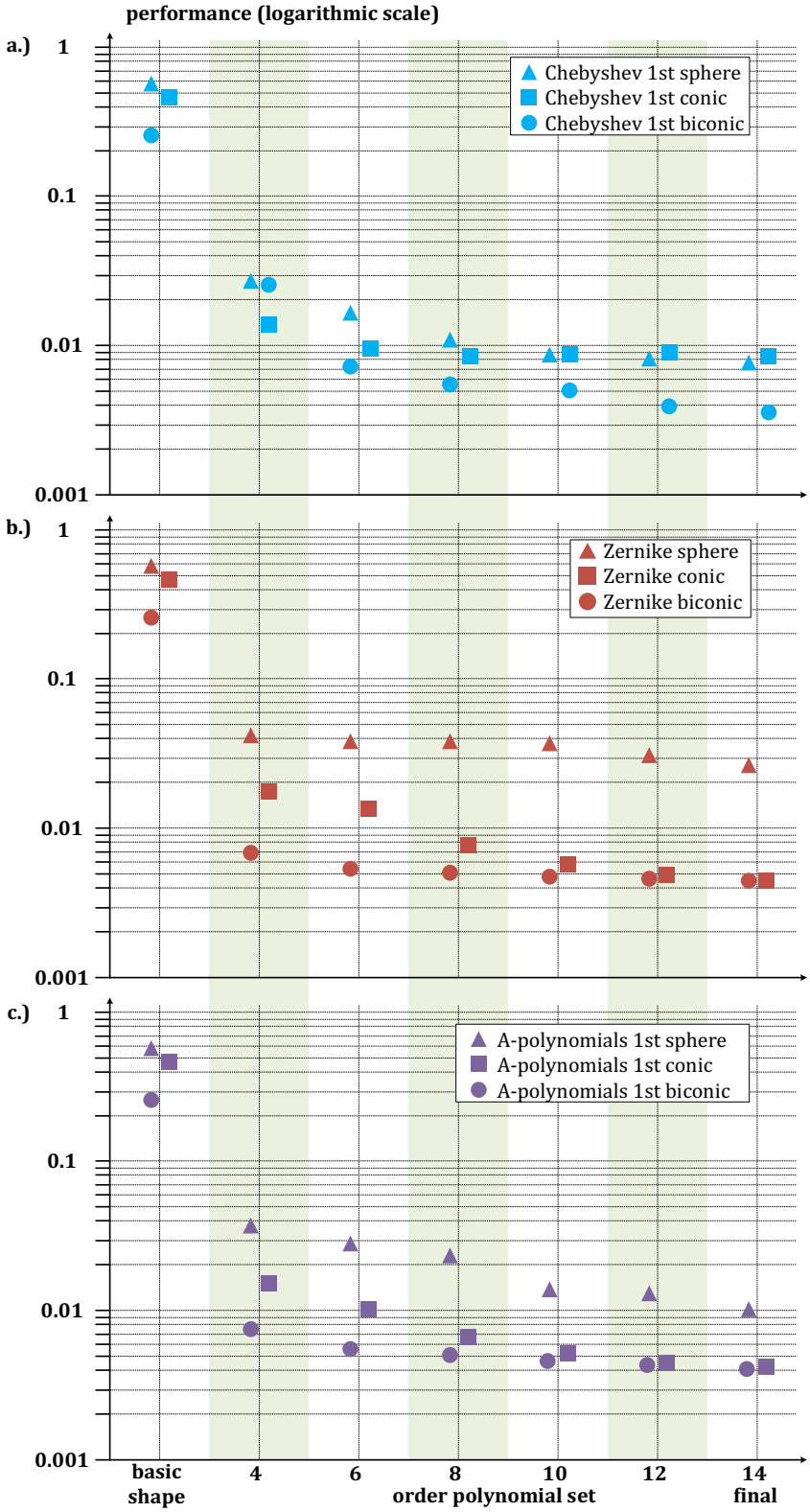

Figure 4.4 Performance for different basic shapes for TMA: a.) Chebyshev 1st kind, b.) Zernike polynomials, c.) A-polynomials 1st kind

Head-mounted display

For the HMD the different polynomial sets have quite similar behaviour: For lower orders, the performance is a factor of 2 better for biconic in case of Chebyshev 1st kind (figure 4.5a) and conic and biconic in case of Zernike (figure 4.5b) and A-polynomials 1st kind (figure 4.5c).

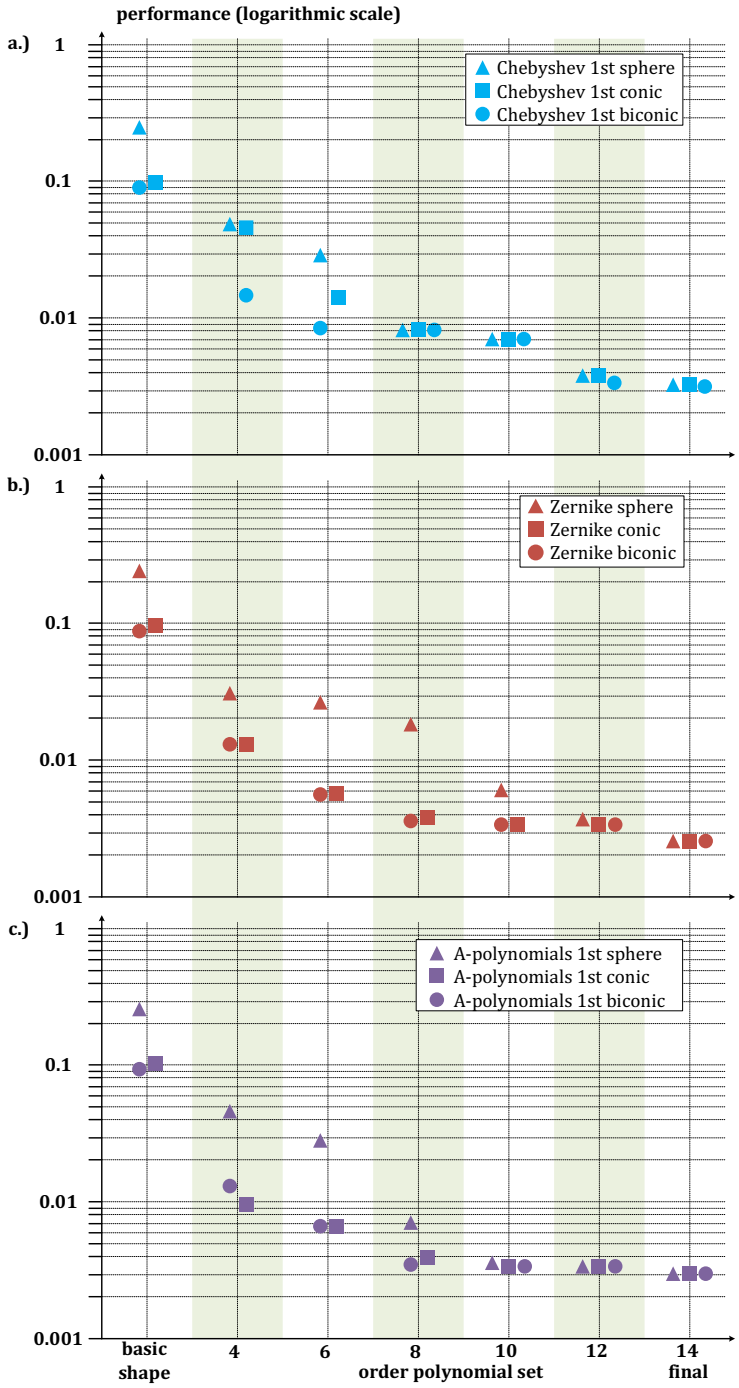

Figure 4.5 Performance for different basic shapes for HMD: a.) Chebyshev 1st kind, b.) Zernike polynomials, c.) A-polynomials 1st kind

With increasing orders, the biconic and conic basic shape is less improving than the spherical one, which results in an equivalent performance at the 8th order for the Chebyshev, 10th for

the A-polynomials and 12th for the Zernike. So, depending on the description, the polynomial sets can compensate with higher order terms for conic and biconic basic shape.

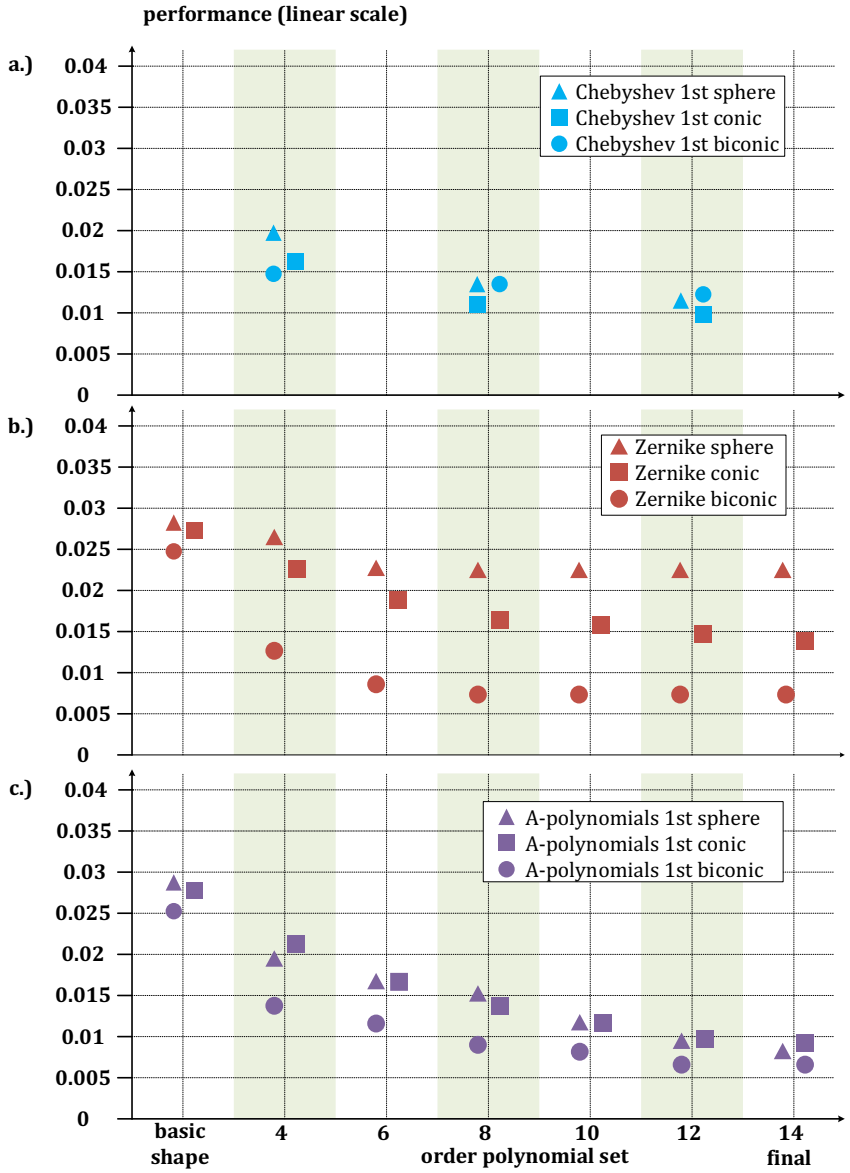

Figure 4.6 Performance for different basic shapes for the anamorphic system: a.) Chebyshev 1st kind, b.) Zernike polynomials, c.) A-polynomials 1st kind

Anamorphic system

Since the anamorphic system is double-plane-symmetric, the Chebyshev 1st kind (figure 4.6a) have only contributing terms in every second order (4th, 8th and 12th). The performance is hereby relatively comparable for all basic shapes over all orders.

In contrary, for the Zernike (figure 4.6b) a difference in performance for each order can be seen. The spherical basic shape leads hereby only to a small improvement at all, whereas for the conical basic shape the impact is small at the beginning but increase at the 8th order significantly.

The biconic has the largest improvement with the 4th order, with performance already better than the final one of the spherical and conical basic shape. For higher orders, this result is than only slightly improved.
The A-polynomials (figure 4.6c) have –similar to the Chebyshev 1st kind – a comparable final result for all basic shape, but with overall better performance for the biconic basic shape for lower orders.

Conclusion for the impact of the basic shape

It can be seen, the impact of the choice of basic shape on the final performance is strongly depending on the system and the selection of the polynomial set.
As the biconic basic shape can correct in special cases for lower order astigmatism and spherical aberration, all investigated systems can theoretically benefit from it. The impact itself is hereby strongly depending on the strength of these aberrations and correction ability of each description. From the result, it can be shown, that it is possible to reduce the number of necessary polynomial orders tremendously to reach a similar result like other basic shapes, like for the Yolo-telescope with the Zernike (figure 4.3b). Here the 6th order correction with biconic basic shape is already better than the final one with sphere and conic.
On the other hand, with the usage of all 14 orders, it is seen, that with a biconic the final result can be significantly better compared to others (e.g. seen in figure 4.4b for the Zernike with a difference in the final result of factor 5 for a spherical vs a biconical basic shape).
Nevertheless, there are also cases, where the basic shape, has either almost no impact at all - like the Chebyshev 1st kind for the Yolo-telescope (figure 4.3a) - or the effect can be completely assumed after the 14th order – like the A-polynomials 1st kind for the Anamorphic system (figure 4.6c) or all three descriptions for the HMD (figure 4.5a-c), due to the very small ray bundle diameter.
Generally, an extension of the basic shape to a biconic is sufficient to reduce the needed parameters and improve the final results significantly. Therefore, for all further investigations in this assessment, a biconic basic shape was used for all descriptions.

4.3 Convergence and final performance of the orders

In this section, the correction ability of the different polynomial sets over the order is considered. So, in other words: How is the individual set able to correct the system.
For the choice of an optimal surface representation, it is important to understand, which aspect of the description influences the performance of the correction. Specifically, in focus are here the properties:

- Domain shape definition (unit square or circle)
- weighting (uniform or with specific weighting)
- boundary function (with restriction or without)
- the defining symmetry (Cartesian or polar)

These properties can be found summarised for each description in section 3.3.
The results for the different representations are hereby shown separately for the Cartesian and polar descriptions. Additionally, the surface sag contribution by basic shape, deformation terms and total freeform surface and the RMS spot (averaged over all fields) for the final result of each description are given. Finally, the best results of the Cartesian and polar defined description are compared.

Yolo-telescope

The Yolo-telescope is a non-symmetric system, with a decoupling of the x and y at the outer boundary, due to the individual tilts of the two mirrors. This leads to larger coma in x and astigmatism in 0°, as well as the relatively small contribution of astigmatism in 45 °, coma y and trefoil.
The Cartesian defined descriptions in figure 4.7 show hereby no difference –except for the 6^{th} order- in the performance over the orders. The main improvement of all polynomials is with the 6^{th} order, where the term 7- corresponds to x^3 in case of Monomials (see table 2.3) - and 10 - corresponds to y^3 in case of Monomials (see table 2.3) - of the set is a combination of primary coma in x, respectively y and trefoil for all Cartesian descriptions. The primary astigmatism correction is only of minor influence. Therefore, almost no change of performance is seen for the 4^{th} order. The further improvement of the 10^{th} and 12^{th} order is due to higher-order aberrations, whereas the 4^{th}, 8^{th} and 14^{th} order have almost no effect on the performance anymore.

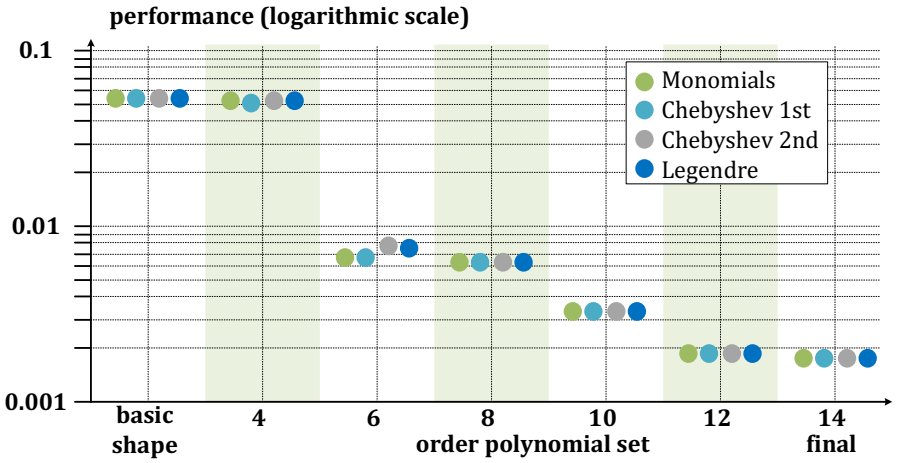

Figure 4.7 Performance for Yolo-telescope: Cartesian descriptions

Table 4.4 Performance data and sag-contribution for the different Cartesian descriptions of the Yolo-telescope

	basic shape	deformation terms	total surface sag
Monomials	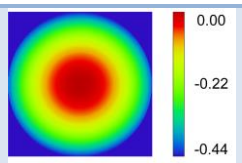	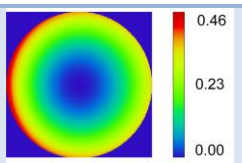	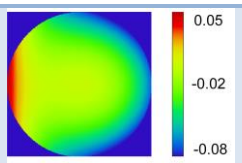
Averaged RMS spot / Airy radius		2.02 µm / 0.86 µm	
Chebyshev 1st kind	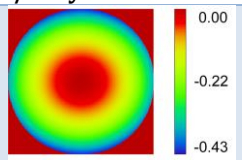	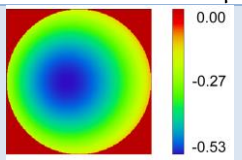	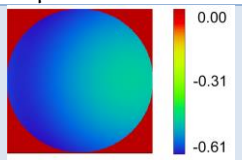
Averaged RMS spot / Airy radius		2.04 µm/ 0.85 µm	
Chebyshev 2nd kind	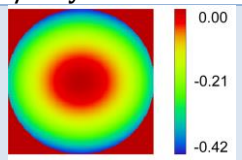	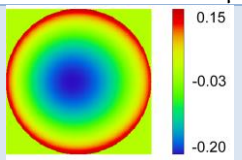	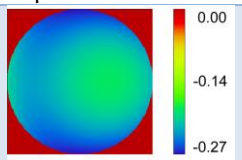
Averaged RMS spot / Airy radius		1.92 µm/ 0.86 µm	
Legendre	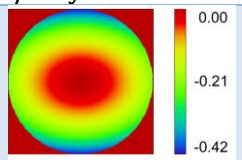	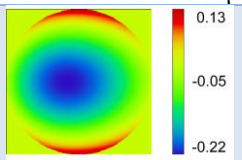	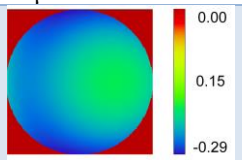
Averaged RMS spot / Airy radius		2.02µm / 0.86 µm	

The averaged spot sizes of the final results for the Cartesian descriptions (table 4.4) are almost identical, whereas the surface shape for the different descriptions slightly differs. For the Chebyshev 1st and 2nd kind, as well as Legendre the basic shape is slightly biconical, with almost identical values for peak-to-valley. The basic shape of the monomials is here more conical, but still in the similar PV-range. The deformation terms show a nearby rotational

symmetric shape with the opposite sign and slight individual deviation in the outer rings: for Monomials asymmetric only in negative x, for Chebyshev 1st kind non, for Chebyshev 2nd kind ring-shaped and for Legendre symmetric for positive and negative y (with similarities to a biconical shape). The overall PV for the deformation terms is hereby almost identical for Chebyshev 2nd and Legendre, whereas the Monomials and Chebyshev 1st kind have twice the PV, in case of the Monomials also with the opposite sign. Despite the differences, the resulting total surface shape, which is of relatively flat and smooth character, looks almost identical for the Chebyshev 1st and 2nd kind and Legendre, with Chebyshev 1st kind having twice the PV. The Monomials, on the other hand, result into a different shape, with much lower total PV and strong deviation in the negative x-direction. So, although there is a certain difference in the shape of the surfaces here, the correction leads to similar results in the overall performance.

Table 4.5 Cartesian descriptions: primary aberration coefficients [λ] for wavefront of final results of the Yolo-telescope

field	Monomials	Chebyshev 1st	Chebyshev 2nd	Legendre
on axis				
astigmatism (Z5/Z6)	0.063/0.000	0.066/0.002	0.067/0.001	0.071/0.001
coma (Z7/Z8)	-0.047/0.001	-0.050/0.000	-0.048/0.000	-0.049/0.000
spherical aberr. (Z9)	0.008	0.009	0.007	0.009
max x /max y				
astigmatism (Z5/Z6)	-0.309/0.202	-0.377/0.244	-0.315/ 0.243	-0.364/0.194
coma (Z7/Z8)	-0.018/0.338	-0.026/ 0.330	-0.020/ 0.334	-0.023/0.335
spherical aberr.(Z9)	-0.020	-0.019	-0.021	-0.019
max x/ min y				
astigmatism (Z5/Z6)	0.492/ -0.104	0.533/-0.040	0.532/ -0.097	0.490/-0.046
coma (Z7/Z8)	0.153/0.235	0.146/0.249	0.151/0.239	0.150/0.243
spherical aberr. (Z9)	0.014	0.016	0.013	0.016
min x/ max y				
astigmatism (Z5/Z6)	-0.562/0.0470	-0.609/-0.128	-0.596/0.039	-0.552/-0.003
coma (Z7/Z8)	-0.113/-0.265	-0.106/0.278	-0.112/0.268	-0.108/-0.274
spherical aberr.(Z9)	-0.023	-0.022	-0.022	-0.023
min x/ min y				
astigmatism (Z5/Z6)	0.238/-0.157	0.305/-0.218	0.251/-0.202	0.302/-0.163
coma (Z7/Z8)	0.059/-0.303	0.068/-0.294	0.060/-0.301	0.065/-0.301
spherical aberr.(Z9)	0.011	0.012	0.011	0.011

The corresponding wavefront coefficients for the primary aberrations (table 4.5) show that there is only a marginal deviation in the values between the descriptions, despite the difference in solution for the Monomials compared to the other representations. The final system is almost perfectly corrected on axis for astigmatism (between 0.000 and 0.071 λ) and suffers only from minor astigmatism in 0° (0.532 to -0.609 λ) and coma in y (-0.303 to 0.338 λ) in the outer field points. Furthermore, an impact of the different weighting of the Chebyshev 1st and 2nd kind, and Legendre cannot be seen.

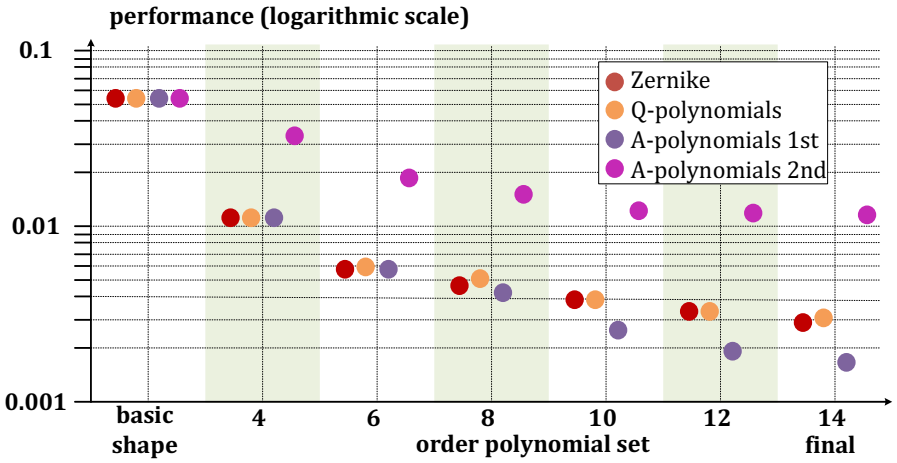

Figure 4.8 Performance for Yolo-telescope: polar descriptions

In figure 4.8 the results for the polar defined descriptions are shown. In contrast to the Cartesian description a difference of performance for the representation can be directly seen. The polynomial sets are all able to improve with the 4th order. For the A-polynomials 2nd kind, this is mainly caused by the term 2 and 3 (see table 3.2), which corresponds to primary coma. The other representations have terms for primary astigmatism and coma (see table 2.5, 2.6 and 3.1 for the corresponding terms) and are therefore able to improve better, as it seems. With higher orders, the results of the A-polynomials 2nd can improve but doesn't overcome the result for the other three descriptions after 4th order, probably caused by the lack of terms corresponding to primary astigmatism. On the other hand, the A-polynomials 1st kind can improve even better compared to the Zernike and Q-polynomials, starting with the 8th order. Since the set is polar defined but developed for a square domain, the terms are adapted for the edges of the domain. These lead to a kind of Cartesian-like behaviour at the boundary. For the Yolo-system with its strong decoupling, this can be an advantage in correction since it combines the classical representation of aberrations with a certain amount of decoupling for the necessary non-symmetric contributions.

The spot sizes and surface sags showed in table 4.6 confirm these results. The Zernike and Q-polynomials are here almost identical for both averaged RMS spot and surface sag contribution. In contrast to the Cartesian descriptions, the basic shapes are almost cylindrical, and the deformation terms have a dominating astigmatic contribution, which results in a similar total surface. The RMS spot of the A-polynomials 1st kind is better than the other two (1.94 to 3.28 respectively 3.39 µm). The corresponding basic shape is also almost cylindrical, but with a larger PV. Furthermore, the deformations terms are not purely dominated by astigmatism contributions, but also have a larger share of coma. Therefore, the resulting total

surface is differing from both the Cartesian descriptions, as well as the other polar ones.

Table 4.6 Performance data and sag-contribution for the different polar descriptions of the Yolo-telescope

	basic shape	deformation terms	total surface sag
Zernike	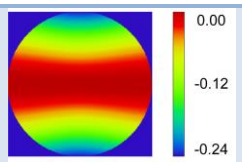	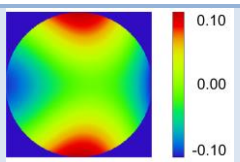	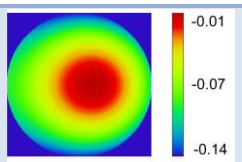
Averaged RMS spot / Airy radius		3.28 µm / 0.91 µm	
Q-polynomials	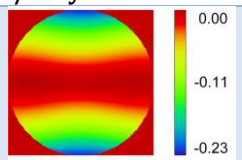	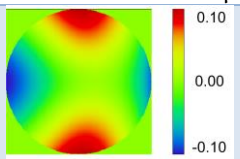	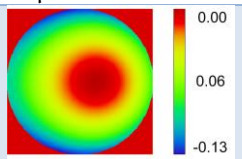
Averaged RMS spot / Airy radius		3.39 µm/ 0.92 µm	
A-polynomials 1st kind	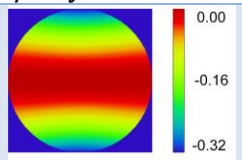	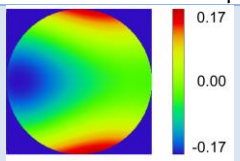	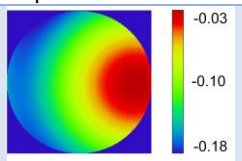
Averaged RMS spot / Airy radius		1.94 µm/ 0.86 µm	
A-polynomials 2nd kind	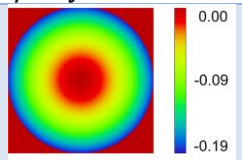	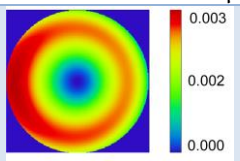	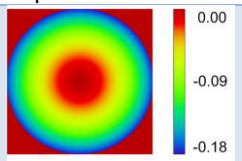
Averaged RMS spot / Airy radius		33.21 µm / 1.27 µm	

The lack of correction ability of the A-polynomials 2nd kind can also be seen in the corresponding RMS spot size, which is a factor of 10 worse than the others, and the sag contribution. The dominating basic shape is here, similar to the Cartesian descriptions more conical, whereas the deformation terms are two magnitudes of order lower in PW and ring-shaped with a bit of asymmetry in the negative x-direction. The resulting freeform surface is therefore not able to correct properly for the aberrations in the system.

In figure 4.9 the best four results, which are for Zernikes, Q-polynomials and A-polynomials 1st kind as well as Chebyshev 1st kind, as one representative of the identical Cartesian descriptions, are shown. In comparison, it can be seen, the lack of correction with the 4th order for the Chebyshev 1st kind, are almost completely balanced out with the 6th order. Where the polar descriptions have more of a uniform improvement over the orders, the Cartesian ones have here specific orders with are of impact, where others have no influence. Specifically, with higher orders (12th and 14th), the Chebyshev 1st kind were able to improve better than the Q-polynomials and Zernike, which leads to a comparable result with the A-polynomials 1st kind. The resulting surfaces for both descriptions have a bit of resemblance, as they both look like

decentred (in positive x-direction) rotational symmetric surface but have totally different contributions by the basic shape and deformation terms.

The corresponding wavefront data (table 4.7) for the A-polynomial 1st kind is very similar to the Cartesian descriptions. The values for the Zernike and Q-polynomials are almost equivalent but in general a factor of 2 higher for astigmatism in ° (1.054 to -1.159 λ) and a factor of 4 for astigmatism in 45° (-0.783 to 1.019 λ). On the other hand, the values for coma in x and y are almost half of the ones by the A-polynomials 1st kind for the maximum field in x and y, as well as the minimum field in both directions. For the other two cases, the values are almost identical. Nevertheless, the coma was almost completely corrected by either of the three descriptions. For the A-polynomials 2nd kind the wavefront contains unchanged values for astigmatism on axis, whereas in the field the astigmatism is balanced in a different way between the outer field points but in total unchanged. Moreover, the coma in x is increased (~ -14.500 λ) and for y only minor improved (~1.800 λ), uniformly for all field points. Although the initial system does not suffer from spherical aberration contains the wavefront of the final results very high contributions (~17.500 λ), again uniformly for all field points.

Table 4.7 Polar descriptions: primary aberration coefficients [λ] for a wavefront of the final results of the Yolo-telescope

field	Zernike	Q-polynomials	A-polynomials 1st	A-polynomials 2nd
on axis				
astigmatism (Z5/Z6)	0.071/0.006	0.073/0.003	0.086/0.001	6.586/-0.643
coma (Z7/Z8)	-0.037/0.000	-0.038/0.000	-0.498/0.000	-14.524/-1.876
spherical aberr. (Z9)	0.006	0.005	0.009	-17.639
max x /max y				
astigmatism (Z5/Z6)	-1.081/0.951	-1.159/1.019	-0.506/0.225	5.565/2.024
coma (Z7/Z8)	-0.015/0.198	-0.014/0.187	-0.027/0.311	-14.429/-1.896
spherical aberr. (Z9)	0.030	-0.318	-0.18	-17.691
max x/ min y				
astigmatism (Z5/Z6)	1.059/0.684	1.111/0.759	0.503/0.105	8.958/-0.031
coma (Z7/Z8)	0.127/0.237	0.126/0.235	0.143/0.249	-14.430/-1.847
spherical aberration (Z9)	-0.005	-0.008	0.015	-17.462
min x/ max y				
astigmatism (Z5/Z6)	-1.086/-0.783	-1.134/-0.868	-0.539/.0,142	4.189/1.754
coma (Z7/Z8)	-0.091/-0.266	-0.094/-0.263	-0.106/-0.281	-14.607/-1.904
spherical aberr. (Z9)	-0.002	-0.001	-0.214	17.630
min x/ min y				
astigmatism (Z5/Z6)	1.054/-0.835	1.138/-0.902	0.470/-0.196	7.583/-2.828
coma (Z7/Z8)	0.052/-0.176	0.046/-0.167	0.070/-0.279	-14.606/1.859
spherical aberr. (Z9)	0.023	0.023	0.011	-17.580

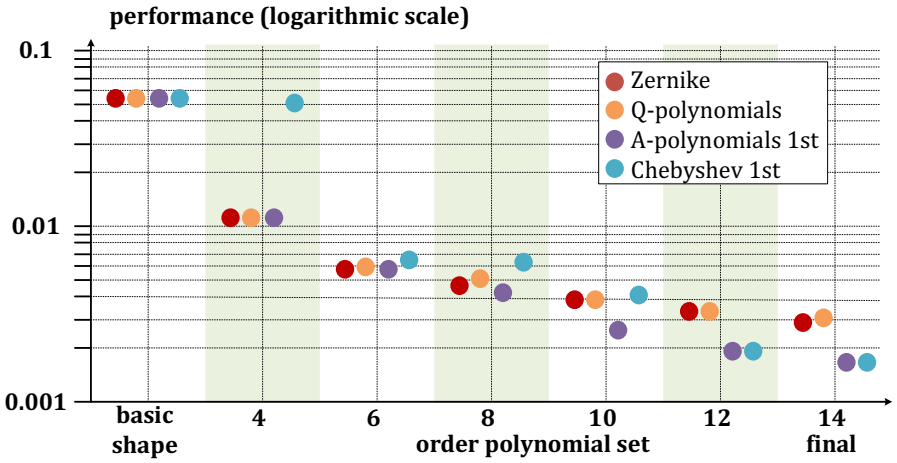

Figure 4.9 Best performances for Yolo-telescope

The results indicate that the descriptions with the best performance in this asymmetric system are the Cartesian ones and the one polar description with a decoupling in x and y at the boundary, whereas the Zernike and Q-polynomials are able to correct nearly as good, due the very good access to the aberrations and the certain remaining coupling in the center of the domain. The A-polynomials 2nd kind fail here completely.

Concerning the domain, the preferable descriptions are the ones with the square-defined domain, which is not coinciding with the footprint at all but is related to the decoupling of the outer boundary in the terms, which only makes sense, if defined on a square domain.

Three-mirror-anastigmat

The TMA is a plane-symmetric system, which is mainly suffering from astigmatism in 0° (-119.255 to -209.254 λ) and coma in y (36.202 to 44.101 λ).

In figure 4. 10 the performance of the Cartesian descriptions for this system can be seen. The main improvement comes hereby with the 4th order, for the astigmatism correction. The small differences in the result for the 4th order is related to the slightly different term in each description, which comes from the different weighting. With increasing orders, the Chebyshev 2nd kind and Legendre are not changing significantly, whereas the Chebyshev 1st kind and Monomials still improve up to the 14th order. The final result here is a factor of two better than the other two descriptions. The effect of the weighting can be directly seen. In case of the Chebyshev 2nd kind and Legendre, the boundary is more emphasised, which doesn't seem to help in correction. For Monomials and also Chebyshev 1st kind the centre and boundary are evenly emphasised, so the difference is specifically for the centre part of the surface. This difference can also be seen in the RMS values for the spot (table 4.8), with the Chebyshev 1st

kind being slightly worse than the Monomials and the Chebyshev 2nd kind, as well as Legendre, being up to a factor of 2 worse.

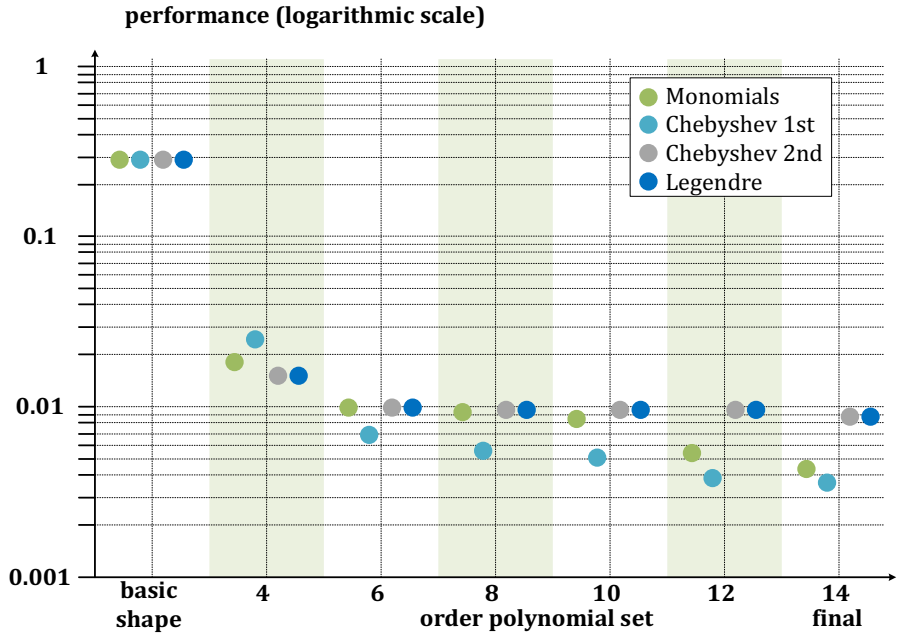

Figure 4.10 Results for TMA-telescope: Cartesian descriptions

Table 4.8 Performance data and sag-contribution for the different Cartesian descriptions of the TMA

	basic shape	deformation terms	total surface sag
Monomials	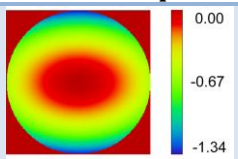	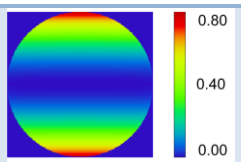	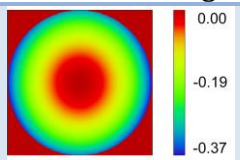
Averaged RMS spot / Airy radius		7.26 µm/ 5.20 µm	
Chebyshev 1st kind	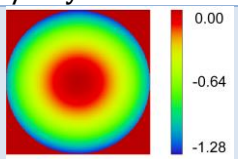	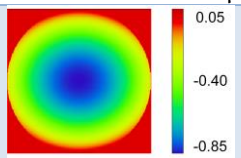	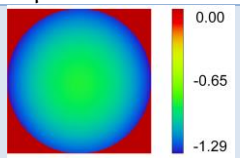
Averaged RMS spot / Airy radius		8.68 µm/ 4.29 µm	
Chebyshev 2nd kind	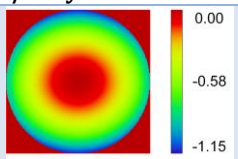	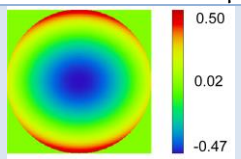	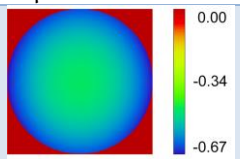
Averaged RMS spot / Airy radius		12.75 µm/ 5.16 µm	
Legendre	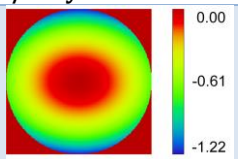	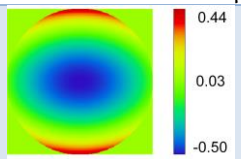	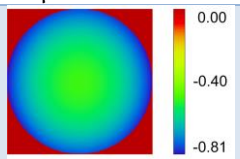
Averaged RMS spot / Airy radius		16.37 µm/ 6.18 µm	

Like the previous system, the corresponding surface contributions for the different Cartesian polynomials look quite similar, specifically for the three (spatial) orthogonal representations. The basic shape of all four descriptions is again a biconic with an only slightly different radius of curvatures/conic parameters in x and y. The deformation terms are also biconical shaped, but with opposite sign. The resulting freeform surface is then mainly rotational symmetric, but with higher order asymmetry, not seen in the total sag plot. The Chebyshev 2nd kind and Legendre are hereby again almost identical.

Looking at the corresponding wavefront of the final results (table 4.9), it can be seen, that four descriptions have quite different values for the individual contributions. The Monomials have the highest contribution of coma y on axis (0.283 λ) and in the field (-0.613 λ), and together with the Chebyshev 1st kind astigmatism in the field (0.240, respectively 0.232 λ) and spherical aberration on axis (0.117, respectively 0.115 λ). The latter one additionally has the highest contribution of astigmatism on axis (-0.227 λ) and spherical aberration in the field (-0.055 λ). Nevertheless, the Legendre, as bad in performance as the Chebyshev 2nd kind, have relatively high contributions for astigmatism (-0.177, respectively 0.195 λ) and spherical aberration (0.101, respectively -0.029 λ) on axis and in the field. The Chebyshev 1st kind, as the best performing Cartesian description has only larger contributions by coma on axis (0.200 λ) and in the field (-0.390 λ), whereas the other values are the lowest of all descriptions.

Table 4.9 Cartesian descriptions: primary aberration coefficients [λ] for a wavefront o the final results of the TMA

field	Monomials	Chebyshev 1st	Chebyshev 2nd	Legendre
on axis				
astigmatism (Z5/Z6)	-0.076/0.000	-0.051/0.000	-0.227/0.000	-0.177/0.000
coma (Z7/Z8)	0.000/0.283	0.000/0.200	0.000/-0.111	0.000/0.016
spherical aberr. (Z9)	0.117	0.064	0.115	0.101
max x /max y				
astigmatism (Z5/Z6)	0.240/0.000	0.110/0.000	0.232/0.000	0.195/0.000
coma (Z7/Z8)	0.000/-0.613	0.000/-0.390	0.000/-0.357	0.000/-0.374
spherical aberr. (Z9)	0.015	0.017	-0.055	-0.029

The results for the polar description for the TMA are seen in figure 4.11. Except for the A-polynomial 2nd kind all descriptions have similar behaviour. The largest improvement by a factor of 40 is with the 4th order, where both primary astigmatism and primary coma are corrected. The remaining aberrations are so small that for the higher orders there is almost

no further improvement of the result. In contrast, the A-polynomials 2nd kind are only able to correct for the coma, but not for astigmatism. The impact on the performance is therefore only small. Nevertheless, with higher orders, the system improves continuously, but is finally still a factor of 5 worse, due to remaining astigmatism.

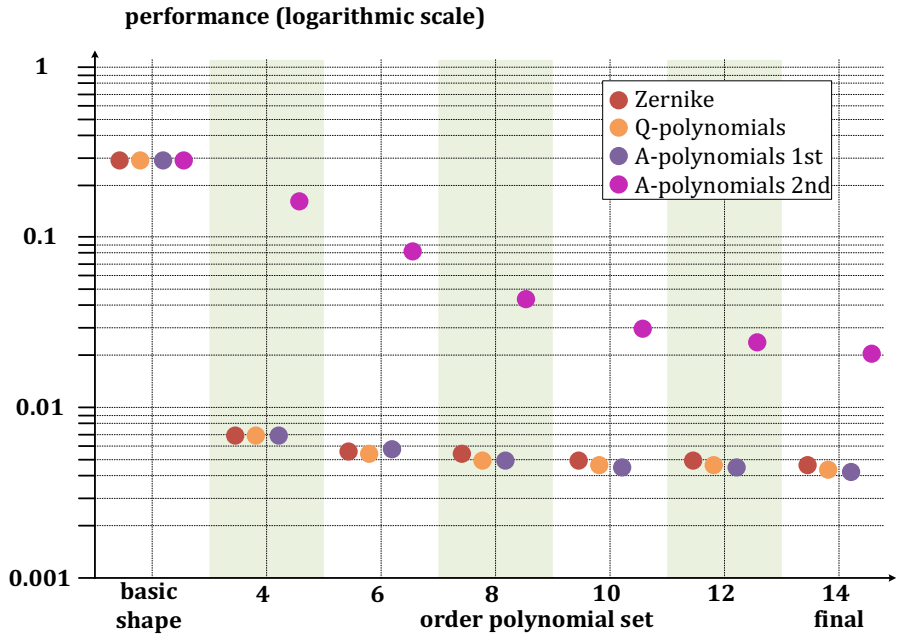

Figure 4.11 : Results for TMA-telescope: polar descriptions

Table 4.10 Performance data and sag-contribution for the different polar descriptions of the TMA

	basic shape	deformation terms	total surface sag
Zernike	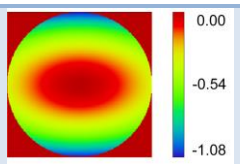	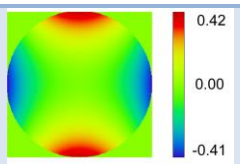	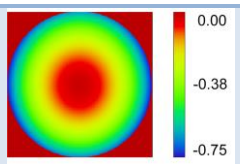
Averaged RMS spot / Airy radius		12.48 µm/ 2.60 µm	
Q-polynomials	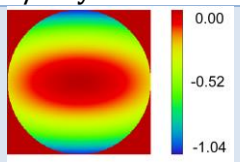	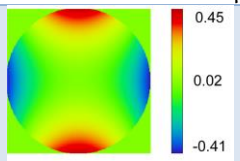	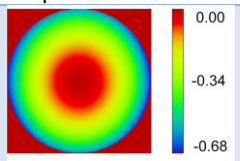
Averaged RMS spot / Airy radius		11.23 µm/ 2.86 µm	
A-polynomials 1st kind	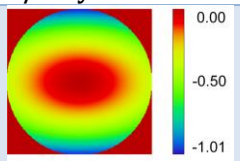	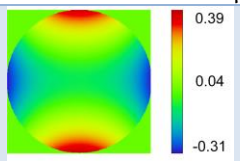	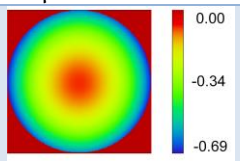
Averaged RMS spot / Airy radius		10.23 µm/ 3.25 µm	
A-polynomials 2nd kind	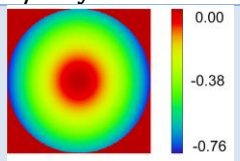	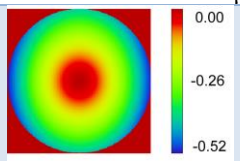	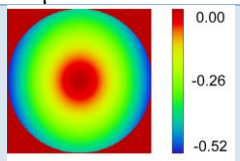
Averaged RMS spot / Airy radius		70.44 µm/ 2.11 µm	

The equivalent result for Zernike, Q-polynomials and A-polynomials 1st kind can also be seen in the averaged RMS spot and surface contribution (table 4.10). The three descriptions have similar RMS values, with A-polynomial 1st kind being slightly better (in reference to the Airy radius) compared to the other two. The basic shape, on the other hand, is almost identical for all three cases in shape (biconic), as well as in PV-value. Moreover, the deformation terms are showing dominant astigmatism, as expected, with similar range. Therefore, the resulting freeform surfaces are almost alike, except for slightly less emphasised centre part for the A-polynomials 1st kind, compared to the other two. For the A-polynomials, 2nd kind, the lack of astigmatism correction is seen both in RMS, which is a factor of 5 worse than for the others, and surface sag, which is mainly rotational symmetric for the basic shape and dominated by the evenly rotational symmetric spherical aberration for deformation terms. Although the final freeform surface looks very similar to the other descriptions, the astigmatism correction is missing.

Table 4.11 Polar descriptions: primary aberration coefficients [λ] for a wavefront of the final results of the TMA

field	Zernike	Q-polynomials	A-polynomials 1st	A-polynomials 2nd
on axis				
astigmatism (Z5/Z6)	0.265/0.000	0182/0.000	0.108/0.000	83.329/0.000
coma (Z7/Z8)	0.000/0.759	0.000/0.622	0.000/0.475	0.000/24.993
spherical aberr. (Z9)	0.094	0.080	0.064	-85.615
max x /max y				
astigmatism (Z5/Z6)	0.071/0.000	0.089/0.000	0.072/0.000	42.876/0.000
coma (Z7/Z8)	0.000/-0.891	0.000/-0.738	0.000/-0.568	0.000/-63.070
spherical aberr. (Z9)	0.092	0.078	0.062	-74.713

The wavefront data for the polar descriptions is shown in table 4.11. For Zernike, Q-polynomials and A-polynomials 1st kind the values for coma y on axis is up to 3 times higher (0.475 to 0.759 λ) than for the Cartesian descriptions, moreover for coma y in the field it is about two times higher (-0.568 to -0.891 λ). On the other hand, astigmatism 0° in the field is only one-third of the Cartesian representations (0.071 to 0.089 λ). The spherical aberration on the axis is slightly smaller (0.064 to 0.094 λ), whereas in the field it is slightly larger (0.062 to 0.092 λ). Generally for the three descriptions the remaining aberrations are uniformly distributed over the field. The A-polynomials 2nd kind fails here, as before for the Yolo-telescope, completely. Astigmatism, both on axis and in the field, is only reduced by a factor of 3 (83.239, respectively 42.876 λ). The coma in y is reduced on an axis by 40% (24.993 λ) and

increased in the field by 75 % (-63.070 λ), whereas the spherical aberration is increased by a factor of about 70 on axis (-85.615 λ) and in the field (-74.713 λ).

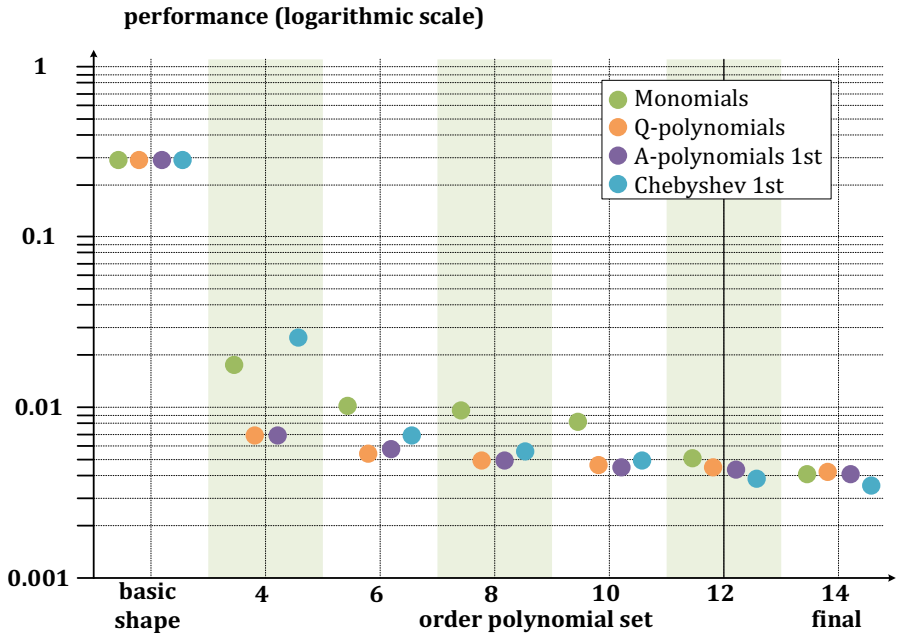

Figure 4.12 Best performances for TMA-telescope

In figure 4.12 the best results are shown both from Cartesian and polar descriptions. As discussed before the Q-polynomials and A-polynomials 1st kind have almost identical behaviour, with a slightly better result for the latter one. The Chebyshev 1st kind and Monomials in comparison have more problems with correction for lower orders, but finally a better performance than the polar-descriptions. As before the surface shape for the polar- and Cartesian-defined description look only slightly similar, although within one group for the different descriptions the correction pattern is quite the same. What can be seen, is the effect of different weighting on the performance, with a preference for descriptions, which are specifically not emphasising the boundary. Additionally, the results of the best descriptions both for Cartesian and polar- defined representations are nearby, which shows that for this kind of systems both kinds have a similar ability of correction since the main aberration - astigmatism- can be covered by both types, except for the A-polynomials 2nd kind.

Head-mounted display

The folded head-mounted display suffers mainly from astigmatism 0° on-axis (-1.539 λ) and the field (2.493 to 6.718 λ), as well as astigmatism 45° in the field (-9.741 to 27.094 λ) and coma in x and y for the positive y field (~2.400 λ) So the main correction should be with the 4th order terms.

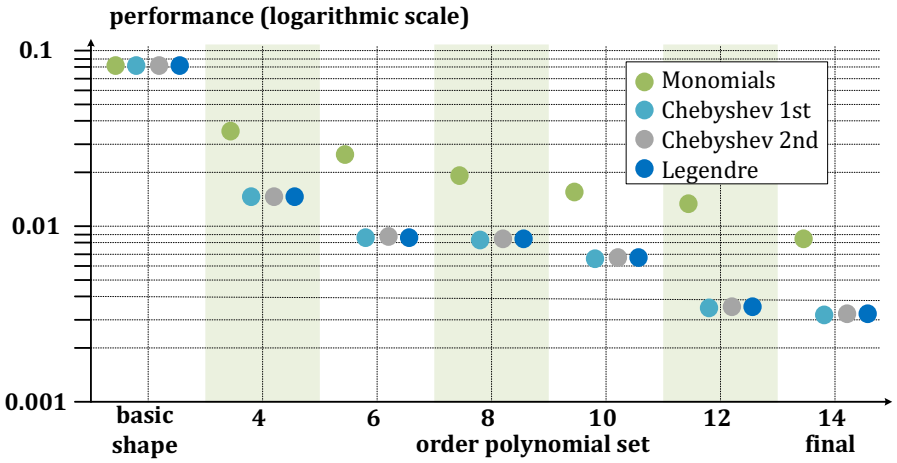

Figure 4.13 Performance for HMD: Cartesian descriptions

In figure 4.13 the performance of the Cartesian descriptions can be seen. Except for the Monomials, all Cartesian descriptions have almost identical results for each order. The major improvement for the Chebyshev 1st and 2nd kind, as well as Legendre, is with the 4th order, as expected, with the correction for astigmatism. Furthermore with 6th and 12th order for coma and higher-order aberrations.

Table 4.12 Performance data and sag-contribution for the different Cartesian descriptions of the HMD

	basic shape	deformation terms	total surface sag
Monomials	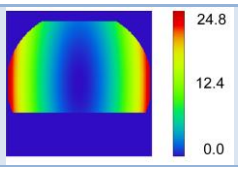	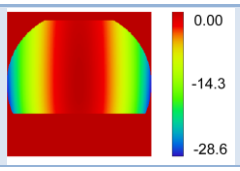	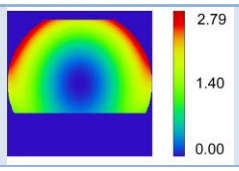
Averaged RMS spot / Airy radius		10.60 µm/ 7.57 µm	
Chebyshev 1st kind	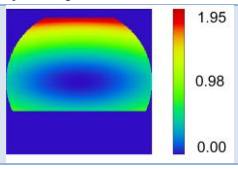	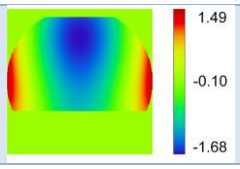	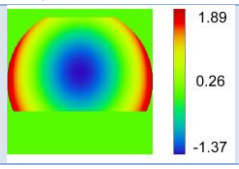
Averaged RMS spot / Airy radius		4.70 µm/ 7.22 µm	
Chebyshev 2nd kind	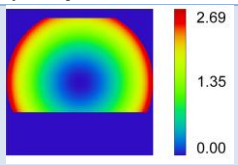	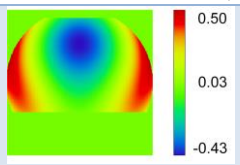	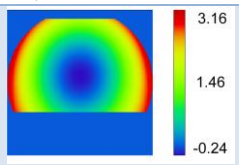
Averaged RMS spot / Airy radius		5.24 µm/ 7.10 µm	
Legendre	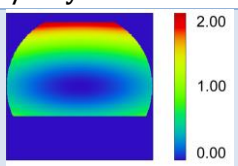	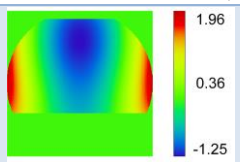	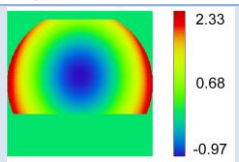
Averaged RMS spot / Airy radius		4.91 µm/ 7.15 µm	

The Monomials, on the other hand, improve mostly with the 4th order. For higher orders, the error function improves slightly, with each order, but is finally three times worse than for the other descriptions.

Table 4.13 Cartesian descriptions: primary aberration coefficients [λ] for a wavefront of the final results of the HMD

field	Monomials	Chebyshev 1st	Chebyshev 2nd	Legendre
on axis				
astigmatism (Z5/Z6)	0.186/0.000	-0.060/0.000	-0.052/0.000	-0.060/0.000
coma (Z7/Z8)	0.000/0.110	0.000/0.075	0.000/0.092	0.0000/0.082
spherical aberr. (Z9)	0.002	0.002	0.002	0.017
max y				
astigmatism (Z5/Z6)-	-0.183/0.152	-0.073/0.015	-0.086/0.014	-0.079/0.017
coma (Z7/Z8)	-0.011/0.084	-0.046/0.061	-0.047/0.073	-0.046/0.067
spherical aberr. (Z9)	0.002	0.000	0.000	0.000
min y				
astigmatism (Z5/Z6)	0.244/0.212	0.141/0.020	0.144/0.026	0.142/0.022
coma (Z7/Z8)	-0.008/0.051	0.014/0.048	0.017/0.059	0.014/0.051
spherical aberr. (Z9)	0.001	0.002	0.002	0.002

This can also be seen in the RMS spot after adding the 14th order for the different descriptions (see table 4.12). Chebyshev 1st and 2nd kind, as well as Legendre, are all diffraction limited and with similar spot size, whereby the 1st kind Chebyshev is slightly better than the other two. Nevertheless, the distribution of the correction between basic shape and deformation terms is quite different. Legendre and Chebyshev 1st kind have a similar biconic basic shape and slightly dominating deformation, whereas the Chebyshev 2nd kind has a dominating conic basic shape with only a minor fraction of deformation terms. However, the resulting freeform surfaces in these three cases are then nearly identical in shape and similar in peak-to-valley.

The corresponding wavefront data, as seen in table 4.13, confirm the performance seen in figure 4.13. The Chebyshev 1st and 2nd kind, as well as the Legendre, have comparable low values for astigmatism in 0° on-axis (~-0.060 λ) and the field (-0.073 to 0.144 λ). The Monomials, on the other hand, have here 0.186 λ on axis and -0.183 to 0.244 λ in the field. Moreover, in case of astigmatism 45° in the field, the Monomials have ten times higher values (0.152 to 0.212 λ) than the other descriptions. For coma x and y on axis and in the field, the four descriptions are in the same range, similar is for the spherical aberration. The difference in performance seems to result from the slightly worse ability of the Monomials to correct for astigmatism.

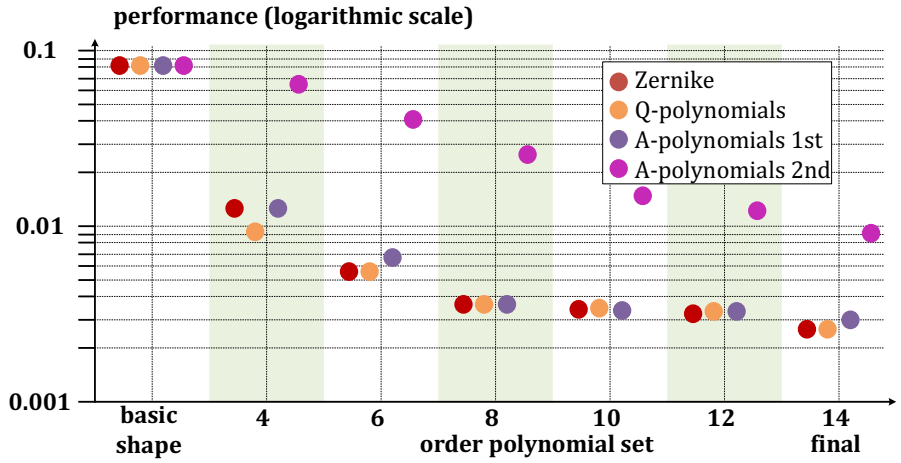

Figure 4.14 Results for HMD-telescope: polar descriptions

For the polar descriptions, the results are relatively similar (see figure 4.14). With the 4th order, the error function is reduced by a factor of about 8 for Zernike and A-polynomials 1st kind and 10 for the Q-polynomials, whereas the A-polynomials 2nd kind have no astigmatism ability, which leads to only a very small improvement. With further orders, the other three descriptions become almost equivalent in error function, whereby the performance is relatively stable for the 8th to 12th order. At the 14th order, the Qs and Zernike improve a bit more than the A-polynomials 1st kind. The 2nd kind A's, on the other hand, have a relatively small but constant reduction of the error function for each order, but the final result is still a factor of three worse than for the other descriptions.

The equivalence in result can also be seen in the almost identical RMS spot values of the three descriptions, compared to the almost three times worse RMS spot value for the A-polynomials 2nd kind. Moreover, the corresponding surface shapes (table 4.14) are not only very much alike in shape and PV-value but also very similar to the Cartesian ones. Hereby the Zernike and Q- polynomials using an approach of a dominating conical basic shape with a very similar shape for the deformation terms. The A-polynomials 1st kind, however, has (similar to the Chebyshev 1st kind) a nearly cylindrical basic shape with slightly dominating deformations terms. The 2nd kind A-polynomials are not near the final results of the other descriptions. Furthermore both, basic shape and deformation terms, are dominated by the rotational symmetric contributions. The resulting freeform surface has some similarities in shape, but, due to the lack of astigmatism correction, isn't as effective as the ones by the descriptions.

Table 4.14 Performance data and sag-contribution for the different polar descriptions of the HMD

	basic shape	deformation terms	total surface sag
Zernike	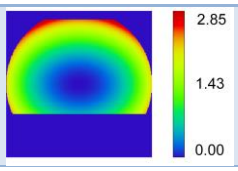	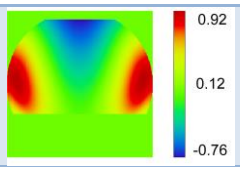	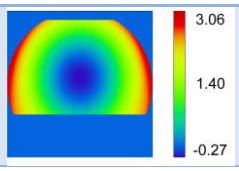
Averaged RMS spot / Airy radius		4,27 µm/ 7,08 µm	
Q-polynomials	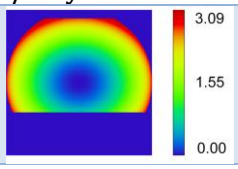	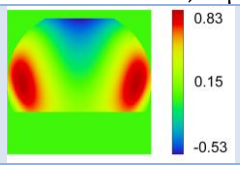	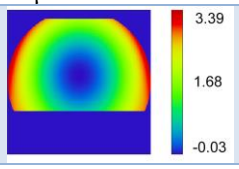
Averaged RMS spot / Airy radius		4.38 µm/ 7.03 µm	
A-polynomials 1st kind	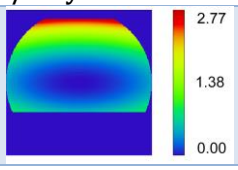	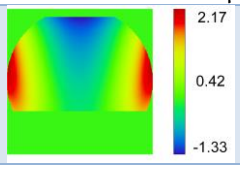	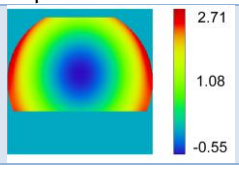
Averaged RMS spot / Airy radius		4,31 µm/ 7,10 µm	
A-polynomials 2nd kind	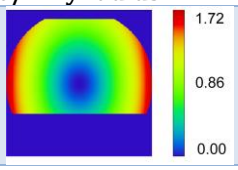	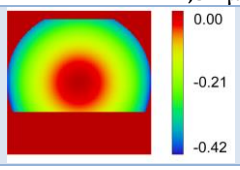	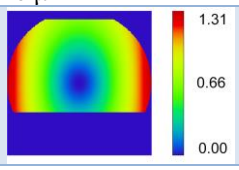
Averaged RMS spot / Airy radius		11,76 µm/ 7,47 µm	

The corresponding wavefront data (table 4.15) show an almost fully corrected wavefront on axis for the Zernike, Q- and A-polynomials 1st kind , as well as similar small contributions for astigmatism 0° (-0.037 to 0.105 λ), 45 ° (-0.09 to -0.032 λ) and coma in x (0.000 to -0.032 λ) and y (0.054 to 0.081 λ) in the field, which can also be seen in the almost identical results for the three descriptions. For the A-polynomials 2nd kind , the astigmatism contribution on axis is increased by a factor of 4 (6.525 λ) and slightly decreased in the field (1.667 to 2.061 λ). Astigmatism 45° is strongly reduced for the positive y field (0.504 λ), but only slightly for the negative one (-3.679 λ). The coma for both on axis and field is almost corrected (0.004 to -0.124 λ).

Since all Cartesian descriptions, except the Monomials, have almost identical results, the Chebyshev 1st kind were chosen for the comparison with the best polar descriptions (see figure 4.15). It can be seen, that for the 4th and the higher orders -starting with the 12th- the difference between the descriptions, specifically Chebyshev 1st kind and the others, are negligible.

Table 4.15 Polar descriptions: primary aberration coefficients [λ] for a wavefront of the final results of the HMD

Field	Zernike	Q-polynomials	A-polynomials 1st	A-polynomials 2nd
on axis				
astigmatism (Z5/Z6)	-0.027/0.000	-0.009/0.000	0.001/0.000	6.525/0.000
coma (Z7/Z8)	0.000/0.001	0.000/0.000	0.000/0.019	0.000/-0.124
spherical aberr. (Z9)	0.001	0.001	0.001	0.005
max y				
astigmatism (Z5/Z6)	-0.045/-0.035	-0.048/-0.035	-0.037/-0.032	1.667/0.504
coma (Z7/Z8)	-0.007/0.074	0.000/0.081	-0.012/0.066	-0.028/0.004
spherical aberr. (Z9)	0.009	0.010	0.000	0.001
min y				
astigmatism (Z5/Z6)	0.105/-0.009	0.078/-0.009	0.081/-0.009	2.061/-3.679
coma (Z7/Z8)	-0.023/0.062	-0.017/0.065	-0.032/0.054	0.084/-0.086
spherical aberr. (Z9)	-0.001	-0.001	-0.001	0.003

The final surfaces of the descriptions are almost identical in shape and PV-values. The corresponding RMS spot radii are diffraction limited and similar for all descriptions, except for Monomials and A- polynomials 2nd kind. An impact on the result of the different weighting for the Cartesian description could not be seen here.

Therefore, as a result it can be concluded that the ability to correct this system is equivalently present in the descriptions, except for the Monomials and A-polynomials 2nd kind and shape of the freeform is almost identical, although the descriptions use different strategies for the basic shape and deformation terms.

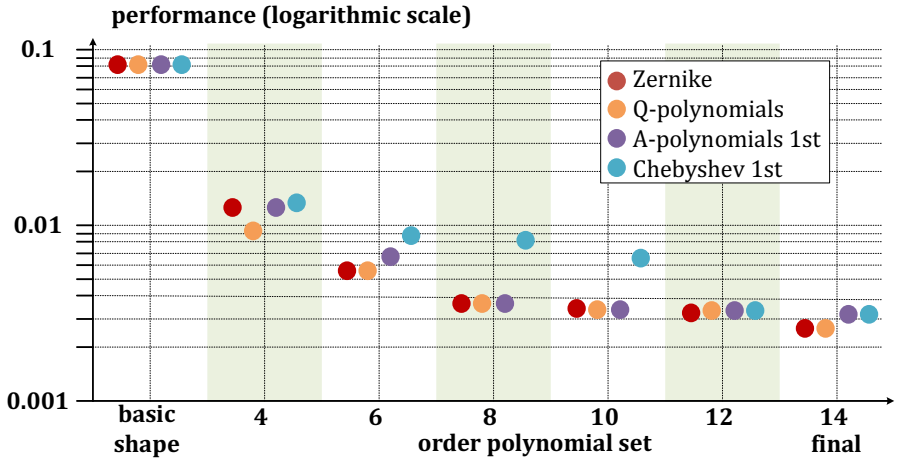

Figure 4.15 best Results for HMD

Anamorphic system

The anamorphic system is a double-plane symmetric system, which different magnifications in x and y. The system mainly suffers from astigmatism 0° (9.175) and spherical aberration (2.975) on axis and astigmatism in 0° and 45° (-13.713, respectively -3.571), as well as coma in x and y (-4.529, respectively 2.248) and spherical aberration (-1.705) in the field.

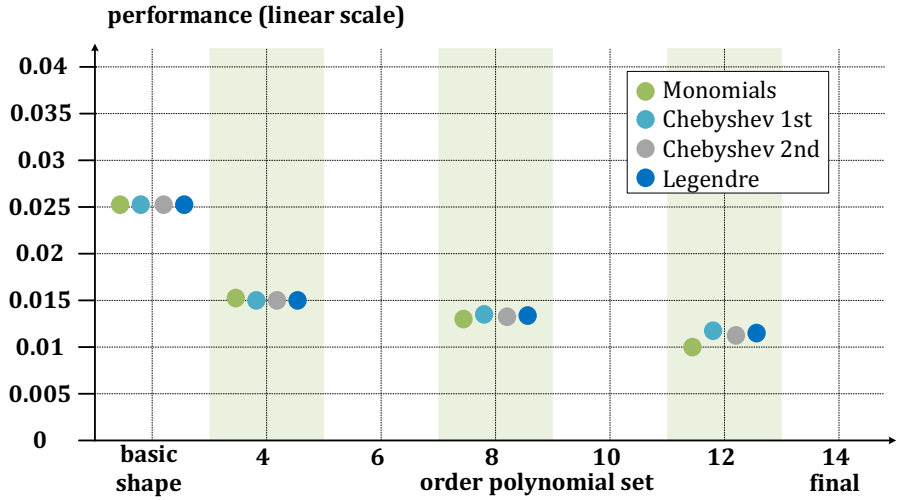

Figure 4.16 Performance for the anamorphic system: Cartesian descriptions

Due to the symmetry of Cartesian description, only even powers of x and y can be used, which results in the 4th, 8th and 12th order. The other polynomial orders are not contributing to the symmetry. The result for the remaining orders is shown in figure 4.16. The behaviour for all description is similar with the only slight difference in the final results. The main correction is with the 4th order, which means for astigmatism. With higher orders, there is almost no further progress, due to the limited number of degrees of freedom.

Although they are quite similar in performance, which can also be seen in the corresponding RMS- values (table 4.16), the surface sag contributions are differing, especially for the deformation terms. The Monomials and Legendre both use a biconical basic shape (with a larger radius of curvature/conic constant in x than y) and stronger biconical shaped deformation terms (with a larger radius of curvature/conic constant in y than in x). The Chebyshev 2nd kind use a similar basic shape, but the deformation terms are dominated by astigmatism, with a higher PV-value than the basic shape. In contrary, the 1st kind Chebyshev have a conical basic shape and deformation terms, which are mainly rotational symmetric. With these different constellations, the resulting freeform surfaces are still very similar, with a dominating rotational symmetric part.

Table 4.16 Performance data and sag-contribution for the different Cartesian descriptions of the anamorphic system

	basic shape	deformation terms	total surface sag
Monomials	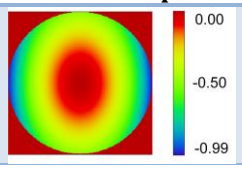	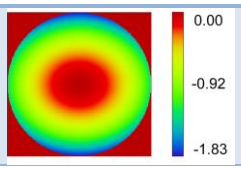	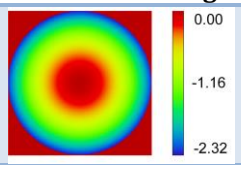
Averaged RMS spot / Airy radius		20.79 µm/ 1.29 µm	
Chebyshev 1st kind	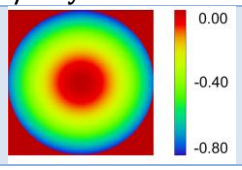	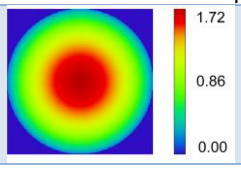	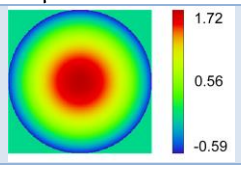
Averaged RMS spot / Airy radius		24.47 µm/ 1.29 µm	
Chebyshev 2nd kind	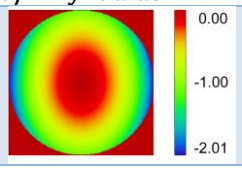	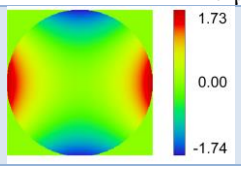	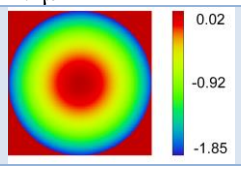
Averaged RMS spot / Airy radius		21.16 µm/ 1.29 µm	
Legendre	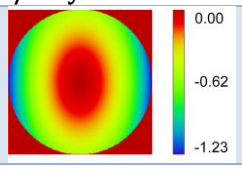	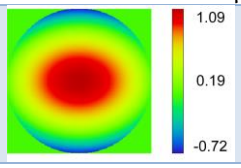	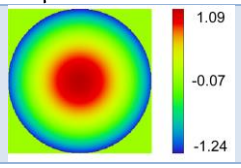
Averaged RMS spot / Airy radius		22.33 µm/ 1.29 µm	

The difference of the descriptions for the surface shape can also be seen in the wavefront data. The Monomials and Chebyshev 2nd kind have hereby similar values for astigmatism 0° in axis (~0.33 λ) and in the field (~-0.180 λ), as well as for coma y in the field (~1.400 λ). For spherical aberration on axis, Chebyshev is two times larger than the Monomials (0.798, respectively 0.430 λ). The same is for astigmatism 45° in the field (0.229, respectively 0.648 λ) and coma x in the field (-0.175, respectively -0.347 λ). The value for spherical aberration is slightly higher for the Chebyshev (0.927, respectively 0.786 λ). The Chebyshev 1st kind and

Table 4.17 Cartesian descriptions: primary aberration coefficients [λ] for a wavefront of the final results of the anamorphic system

field	Monomials	Chebyshev 1st	Chebyshev 2nd	Legendre
on axis				
astigmatism (Z5/Z6)	0.321/0.000	0.896/0.000	0.344/0.000	1.149/0.000
coma (Z7/Z8)	0.000/0.000	0.000/0.000	0.000/0.000	0.000/0.000
spherical aberr. (Z9)	0.430	0.421	0.798	0.219
max x /max y				
astigmatism (Z5/Z6)	-0.179/0.229	-1.293/-0.019	-0.180/0.648	-1.637/-0.904
coma (Z7/Z8)	-0.175/1.488	0.214/2.825	-0.347/1.352	0.160/2.892
spherical aberr. (Z9)	0.786	0.686	0.927	0.689

Legendre have a much larger contribution for astigmatism 0° on axis (0.896, respectively 1.149 λ) and in the field (-1.293, respectively -1.637 λ). Moreover, the coma in x is similar to the Monomials (0.214, respectively 0.160 λ), whereas the coma y two times larger is (~2.800 λ). The spherical aberration on axis is for the Chebyshev 1st kind comparable to the Monomials, for the Legendre only half of the value (0.219 λ). In the field, they are both equivalent (~0.690 λ). However, the major difference between the two descriptions is astigmatism 45° in the field, which is almost corrected in case of the Chebyshev 1st kind, but comparable large for the Legendre (-0.904 λ).

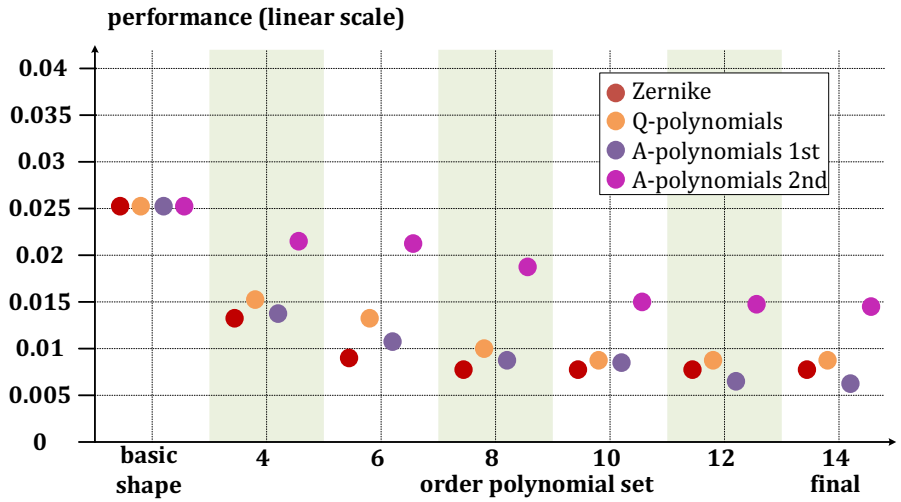

Figure 4.17 Performance for the anamorphic system: polar descriptions

In figure 4.17 the performance of the polar descriptions is shown. The performance of Zernike, Q- polynomials and A-polynomials 1st kind is very nearby over all orders, with a slightly better performance for Zernike for lower and for A-polynomials 1st kind for higher orders. The largest improvement is obtained for the 4th order for astigmatism and 6th order for spherical aberration. For Zernike, the performance is not improving significantly beyond the 6th order, whereas the Q-polynomial converges for the 10th and the A-polynomial for the 12th order. The A-polynomial 2nd kind is also in this system not able to compensate for the lack of astigmatism correction, which results in a two times worse result compared to the other descriptions. The relatively similar performance can also be seen in the RMS spot value, which is best for the A-polynomials 1st kind and in a similar range, but worse for the Zernike and Q-polynomials. The A- polynomials 2nd kind is a factor of two worse than 1st kind set.

The corresponding surface sag contributions are shown in table 4.18. For the first three descriptions, they are very much alike, as the basic shape is a biconic (with a larger radius of curvature/conic constant in x than y) and the deformation terms are dominated by

astigmatism. The freeform surfaces are equivalent, with similar PV-values. For the A-polynomial 2nd kind both basic shape and deformation terms are mainly rotational symmetric and although similar in appearance the final freeform surface also lacks here the astigmatism correction.

Table 4.18 Performance data and sag-contribution for the different polar descriptions of the anamorphic system

	basic shape	deformation terms	total surface sag
Zernike	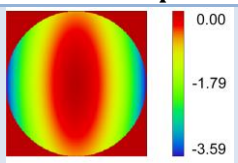	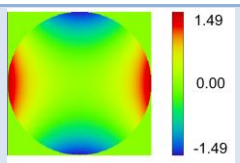	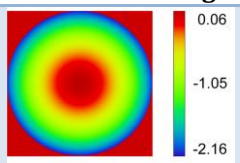
Averaged RMS spot / Airy radius		15.36 µm/ 1.29 µm	
Q-polynomials	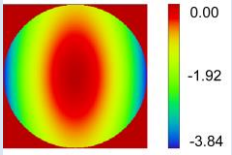	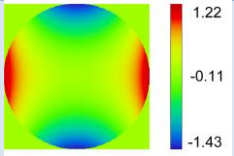	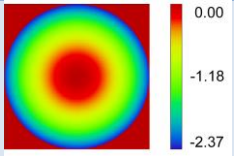
Averaged RMS spot / Airy radius		17.69 µm/ 1.29 µm	
A-polynomials 1st kind	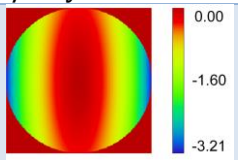	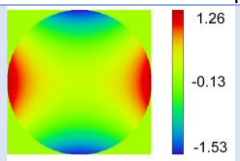	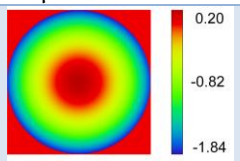
Averaged RMS spot / Airy radius		11.69 µm/ 1.29 µm	
A-polynomials 2nd kind	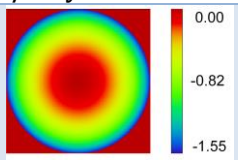	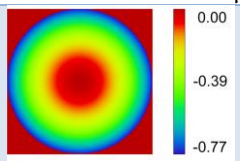	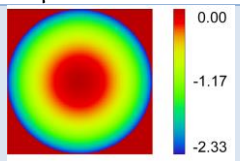
Averaged RMS spot / Airy radius		24.49 µm/ 1.29 µm	

The wavefront data of the remaining aberrations for the final results in table 4.19 show that for the anamorphic system the descriptions have quite different way of correcting. Similar to the Zernike, Q- and A-polynomials is the contribution of spherical aberration on axis (~0.300 λ) and coma x in the field (~-0.250 λ). For astigmatism 0° on axis the Zernike and Qs are almost equivalent (~0.370 λ), but the A-polynomials 1st kind are two times worse (0.696). For astigmatism 0° in the field, Zernike and Q-polynomials have again very low values (-0.035, respectively -0.094 λ), whereas the contribution by the A-polynomials is up to 250 times larger (-0.871 λ). For astigmatism in 45°, on the other hand, are the Q- and A-polynomials identical (-0.097 λ) and more than three times smaller than the Zernike (0.349 λ). The coma y values in the field are very similar for Zernike and Q-polynomials (0.805, respectively 0.953 λ), but ten times smaller for the A-polynomials (-0.098 λ).The spherical aberration in the field is slightly better for the As (0.430 λ) and comparable to the Chebyshev 1st kind and Legendre

for the Zernike (0.604 λ), but almost three times larger for the Q-polynomials (1.529 λ). The A-polynomials 2nd kind show the same picture as for the other three descriptions: for astigmatism, the value is reduced by a factor of 3 (3.205 λ), in the field by 25 % for 0° (-10.923 λ) and increased by a factor of 13 for 45° (40.717 λ). Coma in the field is up to 20 times larger (44.617, respectively 55.663 λ) compared to the initial system and the spherical aberration on axis is ten times higher (23.940 λ) and in the field 20 times (33.009 λ).

Table 4.19 Polar descriptions: primary aberration coefficients [λ] for a wavefront of the final results of the anamorphic system

field	Zernike	Q-polynomials	A-polynomials 1st	A-polynomials 2nd
on axis				
astigmatism (Z5/Z6)	0.352/0.000	0.391/0.000	0.696/0.000	3.205/0.000
coma (Z7/Z8)	0.000/0.000	0.000/0.000	0.000/0.000	0.000/0.000
spherical aberr. (Z9)	0.293	0.341	0.265	23.940
max x /max y				
astigmatism (Z5/Z6)	-0.035/0.349	-0.094/0.097	-0.871/-0.097	-10.923/40.717
coma (Z7/Z8)	-0.235/0.805	-0.287/0.953	-0.239/-0.098	44.617/55.663
spherical aberr. (Z9)	0.604	1.529	0.430	33.090

In figure 4.18 the best performances for Cartesian and polar-defined descriptions are shown. It can be seen, that the polar representations are here generally equal or better in the result for all orders, but specifically the final one. The difference between the best polar (A-polynomials 1st kind) and Cartesian one (Monomials) is almost a factor of 2 in merit function and resulting RMS value of the spot, which is probably caused by the limited number of contributing terms.

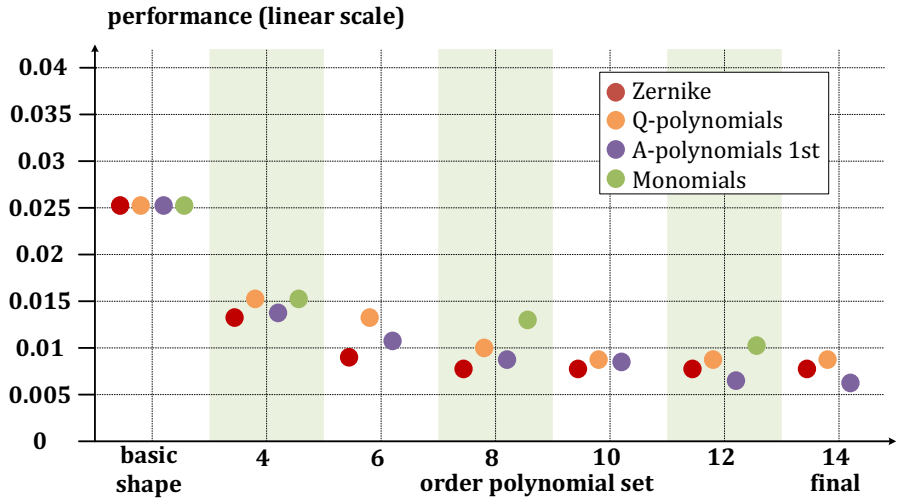

Figure 4.18 Best performances for anamorphic system

Conclusion for the convergence of the orders

For most systems, there was no significant difference in performance for Cartesian and polar descriptions, because both were able to correct for the aberrations significantly. Since the systems used here mainly suffered from astigmatism and coma, the largest improvement came from the 4th order for polar descriptions and 4th (astigmatism) and 6th order for Cartesian descriptions. Although a biconic basic shape was used, an additional correction with the deformation terms for astigmatism is needed for a good result, as it could be seen in the failure of the A-polynomials 2nd kind.

A significant difference in performance of the Cartesian descriptions, among others due to the different weighting, was only seen in case of the TMA. Here the emphasised boundary for Chebyshev 2nd kind and Legendre was disadvantageous for the improvement of the correction. Over all investigated systems the Chebyshev 1st kind seems to be the most flexible Cartesian description, in most cases with the best or nearly the best results out of the four descriptions.

For polar descriptions, the results are similar. Specifically, the Zernikes and Q-polynomials were very much alike in their correction behaviour and are almost interchangeable. The A-polynomials 1st kind showed a comparable performance, whereby for systems with a certain decoupling at the boundary like the Yolo-telescope, they had a significantly better performance.

An impact of the defining domain on the performance of the description was not seen.

The main aspect for the convergence over the orders is the remaining symmetry of the system and the decoupling of x and y at the boundary, due to asymmetry in the system.

For a system with a remaining plane-symmetry and relatively strong coupling, polar descriptions are slightly preferable, like the HMD. For asymmetric systems, the choice is mainly influenced by the degree of decoupling. If only the boundary is affected, Cartesian descriptions and the polar defined A-polynomials 1st kind are of more benefit, but the other polar descriptions are still to a certain extent useful. The stronger the decoupling, so in this case the stronger the asymmetry due to the different tilts in the Yolo-telescope, the more Cartesian descriptions will be preferred. For some systems like the TMA, both descriptions have a comparable impact. Hereby the basic ability of the different descriptions to correct for astigmatism and coma was sufficient.

The anamorphic system is a special case: x and y are to a certain extent decoupled, due to the

different specifications in both directions, but due to the double-plane symmetry and the resulting loss of polynomial terms the Cartesian descriptions have not enough degrees of freedom and are not able to correct appropriately.

This leads to the question: How many of the representations do we really need?

- For asymmetric and strongly decoupled systems:

The Chebyshev 1st kind are the first choice.

- For strongly coupled systems, due to the remaining symmetry:

The Zernike or Q-polynomials are preferable to use.

- However, for neither extreme case:

The A-polynomials 1st kind are a very good choice, with very good performance in systems with different remaining symmetry and coupling.

4.4 Impact of orthogonality on convergence

Previous investigations [64, 95] have indicated that the convergence speed is mainly dependent on the presence of orthogonality, not on the kind of orthogonality. Therefore, for the evaluation of the convergence behaviour within one order, the best performing description in section 4.3 for each orthogonality was chosen:

- Non-orthogonal: Monomials
- Spatial-orthogonal: Zernike
- Gradient-orthogonal: A-polynomials 1st kind

The systems presented here, are the Yolo-telescope and the HMD. Both are with their final results near to or within diffraction limit. Moreover, they have shown a difference for the choice of descriptions, due to the remaining symmetries, as seen in the previous section.

For the optimisation of each description, 300 cycles for each polynomial order were used, with the merit function value being logged after every 5 cycles. The following convergence plot for each system, show therefore order by order the decrease of the error function over the 300 cycles within one order. Compared to the previous sections the performance was normalised here.

Head-mounted display

In figure 4.19 shown is the convergence of the polynomial sets for the HMD. The final results for each order were already shown and discussed in figure 4.13 and 4.14.

The merit function converges typically between 20 and 45 cycles for all descriptions equally over all orders, with a few exceptions (table 4.20): Specifically, the Monomials have more problems in convergence in the 8th and 12th order. Here 55, respectively 135 cycles are needed. In the final 14th order the merit function convergences very slowly, with a relatively large drop after more than 200 cycles. For more cycles, the results improve slightly but converge finally at 245 cycles. The Zernike polynomials also have slight problems 6th and 10th order. In all cases, up to 60 cycles are needed until they finally converge. The A-polynomials converge within the 45 cycles except for the 14th order, there also 160 cycles are needed, and 12th order with 5 cycles. In both cases is the overall change of the merit function minor, but in the latter order is the convergence speed very low. The total number of cycles needed is with 530 cycles for Monomials 2 times larger than for Zernike and A-polynomials 1st kind. The slightly larger value for the As results mainly from the 14th order. Considering only lower orders the 1st kind -polynomials converge almost two times faster than Zernike and Monomials.

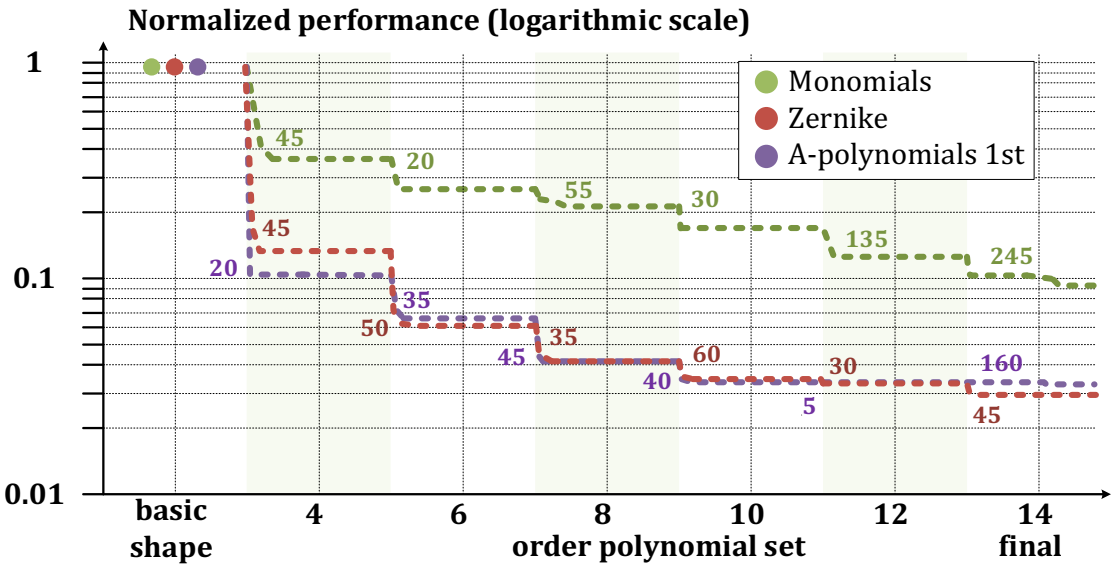

Figure 4.19 Convergence within each order for HMD with the number of cycles needed for the final result (see table 4.20)

Table 4.20 Number of cycles needed for the final result by each order and description for HMD with Zemax DLS

order polynomial set	Monomials	Zernike	A-polynomials 1st kind
4th	45	45	20
6th	20	50	35
8th	55	35	45
10th	30	60	40
12th	135	30	5
14th	245	45	160
total	530	265	305

Yolo-telescope

The results for the Yolo-telescope are shown in figure 4.20. The final performance for each order was presented and discussed before in figure 4.7 and 4.8.

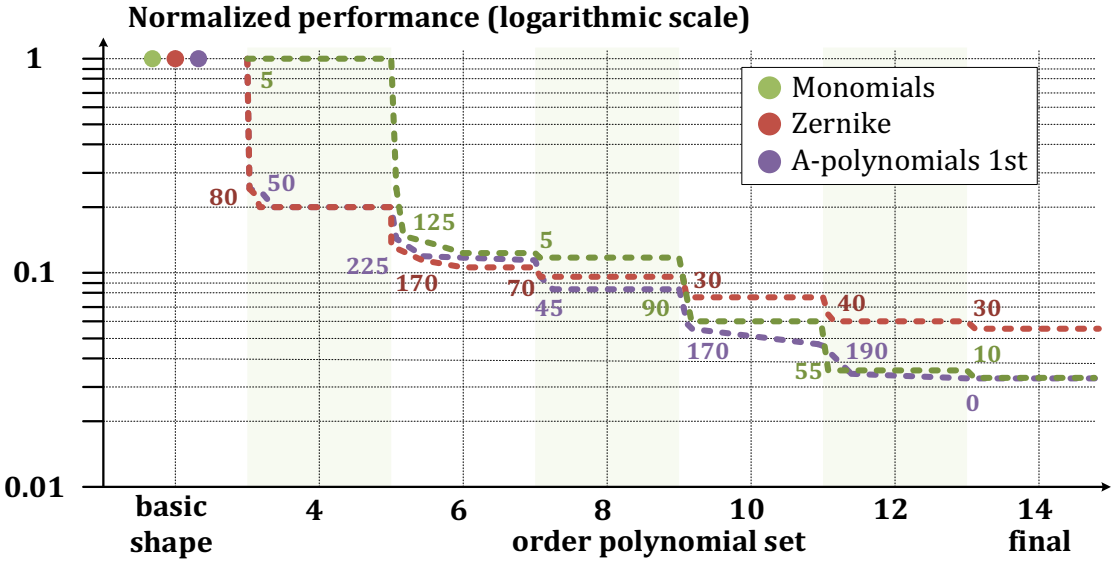

Figure 4.20 Convergence within one order for Yolo-telescope with the number of cycles needed for the final result (see table 4.21)

In case of the non-symmetric Yolo-telescope, the descriptions seem to have much more problems in convergence. Between 30 and90 cycles are needed for all of them (table 4.21), except the Monomials, who need only 5 to 10 cycles in the 4th, 8th and 14th order. This probably results from the minor changes in the merit function, occurring in these orders. With 125 cycles, the descriptions need significantly more cycles for convergence in the 6th order, similar to the Zernikes with 175 cycles. Moreover, the A- polynomials have a problem with the higher orders. Although the major improvement step is within the first 50 cycles, the merit function is reduced by small values constantly over the further cycles. This effect is seen in the 6th, 10th

and 12th order. It has to be noted after the performance is here already within the diffraction limit. The minor changes in merit function are of only small influence in the RMS spots sizes, also seen in the unchanged performance with the 14th order. Contrary to the previous results is the number of total cycles needed here lowest for the Monomials and highest for the A-polynomials, although interestingly both end up with comparable final results.

Table 4.21 Number of cycles needed for the final result by each order and description for Yolo-telescope with Zemax DLS

order polynomial set	Monomials	Zernike	A-polynomials 1st kind
4th	5	80	50
6th	125	170	225
8th	5	70	45
10th	90	30	170
12th	55	40	190
14th	10	30	0
total	290	420	680

Conclusion for the convergence within one order

In case of the HMD, the descriptions have a relatively uniform convergence within a small number of cycles (20 to 45). Nevertheless, for a few orders, the non-orthogonal Monomials and A-polynomials 1st kind show a slower convergence up to a factor of 6 in a number of cycles.

For the Yolo-telescope the convergence is more problematic for all descriptions. The number of cycles typically needed is with 30 to 90 relatively large and as far as it was seen non-deterministic. Moreover, the A-polynomials 1st kind have problems with constantly, but small changes in the merit function, which increases the number of needed cycles tremendously.

Previous work [94], has shown a more significant result. Nevertheless, it can be seen that for higher orders, the convergence can be a problem if the results are already near to the local minimum. Here the merit function usually only changes in small values, with limited impact on the performance.

4.5 Convergence behaviour of other algorithms

As indicated at the beginning of this chapter, there are only a few publications dealing with a comparison and evaluation of surface descriptions. Moreover, the ones known are using either Zemax or CODE V, and no OSLO at all. Therefore, the question is: Are the results and conclusions transferable to algorithms of other software platforms? This question has three aspects:

1. The convergence over the orders, so the choice of description, due to the correction, as shown in section 4.3.
2. The convergence within on order, so the number of cycles needed, shown in section 4.4.
3. Comparability of software platforms, so the question if the results are finally depending on the implemented optimisation algorithm of the software used.

To evaluate this for the first time, the HMD system known from the previous sections with the three descriptions of Monomials, Zernike and A-polynomials 1st kind, was chosen. For the implementation of the descriptions, an interface for the DLLs, written for Zemax, was added to use them also for the CODE V and OSLO. For the optimisation, the DLS algorithm, as before in Zemax, is also used for the other two platforms of CODE V and OSLO. Moreover, in case of CODE V, the DLS was evaluated with and without activating the Step-optimization for a comparison. Only few information is available for the algorithms; this seems to be a confidential issue for the companies. However, from experience with rotational symmetric systems, it can be said, that the DLS (with Step) of CODE V can be much faster and better in the final solution as pure DLS, as demonstrated here [105]. The Step should hereby help to overcome shallow minima. A few years ago, a small comparison between DLS with and without Step for a freeform zoom system was demonstrated [64]. The results indicate that a positive effect of Step is also occurring in case of a freeform system. A comparison between Zemax, CODE V and OSLO, as three of the leading software tools for designing optical systems, could not be found in the literature.

The starting point of this investigation is, therefore, to set up the HMD system in all three software platforms. A small modification had to be done, because a pick-up of the semi-diameter, as used in Zemax to guarantee, that the norm-radius/-width is always within the range, is not possible for CODE V and OSLO using DLLs. Therefore, the norm-values were fixed since the change over all orders is below 3% for the semi-diameter, this has no significant

impact on the result. Table 4.22 shows the system data for the software tools. The settings are identical. Moreover, the spot shapes and wavefronts for all fields are similar. The minor differences in values for the RMS spot and wavefront are probably more to slightly different numeric, but for the final evaluation not of significant relevance.

Table 4.22 Overview of the system data for the HMD for the different software platforms

programs	Zemax	CODE V	OSLO
EFFL	43.584	43.563	43.563
F-number	10.903	10.891	10.891
EPD [mm]	4	4	4
RMS spot radius (averaged over all fields) [µm]	105.72	104.63	108.67
RMS wavefront (averaged over all fields) [waves]	1.92	2.03	2.16

In the following, the performance over and within each order for the individual software tools are discussed. The results for Zemax were shown in section 4.4 and therefore are not repeated here but will be later compared to the other results regarding the comparability. The performance data are here as well normalized, since the different software tools have individual calculation schemes for the merit function and therefore the absolute starting values differ from 0.079, respectively 0.089 -for OSLO and Zemax- to 986 for CODE V. The overall improvement of the error function is a factor of about 40 for OSLO and Zemax and almost 2000 for CODE V. Nevertheless, this gives no indication about the absolute final results, only about the relative improvement within and over the orders. Therefore, the final results are discussed separately.

OSLO™

The performance of error function over the orders and within is shown in figure 4.21. Similar to the previously shown performance by Zemax (figure 4.19) is the main improvement in the 4^{th} order. Moreover, it can be seen that the Monomials are constantly improving, but with less impact by each order, whereas the Zernike and A-polynomials 1^{st} kind have a larger improvement by the 4^{th} to 8^{th} order, which leads to an error function, which is almost a magnitude of order better than for Monomials. The A-polynomials 1^{st} kind and Zernike have almost equivalent results over all orders, similar to Zemax. The convergence within one order is hereby typically between 5 and 25 cycles fo all three descriptions, except the almost 160 cycles the A-polynomials 1^{st} kind needed for the 12^{th} order, as well as the 280 cycles the Zernike needed for the 12^{th} and 165 cycles for 14^{th} order. In both cases, the performance was

already diffraction limited before and the results were more a fine-tuning of the merit function criteria. Moreover, for the 8th order, the Monomials needed 80 cycles for the convergence. The difference in the total number of cycles results mainly by the final orders as before. For lower order, the orthogonal descriptions are about two times faster in convergence.

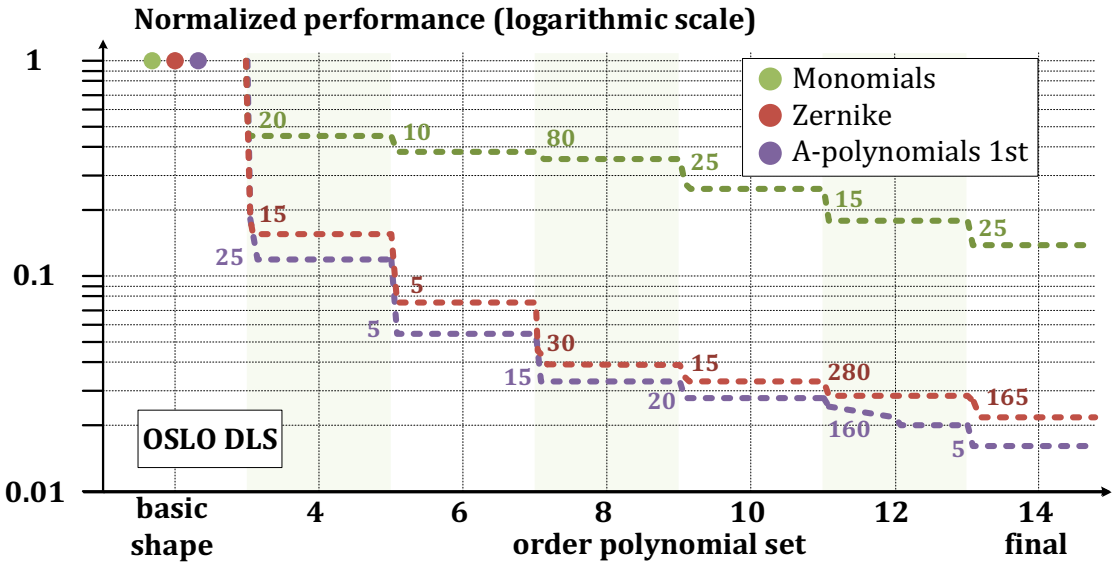

Figure 4.21 Performance of normalised error function for HMD using DLS by OSLO with the number of cycles needed for the final result (see table 4.23)

Table 4.23 Number of cycles needed for the final result by each order and description for HMD using OSLO DLS

order polynomial set	Monomials	Zernike	A-polynomials 1st kind
4th	20	15	25
6th	10	5	5
8th	80	30	15
10th	25	15	20
12th	15	280	160
14th	25	165	5
total	175	510	230

CODE V™

The performance of the standard DLS in CODE V is shown in figure 4.22. One major difference between the previous two calculations is visible (table 4.24): The Monomials are improving much better relative to the other descriptions and are even slightly better than the A-polynomials for the 4th order. Moreover, the Zernike and A-polynomials 1st kind have in this case a relatively different performance over the orders. The first one benefit mostly from the

8th and 14th order, whereas the latter one improves most with the 6th order and less, but still significant with the 8th ,10th and 14th order. Therefore, for the 6th and 12th order, the results of all three are relatively nearby. With the final order, the Monomials are 3 to 4 times worse in error function than the polar descriptions.

For the convergence, within one order the descriptions typically need only 5 to maximum 15 cycles, except for Zernike in the 8th, 12th and 14th order, where 50, 25 and finally 115 cycles were needed. Additionally, for the 8th,10th and 12th order the A-polynomials 1st kind needed 45 cycles, whereby for the 10th order the value kept stable from the previous order for 40 cycles before it dropped within 5 cycles. With a total number of 65 cycles, the Monomials were three times faster than the other two descriptions here.

Table 4.24 Number of cycles needed for the final result by each order and description for HMD using CODE V DLS

order polynomial set	Monomials	Zernike	A-polynomials 1st
4th	5	5	5
6th	5	5	5
8th	5	50	30
10th	30	5	45
12th	5	25	45
14th	15	115	45
total	65	205	175

CODE V™ with Step-optimisation

The DLS using Step optimisation is shown in figure 4.23. Compared to the previous results by the purely DLS, for Monomials and A-polynomials 1st kind no difference in the convergence of the orders can be seen. For the Zernike polynomials, the performance is identical in 4th, 6th and 12th order. The major improvement, seen before in the 10th order is now already appearing in the 8th. Therefore, there is no further progress in the 10th order. Moreover, the improvement in the final order is improved compared to without Step. As for the other algorithms seen, the result of the two polar descriptions is between 3 and 5 times better than for the Monomials.

The convergence within one order is typical with 5 to 10 cycles, with the only exception of the Zernike in the 14th order. Here 60 cycles are needed before the convergence is reached. Moreover, the A-polynomials 1st kind converge 20 cycles in the 8th order, whereas the

Monomials reach the final result in the 14th order after 15 cycles.

Overall compared to the pure DLS in CODE V it can be said, that the convergence speed is about two times faster for the Zernike and A-polynomials and about 50 percent for the Monomial.

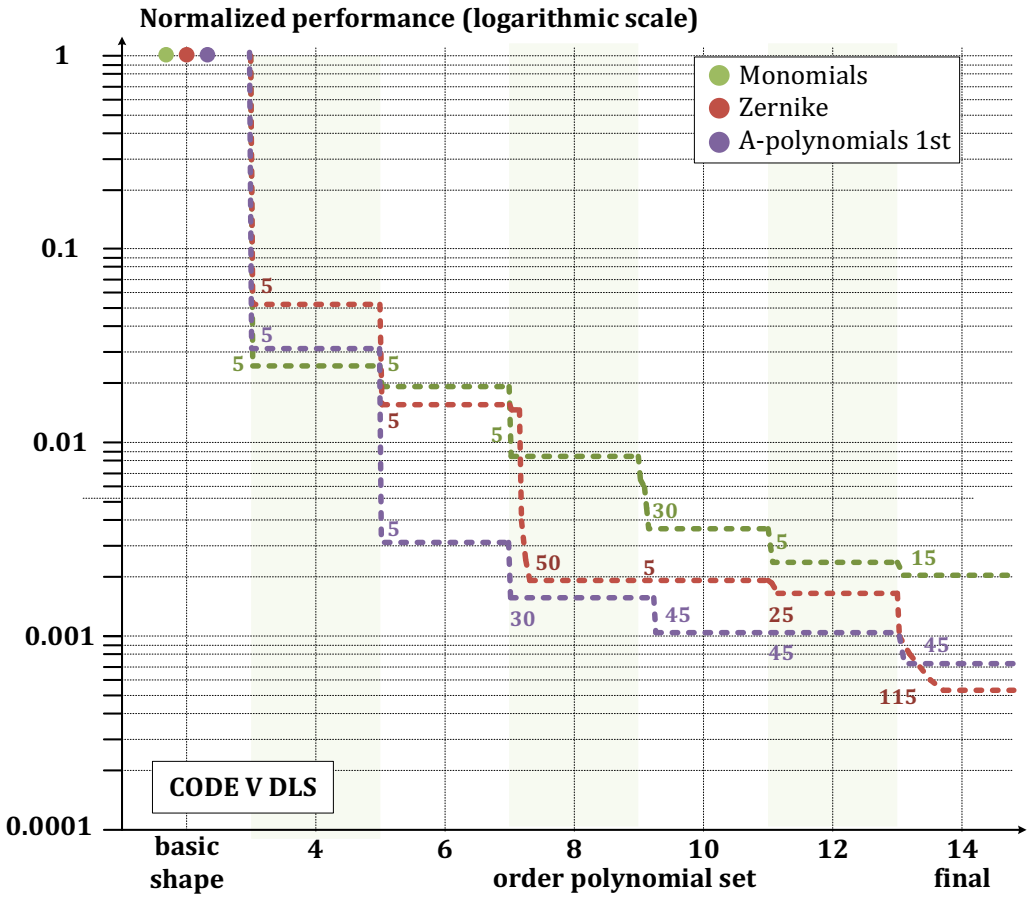

Figure 4.22 Performance of normalised error function for HMD using DLS by CODE V with the number of cycles needed for the final result (see table 4.24)

Table 4.25 Number of cycles needed for the final result by each order and description for HMD using CODE V DLS with Step

order polynomial set	Monomials	Zernike	A-polynomials 1st
4th	5	5	5
6th	5	10	5
8th	5	5	20
10th	10	15	5
12th	5	5	5
14th	15	60	10
total	45	100	50

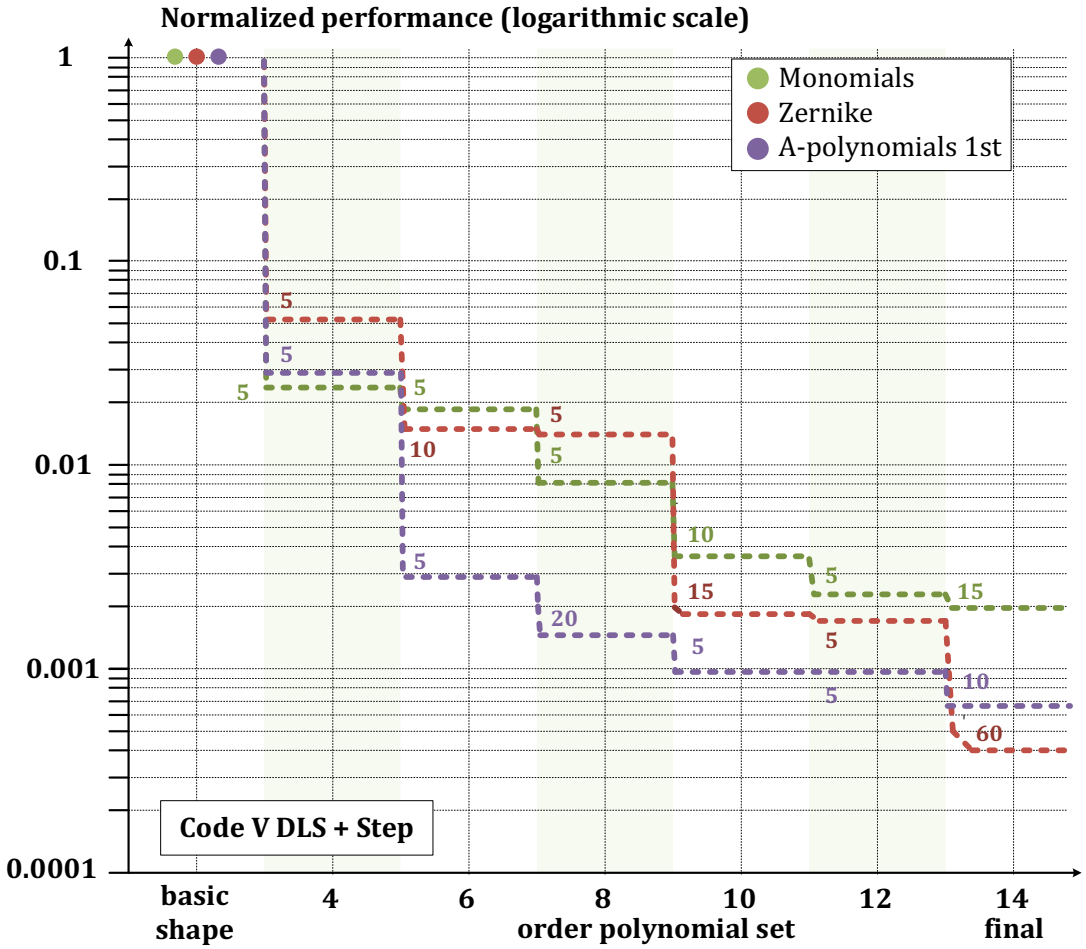

Figure 4.23 Performance of normalised error function for HMD using DLS with Step optimisation by CODE V with the number of cycles needed for the final result (see table 4.25)

Comparison between the different algorithms

It can be seen, that the algorithms have quite similar behaviour and results of final quality. For a comprehensive comparison, a look at the final results for each algorithm is needed. Therefore, in table 4.26 the summarised data for Monomials, Zernike and A- polynomials 1st kind of the four algorithms are shown.

In the error function plots, it was already seen that the polar description gives comparable performance, with slightly better results for the Zernikes compared to the other two descriptions in all software tools except OSLO. The same can be said for the spot and wavefront data here. The difference is hereby between 13 (CODE V) and 26 % (CODE V with Step) in the spot and up to 20 % in the wavefront. Nevertheless, the results for all polar descriptions and the Cartesian ones in CODE V (with and without Step) are diffraction limited. Moreover, the difference between the Monomials and the other two descriptions are, as seen before in the plots, between a factor of 2 (CODE V) and 9 (OSLO).

Table 4.26 Final results for RMS spot and wavefront (both averaged over all fields) for the three descriptions and four algorithms.

	Monomials	**Zernike**	**A-polynomials 1st**
Zemax			
RMS spot / Airy radius [µm]	10.01 /7.64	3.33 / 7.06	3.90 / 7.07
RMS wavefront [waves]	0.184	0.06	0.07
OSLO			
RMS spot / Airy radius [µm]	17.13 / 8.08	2.61/ 7.76	1.86/ 7.40
RMS wavefront [waves]	0.303	0.04	0.06
CODE V			
RMS spot / Airy radius [µm]	4.23 / 7.68	2.11 / 7.06	2.40 / 7.06
RMS wavefront [waves]	0.121	0.06	0.06
CODE V + Step			
RMS spot / Airy radius [µm]	4.23 / 7.68	1.89/ 7.06	2.39/ 7.06
RMS wavefront [waves]	0.121	0.05	0.06

The overall best results are obtained for:

- Monomials: CODE V (with and without Step)
- Zernike: CODE V (with Step)
- A-polynomials 1st kind: OSLO

CODE V and OSLO can achieve up to two times better results for Zernike and A-polynomials, whereas for Monomials CODE V is two times better than Zemax and four times better than OSLO. When we look at the corresponding surface sag contribution (see table 4.27) it can also be seen that for the two CODE V algorithms the contribution is identical, whereas for the A-polynomials 1st kind the surface is similar, but with much more dominating deformation terms.

The OSLO surface has similarities, specifically in the outer shape, but the composition of basic shape and deformation terms with a similar pattern but of opposite sign seems not to be beneficial.

For the Zernike polynomials, seen in table 4.28, the sag contribution of the Zemax, OSLO and CODE V (without Step) look very similar, whereas the slightly better version of CODE V with Step looks slightly different compared to the others. Nevertheless, the distribution between the basic shape and is deformation is completely different for all four algorithms: For Zemax the biconic basic shape is dominating, whereas for OSLO (also with biconic basic shape) the deformations terms are the dominating part. For CODE V, the basic shape is of almost no influence in case of Step and of minor one without Step.

Table 4.27 Sag-contribution for Monomials

	basic shape	deformation terms	total surface sag
Zemax DLS	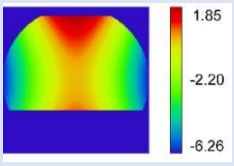	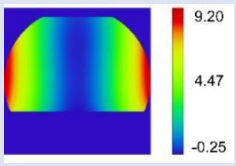	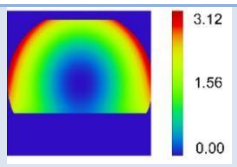
OSLO DLS	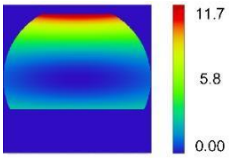	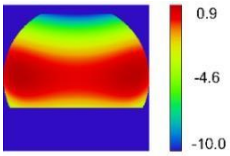	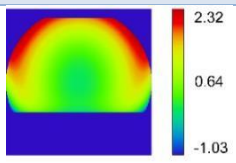
CODE V DLS	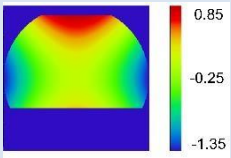	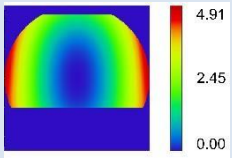	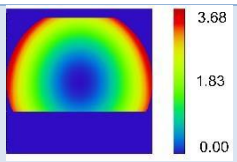
CODE V DLS + Step	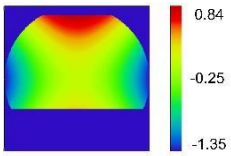	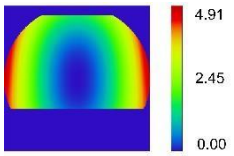	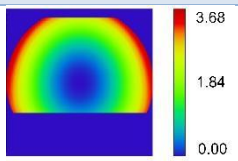

Table 4.28 Sag-contribution for Zernike

	basic shape	deformation terms	total surface sag
Zemax DLS	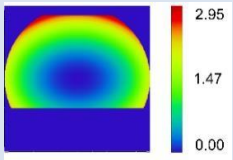	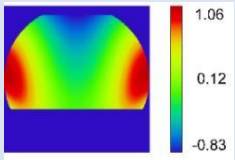	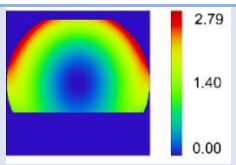
OSLO DLS	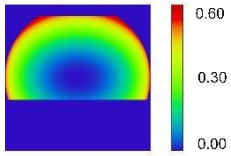	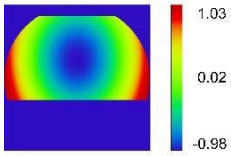	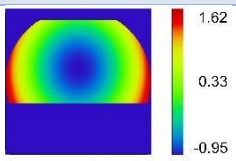
CODE V DLS	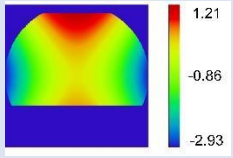	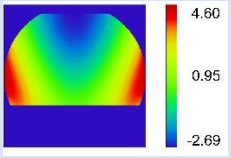	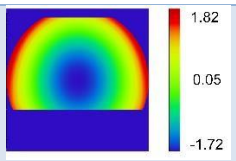
CODE V DLS + Step	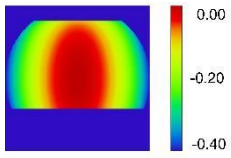	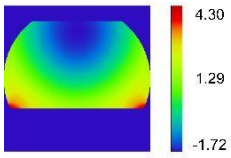	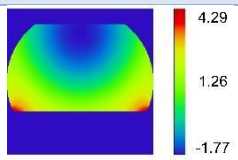

For the A-polynomials 1st kind, the results (table 4.29) for the two CODE V algorithm are identical and so is the surface, including the individual contribution by basic shape and deformation terms. The Zemax surface also uses a biconic basic shape, but of opposite sign and therefore more astigmatism dominated deformation terms are observed. The total surface is similar to the previous results for Zernike and Monomials. OSLO achieves the best performance result with a dominating freeform part, which is similar to the shape of the CODE V approaches. The total surface is then almost identical to the solution by the Zernike set.

Table 4.29 Sag -contribution for A-polynomials 1st kind

	basic shape	deformation terms	total surface sag
Zemax DLS	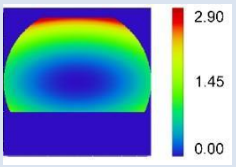	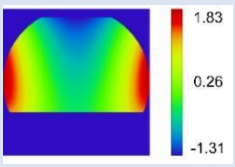	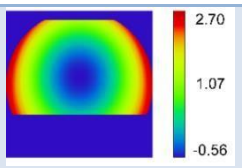
OSLO DLS	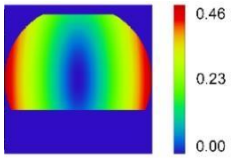	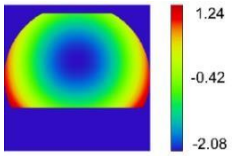	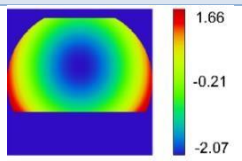
CODE V DLS	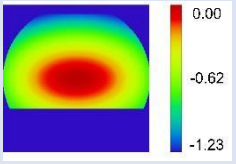	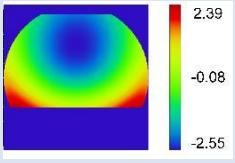	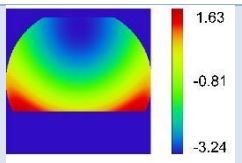
CODE V DLS + Step	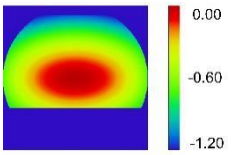	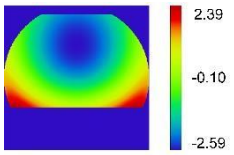	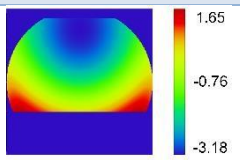

Conclusion for different algorithms

Although the algorithms show different behaviour for lower orders, specifically for CODE V compared to the other two, it can be seen that with the higher orders the results are all nearby. The polar descriptions have the much better performance for all algorithms compared to Monomials. The difference is ranging from a factor of 3 for Zemax and CODE V without Step up to a factor of 10 for OSLO.

Moreover, for the convergence of one order, it can be seen that the DLS algorithm of CODE V, specifically with Step-optimization is improving the typical number of cycles needed up to a

factor of 4. Nevertheless, the total number of needed cycles per order for the other software is with 20 and less still quite low.

The final results of the different algorithm are relatively similar: The Monomial descriptions are not as good as the polar descriptions in all versions. In case of the other two descriptions, the A- polynomials 1st kind are slightly preferred by the OSLO algorithm, whereas the Zernikes are with slightly better performance for the other three ones. It can be seen that the general outcome of the different algorithms is not much different and therefore the choice of description is not influenced by the algorithm used for the optimisation.

It is seen, that OSLO and CODE V are able to reach a better result than Zemax for the polar descriptions, within a factor of two. For the Monomials, on the other hand, OSLO has significantly worse results than the others, which may be caused by the non-orthogonality of the description.

Overall it can be said, that the correction behaviour of the different algorithms is very similar. Therefore, the conclusions from the previous sections can also be applied to the other algorithms in CODE V and OSLO. The final results of the different software tools differ less than a factor of 2 for the convergence within one order, which is for such small number of cycles negligible. For more complex systems with more than one freeform, this might be of more effect.

Part of this work regarding the convergence behaviour of different optimization algorithms can be found in the labwork of Siti Heder [107].

4.6 Summary and conclusion for application

In this chapter, the assessment and evaluation of different freeform surface descriptions were presented. The focus was hereby on the impact of the basic shape, surface descriptions properties like orthogonality, as well as optimisation algorithm on the performance of the description concerning convergence and level of final quality.

The investigated systems, diverse as they were, showed a very similar behaviour: the outer boundary was comparable for all descriptions, with a smaller correction impact. For a better correction, the centre part of the surface was of more importance. Generally spoken, the effect of the domain on the results is minimal. On the other hand, the effect of the defining grid for the description is of much higher influence. Additionally, the higher order contributions by the individual representations made the final difference. Nevertheless, the variation of the

different descriptions was not as strong as might expected. Except for the Monomials in one case, the worst results were less than a factor of 2 than the best. Additionally, the aperture of the freeform surface and description did not influence the results at all. The impact of the orthogonality was only partly seen in the result of faster convergence within one order by the orthogonal sets. Another important aspect is the basic shape, which to some extent has an even more significant impact on the final performance than the choice of description itself. With systems suffering from astigmatism, a more sophisticated basic shape like a biconic can reduce the number of additional needed freeform parameters to a third to represent the same system or improve the system by a factor of 2 with the same number of freeform terms.
Except for the remaining symmetry and a potential decoupling of x and y, a significant impact of the system parameter like a field of view, entrance pupil diameter or F-number could not be seen. Moreover, it could be shown, that the choice of descriptions is not influenced by the used software tools. The final results are comparable both in the speed of convergence and absolute values. This leads to the question: What is the best choice?

Table 4.30 Criteria for choice of description (++ very good, + good, o sufficient, - problematic, -- fail, N/A: not available)

criteria	Monomials	Chebyshev 1st	Chebyshev 2nd	Legendre	Zernike	Q-polynomials	A-polynomials 1st	A-polynomials 2nd
easy access to aberrations	o	o	o	o	++	++	++	+
fast convergence speed (above the diffraction limit)	+				+		++	
direct relation to tolerancing	N/A	N/A	N/A	N/A	N/A	++	++	++
simple and robust import/export of data (conversion)	++	++	++	++	++	o	o	o
simple extension of surface (slopes)	-	-	-	-	-	++	++	++
“ability of correction”:								
non-symmetric system	++	++	++	++	+	+	++	--
plane-symmetric system	o	++	o	o	++	++	++	--
double-plane-symmetry	o	-	-	-	+	+	+	--
large astigmatism	o	+	o	o	+	+	++	--
large coma	o	o	o	o	+	+	++	--

In table 4.30, an evaluation of the criteria for a good freeform surface description, as introduced in section 1.7, is shown. Not explicitly mentioned here is the effective and robust calculation, specifically for intersection points, which is generally given for polynomial descriptions. Moreover, in a recent work [108] the fitting behaviour of the different descriptions were tested, and it can be seen, it generally is possible for all descriptions, with advantages for the representation, which excelled in the optimisation, like Chebyshev 1st kind, Zernike, Q- and A-polynomial 1st kind.

Thinking solely on the final result from each of the presented descriptions should be sufficient, except for the A-polynomials 2nd kind. Nevertheless, there are more detailed aspects to consider. The Chebyshev 1st /2nd kind and Legendre have only about half of the parameter number of the Zernike Fringe set, for example, and can reach similar results, specifically for non-symmetric systems. In contrary, when it comes to higher order correction the Zernike Fringe, Q-polynomial or A-polynomial 1st kind are more beneficial. Moreover, the easy access to the aberration for the three descriptions is an advantage in the handling and optimisation as it can be seen. For data exchange and manufacturing, descriptions of a polynomial structure are preferred. However, since to the projection factor for Q-polynomial and A-polynomials 1st kind cause these descriptions to not be real polynomials anymore, this can be a disadvantage for later processes. On the other hand, the projection factor offers the opportunity to tolerance directly with the coefficients, which is a huge advantage.

Deciding on a sufficient description is therefore highly depending on the further process with the system. However, to cope with a high number of possibilities the following descriptions are highly recommended:

- Zernike Fringe with a biconic basic shape for systems with remaining symmetry: spatial-orthogonal description with fast convergence, simple data transfer for manufacturing, easy access to aberrations (implemented in most of the commercial optical design software)
- Chebyshev 1st kind with a biconic basic shape for strongly asymmetric systems: spatial-orthogonal description with a small number of parameters, simple data transfer for manufacturing (not broadly implemented in most of the commercial optical design software)
- A-polynomials 1st kind with biconic basic shape can be broadly used in symmetric and non-symmetric systems: gradient-orthogonal description with fast convergence, for tolerancing: easy access to tolerancing with the coefficients and simple extension of the basic shape (not yet implemented in any of the commercial optical design software)

Chapter 5 Conclusion and Outlook

In this work, freeform surfaces descriptions were developed and evaluated for use in non-circular symmetric optical imaging systems. It can be said that freeform surfaces can improve the system tremendously with only one sophisticated surface. Crucial for the correction of the aberration in this system and final performance is how good the description can represent the needed correction.

With the requirements from the optical design and manufacturing, like fast and robust calculations, superior results with only a few numbers of parameters and easy access to aberrations, tolerancing and conversion of data for import and export, globally defined polynomial descriptions are a suitable choice.

In a first step, the general approach of this kind of representation and the structure of such a polynomial set was introduced. Moreover, a selection of well-known descriptions used in design and mathematics, as well as a recently published approach for a freeform polynomial set, was described more detailed.

Although a huge variation of descriptions is published, there still seems to be an option missing, which combines the advantages of the individual descriptions. Therefore, two new sets, called A-polynomials 1st kind and 2nd kind were developed. They incorporate a biconic basic shape, for better astigmatism correction, a projection- factor for an easier access to tolerancing along the normal of the surface, a gradient-orthogonal polynomial set for faster convergence, with the Zernike-polynomials as the basic function for an easier access to the aberrations. Moreover, the polar defined polynomial sets were developed on a square domain for better accordance with non-circular shaped domains.

In a comprehensive benchmark, the selection of already existing descriptions and the two new sets were evaluated for their benefit in the design of typical freeform imaging systems.

It could be seen that the extension of the basic shape to a biconic can improve systems suffering from large astigmatism either up to a factor of two or reduce the number of needed freeform terms to a third, compared with a conical basic shape. Nevertheless, although a major part of the astigmatism correction can be done with the basic shape, a higher order contribution by the freeform terms still seem necessary.

The convergence behaviour and final performance of the eight evaluated descriptions have

shown, that the difference is not as significant as expected. Except for the newly developed A-polynomials 2nd kind, which fail completely due to the lack of primary astigmatism contribution and partly the Monomials, due to the lack of orthogonality and complexity for higher orders, are all the descriptions relatively nearby and the results within one magnitude of order.

Contrary to the expectations, neither the system parameters (e.g. EPD, FOV, F/#) nor the coincidence of domain and footprint shape were of significant impact on the performance.

The main criteria for the right choice seem to be the remaining symmetry of the system and the resulting potential decoupling at the boundary, due to asymmetric conditions. Hereby it was seen, that for most systems a choice between Zernike and Q-polynomials is sufficient, due to the remaining plane-symmetry and therefore relatively strong coupling. Moreover, for asymmetric systems, the Chebyshev 1st kind emerged as a very good option. Nevertheless, for the different types of systems, the A-polynomials 1st kind met the expectations placed on them, with a uniformly good to very good performance.

Moreover, an initial investigation on the convergence speed with the commonly used DLS algorithm in the three most frequently used commercial software tools indicated that the optimisation algorithm is only of minor influence on the performance and the final results of different software tools are comparable.

Generally, it can be seen, that the handling and the right choice of criteria and parameter seem to be of more impact than the description itself. At the moment, without many experiences, it is feasible to use relatively simple settings and initial values (like zero for the polynomial terms), as it was done in this benchmark. However, with the experience of more systems, it should be possible in the future to have a better understanding of the influence of the settings for the performance, like merit function definition or weighting. Moreover, in combination with enhanced aberration theory for freeform surfaces, it should be possible to select the terms needed for correction and the initial values target-oriented. This approach would probably also alter the benefit of certain descriptions towards the representations, which directly represents aberrations, like the polar ones.

Nevertheless, for the systems and design problems, we are facing now, the available and new descriptions give us a good selection to choose from, depending on individual preferences and goals in the design.

Appendix A: Sorting

Monomials, Chebyshev 1st kind, 2nd kind and Legendre

With a simple transformation, the double-indices (m,n) can be transformed into a single-index j, which sorts the polynomials -similar to the Zernike Fringe- by aberrational order:

$$j = \left\lfloor \frac{(m+n)(m+n+1)}{2} + (n+1) \right\rfloor , \tag{A.1}$$

with $\lfloor x \rfloor$ = largest integer smaller than x.

Moreover, backwards from a single-index to double-index:

$$\begin{aligned} p &= \left(\left\lceil \sqrt{2j+0.25} - 0.5 \right\rceil \left\lceil \sqrt{2j+0.25} + 0.5 \right\rceil \right) / 2 - j , \\ q &= \left\lceil \sqrt{2j+0.25} - 1.5 \right\rceil - p \end{aligned} \tag{A.2}$$

with $\lceil x \rceil$ = smallest integer larger than x,

Zernike

with the single-index, j can be converted into the double-index (m,n) as

$$\begin{aligned} m &= \begin{cases} \dfrac{(\lfloor \sqrt{j-1} \rfloor + 1)^2 - j}{2} & \text{, if } (\lfloor \sqrt{j-1} \rfloor + 1)^2 \text{ - j is even} \\ \dfrac{j - (\lfloor \sqrt{j-1} \rfloor + 1)^2 - 1}{2} & \text{, otherwise} \end{cases} \\ n &= 2(\lfloor \sqrt{j-1} \rfloor) - |m| \end{aligned} \tag{A.3}$$

Additionally, the double-index can be transformed into the single-index by

$$j=\begin{cases}\left(\frac{n}{2}+1\right)^2 & \text{for } m=0\\ \left(\frac{|m|+n}{2}+1\right)^2-2|m| & \text{for } m>0\\ \left(\frac{|m|+n}{2}+1\right)^2-2|m|+1 & \text{for } m<0\end{cases} \tag{A.4}$$

Q-polynomials

Like the Zernike it is possible to sort the Q-polynomials with a single-index j:

$$j=\begin{cases}1 & \text{for } a_0^1\\ 2 & \text{for } b_0^1\\ (n+3)^2-2 & \text{for } m=0\\ (n+3)^2-2(m+1) & \text{for } m\neq 0,\ m+n>1,\ a_n^m\\ (n+3)^2-2m-1 & \text{for } m\neq 0,\ m+n>1,\ b_n^m\end{cases} \tag{A.5}$$

The transformation back to single-index is than

$$\begin{aligned}&\text{for } j\leq 2:\\ &j=1:\ m=1,\ n=0\ \&\ a_0^1\\ &j=2:\ m=1,\ n=0\ \&\ b_0^1\\ &\text{for } j>2:\\ &\text{if } j=\left\lceil\sqrt{j+2}\right\rceil^2-2:\\ &m=0\ \&\ n=\sqrt{j+2}-3,\\ &\text{if } j\neq\left\lceil\sqrt{j+2}\right\rceil^2-2:\\ &\left\lceil\sqrt{j+2}\right\rceil^2-2-j=\begin{cases}\text{even}: 2m, n=\left\lfloor\sqrt{j+2}\right\rfloor-m, a_n^m\\ \text{odd}: 2m-1, n=\left\lfloor\sqrt{j+2}\right\rfloor-m, b_n^m\end{cases}\end{aligned} \tag{A.6}$$

Symbols

$W(\eta,\rho,\phi)$	wave aberrations
$W_{\eta\rho\phi}$	wave aberration coefficient
S_I	Seidel sum
ρ, ϕ	(normalized) ray coordinates in the pupil
η	normalized height of object
a_{mn}, a_j	coefficient for double-/single-index sorted polynomials
$Z_n^m(\rho,\phi)$	Zernike-polynomials with double-index
w_i	weighting factor for the i^{th} parameter
$f_{tar,j}$	target values in merit function for the i^{th} parameter
$f_i(\vec{x})$	the objective function component of the i^{th} parameter in merit function
$M(\vec{x})$	merit function
γ	damping factor
$\vec{f}$	change vector
J	Jacobian-matrix of derivatives
I	identity matrix
$\Delta\vec{x}$	change of parameter vector in DLS
m,n / j	double-/ single-sorting index
M,N / J	maximum number of terms for double-/single-index sorting
F/#)	F-number
$F_i(\bar{x},\bar{y})$ / $F_j(\bar{r},\varphi)$	polynomial set in Cartesian /polar coordinates
$B(\bar{x},\bar{y})$ / $B(\bar{r},\varphi)$	boundary function in Cartesian /polar coordinates
$P(x,y)$ / $P(\bar{r},\varphi)$	projection factor in Cartesian /polar coordinates
z(x,y)	surface sag
z_{basic}	surface sag of basic shape
$\bar{x},\bar{y},\bar{r},\varphi$	(normalized) Cartesian/polar coordinates

c_x, c_y	curvatures in x and y
R	radius of curvature
κ_x, κ_y	conic constants in x and y
α	angle between normal of the surface and z-axis
δ_{nd}	normal departure
f^m, f^n	basis functions
$w(\bar{x},\bar{y})$	weighting function
C_m	constant for given parameter m
$T_m(\bar{x})$	Chebyshev 1st kind polynomial
$\delta_{mm'}$	Kronecker- delta
$U_m(\bar{x})$	Chebyshev 2nd kind polynomial
$P_m(\bar{x})$	Legendre polynomial
$N(m,n)$	normalization factor of Zernike polynomials
$R_n^m(\bar{r})$	radial part of Zernike polynomials
$\Phi^m(\varphi)$	azimuthal part of Zernike polynomials
$Q_n^0\left(\bar{r}^2\right)$	Q-polynomials (“mild asphere”-terms)
$Q_n^m\left(\bar{r}^2\right)$	Q-polynomials (freeform-terms)
a_n^m, b_n^m	coefficient for double -index sorted Q-polynomials
$A(\bar{x},\bar{y}) / A(\bar{r},\varphi)$	A-polynomials in Cartesian/polar coordinates
λ	waves (unit)

Abbreviations

2D	two-dimensional
bfs	best-fit-sphere
CAD	computer-aided design software
DLS	damned least square
EFFL	effective focal length
EPD	entrance pupil diameter
FOV	field of view
HMD	head-mounted display
MTF	modular transfer function
NAT	nodal-aberration theory
NURBS	non-uniform rational basis-spline
PV	peak-to-valley
RBF	radial basis functions
RMS	root-mean-square
SMS	simultaneous multiple surface method
TMA	three mirror anastigmat

List of tables

List of figures

References

[1] K. Schwarzschild, “Untersuchungen zur geometrischen Optik II. Theorie der Spiegelteleskope“ Abhandlungen der Gesellschaft der Wissenschaften in Göttingen, Mathematisch-Physikalische Klasse, Band IV (2), 1-28 (1905).

[2] P.L. Ruben, “Design and use of mass-product aspheres at Kodak “, Appl. Opt. 24, 1682-1688 (1985).

[3] A. Yabe, “Optical selection of aspheric surfaces in optical design”, Opt. Exp. 13, 7233-7242 (2005).

[4] G. W. Forbes, “Shape specification for axially symmetric optical surfaces,” Opt. Exp. 15(8), 5218–5226 (2007).

[5] R.N. Youngworth and E.I. Betensky, “Lens design with Forbes Aspheres”, Opt. Exp. 19, 21174-21179 (2011), Proc. SPIE 7100, 7100-0W (2008).

[6] B.Ma, L. Li, K. P. Thompson and J. P. Rolland, “Applying slope constrained Q-type aspheres to develop higher performance lenses”, Opt. Exp. 19, 21174-21179 (2011).

[7] J.P. McGuire, Jr., “Manufacturable mobile phone optics: higher order aspheres are not always better”, Proc. SPIE 7652, 7652-1O (2010).

[8] M. Beier, A. Gebhardt, R. Eberhardt and A. Tünnermann, „Lens centering of aspheres for high-quality optics”, Adv. Opt. Techn. 1, 441-446 (2012).

[9] R. Steinkopf, A. Gebhardt, S. Scheiding, M. Rohde, O. Stenzel, S. Gliech, V. Giggel, H. Löscher, G. Ullrich, P. Rucks, A. Duparré, S.Risse, R. Eberhardt and A. Tünnermann, “Metal mirrors with excellent figure and roughness“, Proc. SPIE 7102, 7102-0C (2008).

[10] F. Simon, G. Khan, K. Mantel, N Lindlein, and J. Schwider, "Quasi-absolute measurement of aspheres with a combined diffractive optical element as reference," Appl. Opt. 45, 8606-8612 (2006).

[11] I. Kitajima; “Improvements in lenses”, patent GB250268A (1925).

[12] H. J. Birchall, “Lenses and their combination and arrangement in various instruments and apparatus,” patent US2001952A (1935).

[13] L.W. Alvarez, “Two-element variable-power spherical lens”, patent US3305294A (1967).

[14] W. T. Plummer, “Unusual optics of Polaroid SX-70 Land camera”, Appl. Opt. 21, 196-208 (1982).

[15] B. Tatian, “Testing an unusual optical surface”, Proc. SPIE 554,137-147 (1985).

[16] X. Hu and H. Hua, "High-resolution optical see-through multi-focal-plane head-mounted display using freeform optics," Opt. Express 22, 13896-13903 (2014).

[17] O. Cakmakci, K. Thompson, P. Vallee, J. Cote, and. J. P. Rolland, “Design of a free-form single-element head-worn display,” Proc. SPIE 7618,7618-02 (2010).

[18] D. Cheng, Y. Wang, H. Hua, and M. M. Talha, "Design of an optical see-through head-mounted display with a low f-number and large field of view using a freeform prism," Appl. Opt. 48, 2655-2668 (2009).

[19] L. Li and A. Y. Yi, "Design and fabrication of a freeform microlens array for a compact large-field-of-view compound-eye camera," Appl. Opt. 51, 1843-1852 (2012).

[20] S. Gautam, A. Gupta and G.S. Singh, "Optical design of off-axis Cassegrain telescope using freeform surface at the secondary mirror", Opt. Eng. 54, 025113 (2015).

[21] C. Xu, D. Cheng, J.Chen and Y. Wang, "Design of all-reflective dual-channel foveated imaging systems based on freeform optics", Appl. Opt. 55, 2353-2362(2016).

[22] S. Chang, "Linear astigmatism of confocal off-axis reflective imaging systems with N-conic mirrors and its elimination," J. Opt. Soc. Am. A 32, 852-859 (2015).

[23] D. Korsch, "Reflective Optics", Academic Press (1991).

[24] X. Li and Z. Cen. "Optimization design of zoom lens systems." Proc SPIE 4927, 44-49 (2002).

[25] C. Miñano, P. Benítez, W. Lin, J. Infante, F. Muñoz, and A. Santamaría, "An application of the SMS method for imaging designs," Opt. Express 17(26), 24036–24044 (2009).

[26] Y. Zhong and H. Gross, "Initial system design method for nonrotationally symmetric systems based on Gaussian brackets and Nodal aberration theory", Opt. Express. 25(9) (2017).

[27] X. Yuan and X. Cheng, "Lens design based on lens form parameters using Gaussian brackets," Proc. SPIE 9272, 92721L (2014).

[28] R. V. Shack and K. P. Thompson, "Influence of alignment errors of a telescope system," Proc. SPIE 251, 146–153 (1980).

[29] K. Thompson, "Description of the third-order optical aberrations of near-circular pupil optical systems without symmetry," J. Opt. Soc. Am. A 22, 1389-1401 (2005).

[30] K. Fuerschbach, J. P. Rolland, and K. P. Thompson, "Theory of aberration fields for general optical systems with freeform surfaces," Opt. Express 22, 26585-26606 (2014).

[31] S.H. Brewer, "Surface-contribution algorithms for analysis and optimization," J. Opt. Soc. Am. 66, 8-13 (1976).

[32] W. Welford, "A new total aberration formula", Opt. Acta 19, 179 (1972)

[33] H. Hopkins, "The wave theory of aberrations", Oxford Univ. Press (1950).

[34] J. Sasián, "Theory of sixth-order wave aberrations," Appl. Opt. 49, D69-D95 (2010).

[35] B. Chen and A. M. Herkommer, "High order surface aberration contributions from phase space analysis of differential rays," Opt. Express 24, 5934-5945 (2016).

[36] M. Oleszko, R. Hambach and H. Gross, "Decomposition of the total wave aberration in generalized optical systems", J. of Opt. Soc. of America A. 34 (10), 1856-1864 (2017).

[37] K. Araki, "Analysis of off-axial optical systems (2)", Optical Review 7(4), 326-336 (2000).

[38] M. Maksimovic, “Optical tolerancing of structured mid-spatial frequency errors on free-form surfaces using anisotropic radial basis functions,” Proc. SPIE 9626, 9626-13 (2015).

[39] K.Achilles, K.Uhlendorf and D.Ochse, “Tolerancing the impact of mid-spatial frequency surfaces errors of lenses on distortion and image homogeneity”, Proc. SPIE 9626, 9626-0A (2015).

[40] M. Beier, J. Hartung, T. Peschel, C. Damm, A. Gebhardt, S. Scheiding, D. Stumpf, U. D. Zeitner, S. Risse, R. Eberhardt, and A. Tünnermann, "Development, fabrication, and testing of an anamorphic imaging snap-together freeform telescope," Appl. Opt. 54, 3530-3542 (2015).

[41] F.Z. Fang, X.D. Zhang, A. Weckenmann, G.X. Zhang, C. Evans, Manufacturing and measurement of freeform optics, CIRP Annals 62 (2), 823-846 (2013).

[42] T. Blalock, K. Medicus, J. DeGroote Nelson, "Fabrication of freeform optics", Proc. SPIE 9575, 9575-0H (2015).

[43] J. Hartung, M. Beier, T. Peschel, A. Gebhardt and S. Risse, "Mechanical design implementation and mathematical considerations for ultra-precise diamond turning of multiple freeform mirrors on a common substrate", Proc. SPIE 9628, 9628-29 (2015).

[44] Z. Gu, C. Yan, and Y. Wang, "Alignment of a three-mirror anastigmatic telescope using nodal aberration theory," Opt. Express 23, 25182-25201 (2015).

[45] K.P. Thompson, E. Schiesser, J.P. Rolland, “Why are freeform telescopes less alignment sensitive than a traditional unobscured TMA?”, Proc. SPIE 9633, 9633-17 (2015).

[46] H. Takeuchi, K. Yosizumi, H. Tsutsumi, “Ultrahigh Accurate 3-D Profilometer Using Atomic Force Probe of Measuring Nanometer”, Proc. of ASPE Winter Topical Meeting, 102-107 (2004).

[47] S. Mühlig, J. Siepmann, M. Lotz, S. Jung, J. Schindler and G. Baer, „Tilted Wave Interferometer – Improved Measurement Uncertainty”, Proc. 58th Ilmenau Scientific Colloquium, 1-7 (2014)

[48] M. Breitbarth, C. Braeuer-Burchardt, P. Kuehmstedt, M. Heinze and G. Notni, "Measurement of optical free-form surfaces with fringe projection", Proc. SPIE 7066, 7066-05 (2008).

[49] M. P. Chrisp, B. Primeau, and M. A. Echter, “Imaging freeform optical systems designed with NURBS surfaces,” Opt. Eng. 55(7), 071208 (2016).

[50] P. Jester, C. Menke, and K. Urban, “Wavelet Methods for the Representation, Analysis and Simulation of Optical Surfaces,” IMA J. Appl. Math. 77, 357–363 (2012).

[51] O. Cakmakci, I. Kaya, G. Fasshauer, K. Thompson and J. Rolland, "Application of Radial Basis Functions to Represent Optical Freeform Surfaces", Proc. SPIE 7652, 7652-0A (2010).

[52] Q. Meng, W. Wang, H. Ma, and J. Dong, “Easy-aligned off-axis three-mirror system with wide field of view using freeform surface based on integration of primary and tertiary mirror,” Appl. Opt. 53(14), 3028–3034 (2014).

[53] K. Fuerschbach, G. E. Davis, K. P. Thompson, and J. P. Rolland, “Assembly of a freeform off-axis optical system employing three φ-polynomial Zernike mirrors,” Opt. Lett. 39(10), 2896–2899 (2014).

[54] F. Liu, B. M. Robinson, P. Reardon and J. M. Geary, "Analyzing optics test data on rectangular apertures using 2-D Chebyshev polynomials," Optical Engineering 50(4), 043609 (2011).

[55] M. Nikolic, P. Benítez, J.C. Miñano, D. Grabovickic, J. Liu, B. Narasimhan, and M. Buljan, “Optical design through optimization using freeform orthogonal polynomials for rectangular apertures”, Proc. SPIE 9626, 9626-0W (2015).

[56] D. Ochse, K. Uhlendorf, L. Reichmann, "Describing freeform surfaces with orthogonal functions", Proc. SPIE 9626, 9626-34 (2015).

[57] E. Muslimov, E. Hugot, W. Jahn, S. Vives, M. Ferrari, B. Chambion, D. Henry, and C. Gaschet, “Combining freeform optics and curved detectors for wide field imaging: a polynomial approach over squared aperture,” Opt. Express 25, 14598–14610 (2017).

[58] M. Bray, “Orthogonal polynomials: a set for square areas”, Proc. SPIE 5252, 314-321 (2004).

[59] G.W. Forbes,“Characterizing the shape of freeform optics,” Opt. Exp. 20, 2483–2499 (2012).

[60] M. Nikolic, P. Benítez, B. Narasimhan, D. Grabovickic, J.liu and J.C. Miñano, “Optical design through optimization for rectangular apertures using freeform orthogonal polynomials: a case study”, Opt. Eng. 55, 071204 (2016).

[61] I. Kaya, K.P. Thompson and J.P. Rolland, “Comparative assessment of freeform polynomials as optical surface descriptions”, Opt. Exp. 20, 22683-22691 (2012).

[62] C. Menke and G.W. Forbes, “Optical design with orthogonal representations of rotationally symmetric and freeform aspheres”, Adv. Opt. Technol. 2, 97-109 (2013).

[63] M. Maksimovic, “Design and optimization of a compact freeform lens array for laser beam splitting: a case study in optical surface representation”, Proc. SPIE 9131, 9131-07(2014)

[64] C. Menke, “What's in the Designer's Toolbox for Freeform Systems?”, Proc. OSA Topical meeting “Freeform optics”, FM4B.1 (2013).

[65] J.Y. Wang and D.E. Silva, “Wave-front interpretation with Zernike polynomials”, Appl.Opt.19 (9), 1510-1518 (1980).

[66] H. Gross, “Handbook of Optical Systems, Vol. 1 Fundamentals of Technical Optics”, Wiley-VCH (2007).

[67] H. Gross, H. Zügge, M. Peschka und F. Blechinger, “Handbook of Optical Systems, Vol. 3: Aberration Theory and Correction of Optical Systems”, Wiley-VCH (2007).

[68] M. Brunelle, J. Yuan, K. Medicus and J. DeGroote Nelson, "Importance of fiducials on freeform optics", Proc. SPIE 9633, 9633-18 (2015).

[69] “CodeV Optimization Reference Manual”, Synopsys Version 11.1 (2017).

[70] “OSLO Program Reference”, Lambda Research Corporation, 339-398 (2016).

[71] “Zemax 13 User’s Manual”, Radiant Zemax, 539-608 (2013).

[72] K. Fuerschbach, “Freeform, φ-Polynomial Optical Surfaces: Optical Design, Fabrication and Assembly”, PhD-thesis Rochester (2014).

[73] K. P. Thompson, T. Schmid, and J. P. Rolland, “The misalignment induced aberrations of TMA telescopes,” Opt. Express 16(25), 20345–20353 (2008).

[74] H. J. Juranek, R. Sand, J. Schweizer, B. Harnisch, B. P. Kunkel, E. Schmidt, A. Litzelmann, F. Schillke, and G. Dempewolf, “Off-axis telescopes: the future generation of Earth observation telescopes,” Proc. SPIE 3439, 104–115 (1998).

[75] P. Ott, “Optic design of head-up displays with freeform surfaces specified by NURBS”, Proc. SPIE 7100 (2008).

[76] T. H. Kim, H. J. Kong, T. H. Kim, and J. S. Shin, “Design and fabrication of a 900–1700 nm hyper-spectral imaging spectrometer,” Opt. Commun. 283, 355–361 (2010).

[77] A. S. Leonard in A. Mackintosh, “Advanced Telescope Making Techniques Volume 1 Optics”, Willmann-Bell (1986).

[78] Y. Liu, Y. Li and Z. Cao, “Design of anamorphic magnification high-numerical aperture objective for extreme ultraviolet lithography by curvatures combination method”, Appl. Opt. 55(18), 4917-4923(2016).

[79] L. W. Alvarez, “Development of variable- focus lenses and a new refractor,” J. Am. Optom. Assoc. 49(1), 24–29 (1978).

[80] C. Bakolias and A. K. Forrest, “Dark-field Scheimpflug imaging for surface inspection,” Proc. SPIE 3029, 57–68 (1997).

[81] Q. Wang, D. Cheng, Y. Wang, H. Hua and G. Jin, “Design, tolerance, and fabrication of an optical see-through head-mounted display with free-form surface elements”, Appl. Opt. 52(7), C88-C99 (2013).

[82] R.R. Boye, W.C. Sweatt, B.H. Jared, A.M. Ison, E.G. Winrow, M.- P. Saavedra and J.P. Hunt, “Design of head-mounted binoculars utilizing freeform surfaces,” Opt. Eng. 53(3), 031310, (2014).

[83] Y. Nie, F. Duerr and H. Thienpont, “Direct design approach to calculate a two-surface lens with an entrance pupil for application in wide field-of view imaging”, Opt. Eng. 54, 015102 (2015).

[84] W.T. Welford, “Aberrations of Optical Systems”, Taylor & Francis (1986).

[85] J. Hoffman, “Induced aberrations in optical systems,” Ph.D. dissertation, University of Arizona (1993).

[86] H. Gross and C. Liu, “Generalized Surface Aberration Contributions”, Talk EOSAM, “Optical System Design and Tolerancing” (2014).

[87] C.Liu, “Surface contribution of aberration”, Research labwork Jena (2014).

[88] G. W. Forbes, "Never-ending struggles with mid-spatial frequencies", Proc. SPIE 9525, Optical Measurement Systems for Industrial Inspection IX, 9525-1B (2015).

[89] J. Stock, A. Broemel, J. Hartung, D. Ochse, and H. Gross, "Description and reimplementation of real freeform surfaces," Appl. Opt. 56, 391-396 (2017).

[90] H. Gross, A. Brömel, M. Beier, R. Steinkopf, J. Hartung, Y. Zhong, M. Oleszko, and D. Ochse, “Overview on surface representations for freeform surfaces,” Proc. SPIE 9626, 9626-0U (2015).

[91] R. Steinkopf, L. Dick, T. Kopf, A. Gebhardt, S. Risse and R Eberhardt, "Data handling and representation of freeform surfaces", Proc. SPIE 8169, Optical Fabrication, Testing, and Metrology IV, 8169-0X (2011).

[92] E. Goodwin, U. Fuchs, S. Gangadhara, S. Kiontke, V. Smagley, and A. Yates, "Design and Implementation of a New Freeform Surface Based on Chebyshev Polynomials", Proc. OSA Topical meeting “Freeform optics”, FT2B.3. (2015).

[93] J. Ye, Z. Gao, S. Wang, J. Cheng, W. Wang, and W. Sun, "Comparative assessment of 2 orthogonal polynomials for wavefront reconstruction over the square aperture," J. Opt. Soc. Am. A 31, 2304-2311 (2014).

[94] J. A. Díaz and R. Navarro, “Orthonormal polynomials for elliptical wavefronts with an arbitrary orientation”, Appl. Opt. 53, 2051-2057 (2014).

[95] V. Mahajan and G. Dai, “Orthogonal polynomials for hexagonal pupils”, Optics Letters 31, 2462-2464 (2006).

[96] G. W. Forbes, “Manufacturability estimates for optical aspheres,” Opt. Exp. 19(10), 9923–9941 (2011).

[97] A. Broemel, H. Gross, D. Ochse, U. Lippmann, C. Ma, Y. Zhong and M. Oleszko, “Performance comparison of polynomial representations for optimizing”, Proc. SPIE 9626, 9626-27 (2015).

[98] M. Abramowitz and I. Stegun, “Handbook of Mathematical Functions with Formulas, Graphs, and Mathematical Tables”, NIST (1964).

[99] V. Mahajan, “Zernike circle polynomials and optical aberrations of systems with circular pupils”, Appl. Opt. 33, 8121-8124 (1994).

[100] J.C. Wyant and K. Creath, “Applied Optics and Optical Engineering”, Vol. XI, Academic Press, Chapter 1 (1992).

[101] B. Dörband, H. Müller, H. Gross, “Handbook of Optical Systems, Vol. 5 Metrology of Optical Components and Systems”, Wiley-VCH (2012).

[102] A.Broemel, U. Lippmann and H. Gross, “Freeform surface descriptions. Part I: Mathematical presentations”, Adv. Opt. Tech., Vol.6, 327-336 (2017).

[103] A.Broemel, C. Liu, Y. Zhong, Y. Zhang and H. Gross, “Freeform surface descriptions. Part II: Application benchmark”, Adv. Opt. Techn., Vol. 6, 337-347 (2017).

[104] B. Chen and A. Herkommer, “Alternate optical designs for head-mounted displays with a wide field of view”, Appl. Opt. 56, 901-906 (2017).

[105] R. Wartmann and U. Schauss,” Anastigmatic anamorphic lens”, US6310731 B1 (2001).

[106] Synopsys, “Choosing the right optical design software”, white paper, 3-4 (2017).

[107] S. Heder, “Comparison of different algorithms for optimizing optical freeform systems with polynomial representations”, Research labwork Jena (2018).

[108] T. Pelgen, “Beschreibung und technologiebedingte Optimierung von Freiformlinsen für Projektionsscheinwerfer im Automotivbereich”, Master-thesis Jena (2017).

Ehrenwörtliche Erklärung

Hiermit erkläre ich ehrenwörtlich, dass ich die vorliegende Arbeit selbstständig, ohne unzulässige Hilfe Dritter und ohne Benutzung anderer als die angegebenen Hilfsmittel und Literatur angefertigt habe. Die aus anderen Quellen direkt oder indirekt übernommenen Daten und Konzepte sind unter Angabe der Quellen gekennzeichnet.

Bei der Auswahl und Auswertung folgender Materialien haben mir nachstehenden Personen in der jeweiligen Weise ~~entgeltlich~~/unentgeltlich geholfen:

- Herbert Gross, Betreuer
- Siti Heder, Research-lab-Studentin: Die im Kapitel 4.5 gezeigten Optimierungen mit CODE V und OSLO wurden von Siti Heder im Rahmen ihres Research- labs nach meiner Anleitung durchgeführt.

Weitere Personen waren an der inhaltlich-materiellen Erstellung der vorliegenden Arbeit nicht beteiligt. Insbesondere habe ich hierfür nicht die entgeltliche Hilfe von Vermittlungs- bzw. Beratungsdiensten (Promotionsberater oder andere Personen) in Anspruch genommen. Niemand hat von mir unmittelbar und mittelbar geldwerte Leistungen für Arbeiten erhalten, die im Zusammenhang mit dem Inhalt der vorgelegten Dissertation stehen.

Weder diese Arbeit noch eine andere wurde bisher im In- oder Ausland in gleicher oder ähnlicher Form einer anderen Prüfungsbehörde vorgelegt.

Die geltende Promotionsordnung der Physikalisch-Astronomischen Fakultät ist mir bekannt.

Ich versichere ehrenwörtlich, dass ich nach bestem Wissen die reine Wahrheit gesagt und nichts verschwiegen habe.

Jena, 22.05.2018 Anika Brömel

Acknowledgement

14 years ago, when I was looking forward to study physics here in Jena, I had no idea, what a journey it will be. Over the years I had the pleasure to work with many great people, who contributed directly or indirectly to this work. Naming all would go way beyond the page limit, but nevertheless I would like to acknowledge some very special ones:

When I met Herbert Gross 5 years ago, I was on a very different path scientifically. Shortly after, my situation changed, and you gave me the opportunity to work in your group and specifically on a new project. During my time in your group, I grew as a scientist and person. As a part of fo+, I learned a lot about the background of such a huge project and at the same time took actively part in shaping the project work. I am grateful for this chance and the experience I gained with it. But most of all I appreciate the support you gave me scientifically and personally through the years.

Another important person is Yi. I hardly remember our first meeting (I know you do), but with the time you became my dear friend. I am grateful for your help and support and your endless optimism. I will miss our spontaneous after work dinners in our favourite restaurant and the discussions about everything and nothing. I enjoyed learning from and with you, even when it was weird German grammar.

I would also like to thank my student Siti for her contribution to my investigations with her research lab. I appreciate your effort and patience with me very much, specifically when I bothered you with a whiteboard full of equations and explanations, and the little swan, who has a very special place now.

Special thanks go to Uwe for his tremendous help in coding the DLLs for the surface descriptions and to Manuel for answering every question I had about Mathematica.

Moreover, I would like to acknowledge my other students Changlong, Eva, Tobias and Chonghuai and colleagues Johannes, Danyun and Yueqian for the help and fruitful discussions throughout the years.

I would also like to thank all the other members of our group, I haven't mentioned and our little sister group at IOF, as well as the administration of IAP. It was pleasure to work with you

and not only because you ate every cookie or cake I brought. I appreciate the open and relaxed atmosphere in the group and specifically in our “cookie-office”.

Besides, there are some very special people, I’d like to acknowledge:

Some years ago, I had the honour to work with Hans-Peter Gemünd. Although I was not meant to continue your work, I appreciate everything you taught me There will always be a special bond to the R(h)einraum in Endenich.

Moreover, I would like to thank Andreas for his support and care of my little girls. I will miss our coffee breaks and whine evenings.

Special thanks go to Tine. I cherish our friendship and your unconditional support through all the years, specifically in the last months. I am very proud to be your “sister”.

Last, but not least I would like to thank my family for their support from the very beginning on. I appreciate that they encouraged me, to go my own way, but that were always there, when I needed them.

In particular, I’d like to thank my other half Christian, for being my partner in crime throughout this whole journey. I could not write this thesis without your tremendous mental support, even from afar. With you by my side, I am looking forward to every new adventure coming.

Curriculum Vitae

Name:	Anika Brömel
Date of birth:	19.09.1984 in Waren (Müritz)

Education:

09/2004 – 11/2010	Diploma in Physics Friedrich-Schiller-Universität, Jena
09/1995 – 06/2004	Abitur Richard-Wossidlo-Gymnasium, Waren (Müritz)
09/1991-08/1995	Primary School Goetheschule, Waren (Müritz)

Work experience:

06/2018-	Projectmanager and development engineer Semicon Modules SwissOptic AG, Heerbrugg, CH
01/2014 – 03/2018	Research assistant and doctoral candidate Group: Optical System Design (Prof. Dr. Herbert Gross) Institute of Applied Physics Friedrich-Schiller-Universität, Jena
12/2010 – 11/2013	Research assistant Department: Quantumdetection (Prof. Dr. Hans-Georg Meyer) Institute of Photonic Technologies, Jena with Carl-Zeiss-scholarship (Abbe school of photonics)

Anika Brömel

Jena, 22.05.2018 Anika Brömel

Publications

Journals

A.Broemel, U. Lippmann and H. Gross
“Freeform surface descriptions. Part I: Mathematical representations”,
Adv. Opt. Tech., Vol. 6, 327-336 (2017)

A.Broemel, C. Liu, Y. Zhong, Y. Zhang and H. Gross
“Freeform surface descriptions. Part II: Application benchmark”,
Adv. Opt. Tech., Vol. 6, 337-347 (2017)

J. Stock, A. Broemel, J. Hartung, D. Ochse and H. Gross,
“Description and reimplementation of real freeform surfaces”,
Appl. Opt. 56, 391-396 (2017)

T. May, E. Heinz, K. Peiselt, G. Zieger, D. Born, V. Zakosarenko, A. Brömel, S. Anders and H. -G. Meyer
“Next generation of a sub-millimetre wave security camera utilising superconducting detectors”,
J. Instrum., Vol. 8, P01014 (2013)

C. Kraft, A. Broemel, S. Schoenherr, M. Haedrich, U. Reisloehner, P. Schley, G. Gobsch, R. Goldhahn, W. Wesch and H. Metzner,
“Phosphorus implanted cadmium telluride solar cells”,
Thin Solid Films, 519(21), 7153-7155 (2011)

Conference proceedings

A. Brömel, H. Gross, D. Ochse, U. Lippmann, C. Ma, Y. Zhong and M. Oleszko,
“Performance comparison of polynomial representations for optimizing optical freeform systems”,
Proc. SPIE 9626, 9626-0W (2015)

H. Gross, A. Brömel, M. Beier, R. Steinkopf, J. Hartung, Y. Zhong, M. Oleszko, and D. Ochse, “Overview on surface representations for freeform surfaces,”
Proc. SPIE 9626, 9626-0U (2015).

Y. Zhong, H. Gross, A. Broemel, S. Kirschstein, P. Petruck and A. Tuennermann,
"Investigation of TMA systems with different freeform surfaces",
Proc. SPIE 9626, 9626-0X (2015)

G. Zieger, D. Born, S. Anders, E. Heinz, K. Peiselt, A. Brömel, V. Zakosarenko, T. May, and H.-G. Meyer,
"A passive submillimeter video camera for security applications,"
Proc. IRMMW-THz, 1–2 (2013)

E. Heinz, T. May, D. Born, G. Zieger, K. Peiselt, A. Brömel, S. Anders, V. Zakosarenko, T. Krause, A. Krüger, M. Schulz and H.-G. Meyer,
"Development of passive submillimeter-wave video imaging systems"
Proc. SPIE 8715, 8715-0E (2013)

E. Heinz, T. May, D. Born, G. Zieger, A. Brömel, S. Anders, V. Zakosarenko, T. Krause, A. Krüger, M. Schulz, F. Bauer and H.-G. Meyer,
"Development of passive submillimeter-wave video imaging systems for security applications",
Proc. SPIE 8544, 8544-02 (2012)

A. Brömel, U. Schinkel, S. Anders, T. May and H.-G. Meyer,
"Polymer filters for far-infrared spectroscopy",
37th International Conference on Infrared, Millimeter, and Terahertz Waves, Wollongong, NSW,1-2 (2012)

Talks (only own)

A. Brömel, J. Stock and H. Gross
"Beschreibung von Freiformflächen in Design und Fertigung"
Keynote, 1. OptecNet Jahrestagung, Mainz (2017)

A. Brömel, H. Gross, D. Ochse, U. Lippmann, C. Ma, Y. Zhong and M. Oleszko,
"Performance comparison of polynomial representations for optimizing optical freeform systems",
Optical Systems Design 2015: Optical Design and Engineering VI (2015)